Nanostructured Liquids, Colloids and Environmentally Acceptable Liquid Media

Dissertation

zur

Erlangung des Grades eines Doktor rer. nat.

der

Universität Regensburg

im

Bereich der Physikalischen Chemie

vorgelegt von

Michael Lorenz Klossek

aus Vilshofen

2013

Promotionskomitee:

1. Gutachter:	Prof. Dr. Werner Kunz, Universität Regensburg
2. Gutachter:	Prof. Dr. Thomas Zemb, CEA, ICSM, UMR
3. Prüfer:	Prof. Dr. Hubert Motschmann, Universität Regensburg
Vorsitzender:	Prof. Dr. Henri Brunner (Emeritus), Universität Regensburg
Tag der Disputation:	10.04.2013

Acknowledgement

This doctoral thesis was carried out at the Institute of Physical and Theoretical Chemistry, Faculty of Natural Science IV, University of Regensburg, between October 2010 and April 2013, under the supervision of Prof. Dr. Werner Kunz. This work would not have been possible without the help from many people.

First of all, I want to thank my supervisor, Prof. Dr. Werner Kunz, for giving me the opportunity to carry out my thesis at his institute. I thank him for his commitment to guide me through my research, for this interesting subject, the countless time he has spent supporting me on this subject and the numerous possibilities to present my work at national and international conferences.

I would like to show my gratitude to Prof. Dr. Thomas Zemb for the many discussions we shared on the subject of surfactant-less microemulsions and the trust he gave to my work.

Further, I owe sincere and earnest thankfulness to Dr. Didier Touraud. Without all his ideas and incitations, I would not have finished my thesis as quick as i did now. I am very pleased for the countless discussions we had and the very comfortable collaborations while supporting me with many experimental ideas.

I would like to thank PD Dr. Rainer Müller, and Prof. Dr. Richard Buchner for supporting my work by providing their equipment.

I want to thank Dr. Roland Neueder for several discussions on the field of thermodynamics in combination with the concept of surfactant-less microemulsions.

Further, thanks go to the secretaries Rosi and Sonja. I want to thank them for the numerous discussions and for the help I got. I think now is the time to apologise for distracting them from their work several times. Further, i want to thank Wolfgang Simon and Georg Berger.

I would like to show my gratitude to Julien Marcus, my former Master student. Without his enthusiasm and purposefulness my thesis would not have been finished

in that short time. I thank him for the fun and the good working atmosphere in the lab.
Additionally, I would like to acknowledge and thank the students Daniel-Fabian Wutz, Sylvia Adlersberger, Marco Dehling, Stefan Ruider, Josef Baumann, Dominik Kellner, Laura Egel, Emilien Folzer, Julia Grapinet, Houria Misbahi, Florence Jacob, and Juan Luis Diaz for their contribution, dedication, and cooperative efforts on helping me with some experiments throughout the scope of this work.
I would like to individually thank, Andreas Eiberweiser, Eva-Maria Schön, Katrin Ledermüller, Andreas Seitz, Oliver Masur, Veronika Fischer, and Julien Marcus for their invaluable assistance on assessing my thesis and providing me feedback on recommendations and suggestions.
I am also very grateful to all colleagues from the lab for scientific collaborations. Among those special thanks should go to Andi, Evi, Julien, Susanne, and Vroni for the numerous funny moments, for all the lunch times we spent in the Cafeteria and all the other events.
Further I want to thank all my fellow students with whom I passed the last seven years at the University of Regensburg. Especially, I want to mention Eva, Katrin, Oli, and Tobi.
Special thanks go to the members of the Kaffeerunde, Andi, Evi, Georg, Julien, Roland, Richard, Tom, and Vroni. Only due to their mental practice it was possible to endure this time and to be prepared for the "real" life outside university.
Am Ende möchte ich vor allem meinen Eltern, Edgar und Margit Klossek, danken. Ohne ihre Hilfe und Unterstützung wäre nicht nur die Promotion sondern auch meine gesamte Zeit in Regensburg nicht möglich gewesen.

Abstract

In this study, two major fields of interest were investigated. The first one was the formulation of greener and more sustainable microemulsions and the second one was the examination of the phenomenon of surfactant-less microemulsions. Both topics can be summarised under the big heading "Green Solvents".

In the first part of the work, the main components of classical microemulsions were successively replaced by greener or more sustainable alternatives. Instead of n-alkanes as oil phase, limonene, biodiesel from different sources, mixtures of limonene and biodiesel, or dibasic esters were used. A sustainable and non-toxic alternative for sodium dodecyl sulfate as surfactant was sodium oleate. The most difficult task was to replace 1-pentanol as cosurfactant. The most green cosurfactant used in this study was citronellol. Beside this, 1-heptanol, in terms of sustainability, and 1-dodecanol or Guerbet Alcohols, as low toxic components, were other alternatives. To optimise the microemulsion systems, a short chain alcohol as cosolvent was added to extend the microemulsion area. The increase of the film flexibility with addition of cosolvent, in this study ethanol, was determined to be a major reason for the enlargement of the area. The incorporation of ethanol in the amphiphilic film makes it more flexible and turns the system from an anti-percolative to a percolative one. With the concept of extending the microemulsion area, it was even possible to formulate highly (with sodium oleate) and fully (with sodium dodecyl sulfate) water dilutable green microemulsions. Further, the limitations of this concept were investigated as well. The partition of the cosolvent plays an important role. With a too high hydrophobicity difference between the cosolvent and the oil or cosurfactant, the cosolvent will be only dissolved in the aqueous phase and will not contribute to the interfacial film. The nanostructures and the film flexibility were investigated using electrical conductivity measurements. Moreover, with dynamic light scattering

experiments, the homogeneous single phase areas were characterised to distinguish real solutions from microemulsions.

In the second part of this work, a study of the monophasic region in the ternary systems containing water, ethanol and octanol was made based on dynamic and static light scattering. It was surprising that it became evident from these experimental results that well-defined micellar structures and consequently two distinct pseudo-phases exist in these ternary mixtures. The particle sizes close to the two-phase boundary were approximately 10 nm which is comparable to microemulsion systems. Light scattering results were confirmed by Prof. Thomas Zemb and Dr. Olivier Diat by small angle X-ray and small angle neutron scattering experiments. To get further information about the partition of ethanol between the pseudo-phases (one is water-rich, the other one is rich in octanol) the partial pressure of ethanol above the liquid medium was considered. The calculation of the vapour pressure compositions were made by the group of Prof. Gmehling. In addition, ternary systems with water, sugar-based solvents (ethanol, ethyl lactate and γ-valerolactone) and benzyl alcohol were investigated with regard to the concept of facilitated hydrotropy. Again, significant correlation functions in light scattering were found, indicating the formation of structure. But the calculated sizes were to small to consider them as well-defined particles. In this case, it is better to call these structures nano-clusters. Finally, it was possible to find a correlation between the occurrence of structure and hydrotropic efficiency.

Zusammenfassung

In dieser Arbeit wurden zwei wichtige Themengebiete untersucht. Das Erste war die Formulierung von grünen und nachhaltigen Mikroemulsionen und das Zweite die Untersuchung des Phänomens von tensidfreien Mikroemulsionen. Beide Bereiche können zudem unter dem Begriff "Grüne Lösungsmittel" zusammengefasst werden.

Im ersten Teil der Arbeit wurden die Komponenten klassischer Mikroemulsionen schrittweise durch grünere oder nachhaltigere Alternativen ersetzt. Es war möglich, n-Alkane durch Limonen, Biodiesel oder deren Mischungen, oder dibasische Ester auszutauschen. Als nachhaltige und ungiftige Alternative zu Natriumdodecylsulfat wurde Natriumoleat verwendet. Die schwierigste Aufgabe war, einen angemessenen Ersatz für 1-Pentanol zu finden. Das "grünste" Cotensid, das in der Arbeit verwendet wurde, ist Citronellol. Des Weiteren wurden 1-Heptanol, ein Alkohol, der aus nachhaltigen Rohstoffen erzeugt werden kann, oder 1-Dodecanol bzw. Guerbet Alkohole, welche beide in kosmetischen Produkten erlaubt sind, benutzt. Um den Bereich der Mikroemulsionen im ternären Phasendiagramm zu vergrößern, wurde zusätzlich ein kurzkettiger Alkohol als Co-Lösungsmittel hinzugefügt. In dieser Arbeit wurde Ethanol verwendet. Die dadurch erhöhte Filmflexibilität war die maßgebliche Ursache der Vergrößerung des Mikroemulsionsbereichs. Die Ethanol-Moleküle lagern sich in der Grenzschicht an, wodurch diese flexibler wird. Dies begünstig eine Umwandlung des anti-percolativen Systems in ein percolatives. Durch das Konzept der Vergrößerung des Mikroemulsionsbereiches konnten auch stark (mit Natriumoleat) und vollständig (mit Natriumdodecylsulfat) mit Wasser verdünnbare grüne Mikroemulsionen hergestellt werden. Außerdem wurden noch die Grenzen dieses Konzepts aufgezeigt. Die Verteilung des Co-Lösungsmittels zwischen den auftretenden pseudo-Phasen spielt die entscheidende Rolle. Unterscheidet sich die Hydrophobizität zwischen Co-Lösungsmittel und Cotensid oder Ölen zu stark, wird

das Co-Lösungsmittel nur in der wässrigen Phase gelöst sein. Dadurch wird es keinen Beitrag zur Erhöhung der Filmflexibilität leisten. Die Nanostrukturierung und die Filmflexibilität wurden mit Hilfe von elektrischen Leitfähigkeitsmessungen überprüft. Des Weiteren wurden einphasigen Gebiete mit Lichtstreuexperimenten untersucht.

Der zweite Teil der Arbeit handelt von der Untersuchung des einphasigen Bereichs im ternären System Wasser, Ethanol und Octanol. Dabei wurden dynamische und statische Lichtstreuexperimente verwendet. Erstaunlicherweise ergaben diese Messungen, dass bei bestimmten Zusammensetzungen klar strukturierte Systeme vorlagen. Die Teilchengröße betrug in der Nähe des zweiphasigen Bereichs etwa 10 nm, was vergleichbar mit deren in Mikroemulsionen ist. Die Lichstreuergebnisse wurde mit SAXS und SANS-Messungen bestätigt, die von Herrn Prof. Thomas Zemb und Herrn Dr. Olivier Diat durchgeführt und interpretiert wurden. Um mehr Informationen über die Verteilung der Ethanol Moleküle in den beiden pseudo-Phasen (eine reich an Wasser, die andere reich an Öl) zu erhalten, wurden Berechnungen von der Gruppe von Prof. Gmehling durchgeführt. Im nächsten Schritt wurden die ternären Systeme mit Wasser, Benzylalkohol und auf Zuckern basierenden Lösungsmitteln (Ethanol, Ethyl Laktat oder γ-Valerolacton) in Hinsicht auf das Konzept "facilitated hydrotropy" untersucht. Wiederum wurden mittels Lichtstreumessungen klare Strukturen bei bestimmten Zusammensetzungen im einphasigen Bereich gefunden. Aber in diesem Fall waren die berechneten Größen zu klein, um von Teilchengrößen sprechen zu können. Besser ist es, die Teilchen als Nanocluster zu bezeichnen. Schlussendlich war es möglich, eine Beziehung zwischen dem Auftreten von Strukturen und der Effizienz von Hydrotropen zu erhalten.

Contents

Chapter I.

Fundamentals

I.1. Green Solvents

I.1.1. General Information

Solvents are substances that are liquid under the condition of application. They can dissolve, dilute or extract other substances, so called solutes, and form a solution. Such solutes can be recovered without any modification of the chemical structure by removing the solvent [1, 2]. Further properties are the regulation of temperature, formation of azeotropes for separation, to aid in mass and heat transfer, etc. Solvents have already been used in industry and science for many hundreds of years. In the 15th century, alchemists searched for the universal solvent, the "*menstruum universale*", which has the power to remove all seeds of disease from the human body [3]. Nowadays, solvents can be found in almost all industries such as food, mining, automotive, electronics, cleaning, chemicals, pharmaceuticals etc. All together, these industries need approximately 15 billion kilograms of organic and halogenated solvents worldwide per year [4]. In the pharmaceutical industry, for example, 85% of the total mass of chemicals used in processes are solvents [5] and the recovery efficiency is approximately 50-80%. Still, aliphatics, aromatics, terpenic and chlorinated hydrocarbons, alcohols, esters, ketons and glycol ethers are very often used solvents in industrial processes [6]. The use of such organic solvents is still a ma-

jor source for VOC (volatile organic compound) emissions from chemical industries. Interestingly, the reduction of the VOC emission in Germany by almost 50 % from 1990 to 2000 was mainly achieved in other sectors. The total emission from solvents remained almost constant at 1000 kilotons per year [7]. The major problem of these VOCs is the formation of lowlevel ozone and smog through free radical air oxidation processes [8]. Additionally, some VOCs are also known or suspected carcinogens. In the following part some solvent applications and the resulting problems are mentioned.

I.1.2. Common industrial applications

Huge amounts of water are needed in textile industries. To dye fibers, approximately 100 litres of water per kilogramme fiber [9] are required. For example, in the US, a big problem is that the waste water is allowed to be returned in rivers in the contaminated form. Another problem is the adsorption of water on the fiber materials. A lot of energy is needed to dry the dyed fibers afterwards.

Another solvent-intensive industry is the dry cleaning. The primary solvent in these processes is perchloroethylene. This solvent is highly toxic and affects plant workers and consumers who use dry cleaners. Everything which comes into contact with perchloroethylene must be treated as "hazardous waste", except clothes [10].

In food industry hexane is still used to extract tons of fats, oils and flavourings from nuts, seeds and other raw materials. More than 20 million kilograms of hexane are released per year into the atmosphere during the extraction. The concentration of n-hexane in commercially available hexane is between 20 and 80 %. The allowable concentrations of pentane and heptane isomers, acetone, methyl ethyl ketone,

dichloromethane, or trichloroethylene is $\leq$0.4% [11]. Hexane poses a health danger to the employees working in food-processing plants because of its neurotoxicity.

I.1.3. What is "green"?!

Since the beginning of the Green Chemistry movement ten years ago, the need and the search for green solvents has been one of the major issues. But there is usually a controversy on the term "green". Everybody has more or less his own definition. Usually the 12 principles of Green Chemistry [12] are used as a first approach:

1. Waste prevention instead of remediation
2. Atom efficiency
3. Less hazardous/toxic chemicals
4. Safer products by design
5. Innocuous solvents and auxiliaries
6. Energy efficient use by design
7. Use of renewable raw materials and solvents
8. Shorter synthesis
9. Biocatalytic or catalytic rather than thermal processes
10. Product design for degradation without pollutant problems
11. Efficient analytical methodologies for pollution detection and prevention
12. Inherently safer processes

Solvents are explicitly mentioned in point 5 which shows the qualitative and quantitative importance of them in chemical processes. But a solvent cannot fulfill all of these 12 principles at once and you can even read in textbooks that "the greenest solvent is no solvent at all" [13]. So, in a lot of cases, instead of "green" the term "greener" or "sustainable" is more appropriate. Several suggestions for such solvents have already been given: inorganic systems (water, supercritical CO_2) [14, 15], involatile systems (ionic liquids) [16–18], easily recyclable systems (fluorous solvents, supercritical CO_2) [19, 20] and no solvents at all [21]. So, this variaty of approaches towards green solvents shows its complexity. In a recent article, Jessop [22] presented a survey where he asked the question

> *"If the adoption of greener solvents over the next 20-30 years will reduce environmental damage from human activities, then the adoption of what class of solvents will be responsible for the greatest reduction in environmental damage?"*

to the top academic researchers in the field of green solvents at a conference in Germany in October 2010. He compared their answers with the amounts of articles published in the journal *Green Chemistry* in 2010 describing each class of solvents. The results are shown in Figure I.1.

Capello *et al.* [23] defined the use of green solvents...

> *"... to minimise the environmental impact resulting from the use of solvents in chemical production."*

They also defined four points directing towards green solvents:

- replacement of hazardous solvents by solvents with better properties in the fields of environment, health and safty [24, 25]
- use of so called "bio"-solvents which are obtained from renewable feedstock [26]

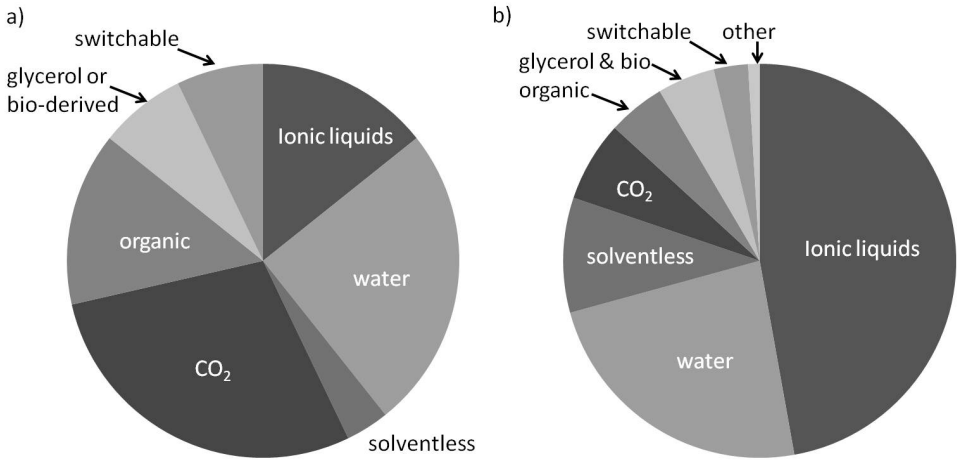

Figure I.1.: a) Results of the survey, which class of green solvents will reduce the damage on environment in the next years. The water part means liquid, supercritical and on-water. The CO_2 part includes supercritical, liquid and CO_2 expanded liquid. b) Articles published in the journal *Green Chemistry* in 2010 describing each class of solvents. The figure is redrawn from [22], the absolute values are not known and only the trends are presented.

- use of supercritical fluids like supercritical CO_2 [27], or

- ionic liquids [16–18].

Further, they presented a study about the use of two methods to classify solvents [23]. They investigated the EHS (Environmental-Health-Safety) properties [28] of 26 chemicals and evaluated them with the LCA (Life-Cycle Assessment) method [29]. Depending on the EHS criteria, Capello *et al.* used nine categories to assess chemicals: release potential, fire/explosion, reaction/decomposition, acute toxicity, irritation, chronic toxicity, persistency, air hazard and water hazard. In each of these categories, chemicals can score points. The more criteria can be applied to a chemical, the higher are the scored points. Thus, chemicals with few points are, of course, more favourable. In the LCA, the whole "life-time" of a solvent, beginning from the production and ending with the waste disposal, is evaluated. As waste, solvents can either be recycled or treated in a hazardous waste incineration plant.

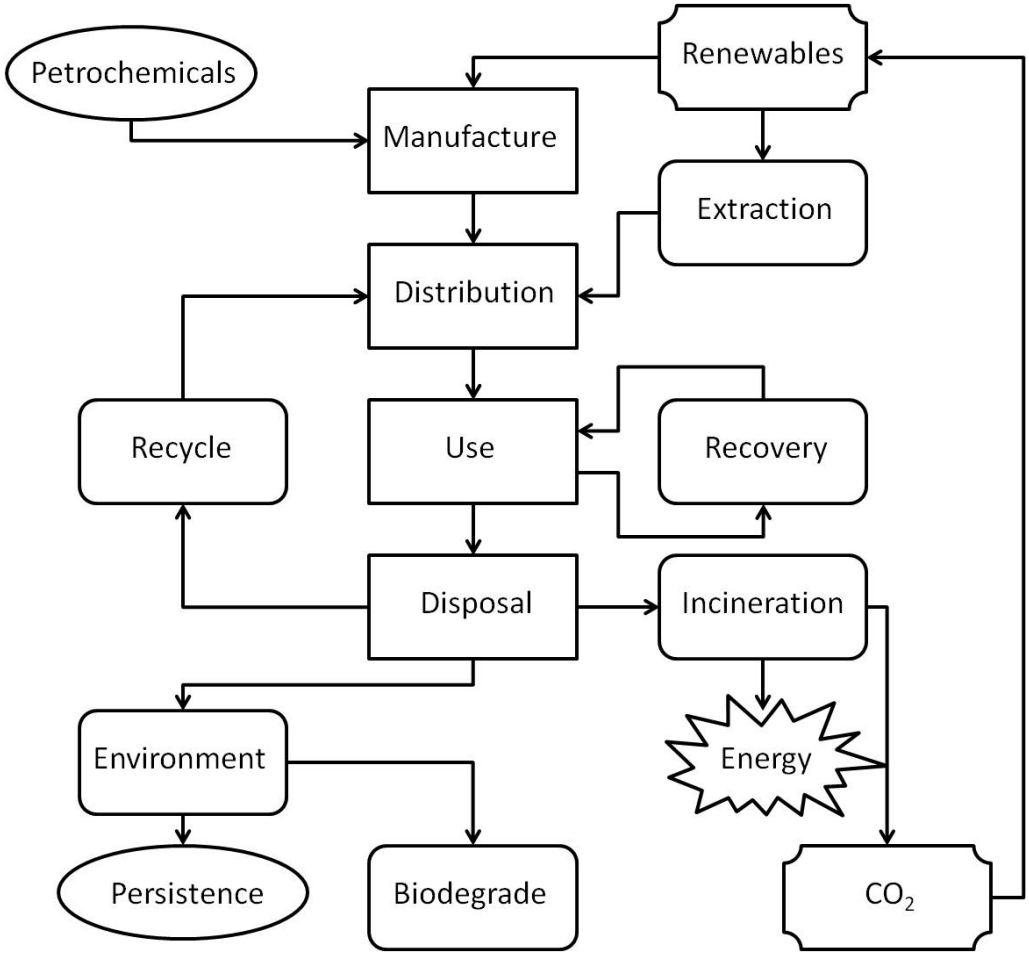

Figure I.2.: Life cycle flow chart for solvent usage [23].

In Figure I.2 an illustration of a life cycle of a chemical is shown.

Another attempt to characterise and evaluate solvents was made by the group of Alfonsi *et al.* [30]. The study describes the investigation of the pharmaceutical company Pfizer in developing a solvent selection tool for their medicinal chemists. Their motivation was, referring to the work of Capello *et al.* [23], to obtain an extremely simple tool for the end user scientist. Solvents were assessed in three major areas: worker safety, process safety and environmental and regulatory considerations. The results of this assessment are presented in Figure I.3 a). This list does not claim to

a)

Preferred
Water, Acetone, Ethanol, 2-Propanol, 1-Propanol, Ethyl acetate, Isopropyl acetate, Methanol, Methyl ethyl ketone, 1-Butanol, t-Butanol

Usable
Cyclohexane, Heptane, Toluene, Methylcyclohexane, Methyl t-butyl ether, Isooctane, 2-Methyl THF, Cyclopentyl methyl ether, DMSO, Acetic Acid, Ethylene glycol

Undesirable
Pentane, Hexane(s), Di-isopropyl ether, Diethyl ether, Dichloromethane, Dichloroethane, Chloroform, DMF, NMP, Pyridine, DMA, Acetonitrile, THF, Dioxane, DME, Benzene, Carbon tetrachloride

b)

Undesirable	Alternative
Pentante	Heptane
Hexane(s)	Heptane
Di-isopropyl ether or diethyl ether	2-MeTHF or tert-butyl methl ether
Dioxane or dimethoxyethane	2-MeTHF or tert-butyl methl ether
Chloroform, dichloroethane or carbon tetrachloride	Dichloromethane
Dimethyl formamide, dimethyl acetamide	Acetonitrile
Pyridine	Et_3N (if pyridine used as base)
Dichloromethane (extraction)	EtOAc, MTBE, toluene, 2-MeTHF
Dichloromethane (chromatography)	EtOAc/heptane
Benzene	Toluene

Figure I.3.: a) A selection of solvents from Pfizer's solvent selection guide for medicinal chemistry. b) Alternatives for common organic solvents. Taken from [30].

be complete but it comprises the most used solvents in medicinal chemistry. Moreover, a list was given with suggestions how undesirable solvents can be replaced by useable ones, see Figure I.3 b). But in most cases, it is not so easy to perform one-to-one replacements. A well adopted strategy to search for green alternatives is to compare the physico-chemical properties of solvents. A classical approach of comparing the solubilisation properties of solvents is the use of the Hansen solubility parameters [31]. The theory of Hansen is based on the "like seeks like" principle. The so called Hildebrand parameter, obtained from the vaporisation enthalpy of the component, can be splitted into three parts, which represent the three major intermolecular forces in liquids: dispersive forces (δd), permanent dipole permanent dipole interactions (δp) and H-bonding (δh).These three parameters of a solvent are usually plotted in a three-dimensional chart. But, if no literature datas on Hansen parameters are available, they either have to be measured, what can be very time consuming, or they can be calculated. But these calculated values are often not consistent with experimental data. Another possibility of comparing physico-chemical properties is to use the Kamlet-Taft plot [32–34]. It is a two-dimensional representation. On the x-axis the π^* value (a measure of the polarity and polarisability) is plotted against the β value (a measure of the basicity or hydrogen-bond accepting ability) on the y-axis. Another important value is α which corresponds to the "proticity" or hydrogen-bond donating ability. Protic solvents have α values higher than 0.5 and aprotic ones below 0.5. These plots were presented by Jessop [22] (see Figure I.4). He included green solvents according to Pfizer's list [30]. In these diagrams, ionic liquids were not included, because in the believe of the author, they are not greener than the conventional solvents. In Figure I.4 a) and b), the areas covered with common organic solvents are represented in grey. Figure I.4 a) presents aprotic solvents and b) the protic ones. The parts (i) show the common organic solvents and (ii) the green alternatives. As can be seen from these figures, the area is cov-

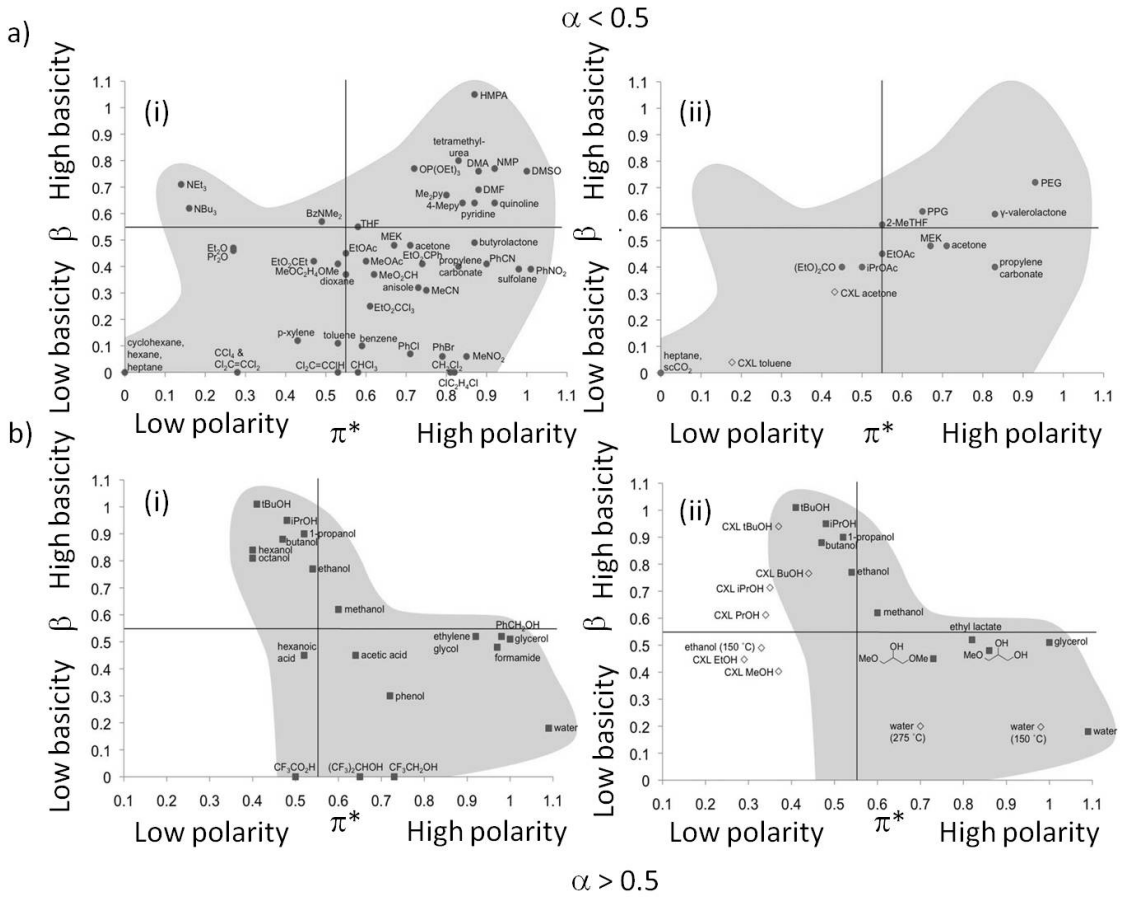

Figure I.4.: Kamlet-Taft plot of a) aprotic and b) protic (i) commonly used organic solvents and (ii) green solvents. The grey area presents the area covered with organic solvents [22].

ered sufficiently well in the case of protic solvents, whereas there is still a lack of alternatives for polar aprotic solvents.

In a recent study, Moity *et al.* presented a way of classifying organic and green solvents using σ-potentials derived from COSMO-RS calculations [35]. In a former work [36], COSMO-RS was already applied to develop a classification system for organic solvents. In their study 153 solvents were used, only from the knowledge of their chemical structure. They found 10 clusters: (I) strong electron pair donor bases, (II) weak electron pair donor bases, (III) aprotic dipolar, (IV) aprotic highly

polar, (V) apolar, (VI) asymmetric halogenated hydrocarbons, (VII) amphiprotic, (VIII) polar protic, (IX) organic acidic compounds and (X) polar structured. Moity tried to characterise 138 green solvents in the same way [35]. As result, no green alternatives to organic solvents in the classes I and VI were found.

Beside the use of greener and more sustainable solvents another alternative is to use solvent-free systems or at least as less solvents as possible. In order to reduce the quantity of solvent in a process water can be added [37]. Moreover, the addition of water to oils leads to a higher heat capacity which is a benefit in lubricants and cutting fluids [38]. An elegant way is to transform the system into a microemulsion. Beside this aspect, very often the physico-chemical properties of microemulsions are favourable as well. For example, low interfacial viscosity is important in cleaning processes and enhanced oil recovery [38].

I.2. Microemulsions

I.2.1. General Information

Microemulsions are isotropic, optically transparent, thermodynamically stable solutions [39, 40] and were first observed by Schulman [41] and Winsor [42]. But, Schulman *et al.* were the first to call these solutions, consisting of water, oil, surfactant, and alcohol, "micro-emulsions" [43] in 1959. However, the word micro does not reflect the nanostructure in these systems, therefore some preferred the names "micellar emulsion" [44] or "swollen micelles" [45]. Another definition was given by Danielsson and Lindman in 1981 [46]:

> *"...a microemulsion is a system of water, oil and an amphiphile which is a single optically isotropic and thermodynamically stable liquid solution."*

Due to the oil crisis in the 1970s, especially oil companies focused on the research of microemulsions because they could be used as a tool for optimising oil recovery. Besides the economic interest, in the 1980s researchers took an interest in the understanding of the various nanostructures. Several techniques were adopted to investigate these structures: NMR self-diffusion [47], transmission electron microscopy (TEM) [47, 48], small angle X-ray scattering (SAXS) [49], or small angle neutron scattering (SANS) [50], to name some examples.

I.2.2. Classification

Microemulsions consist of at least three components, a polar liquid (usually water) and an apolar one (usually an oil) separated by a surfactant molecular film [51, 52]. In most cases a cosurfactant is necessary too. Already in 1955 Bowcott and Schulman stated that their microemulsions needed alcohols (often short or mid-chain [53]) as cosurfactants to stabilise the system [54]. On the microscopic scale microemulsions are structured in terms of domains of well defined droplets (either water in oil (w/o) or oil in water (o/w)) [41, 55] or bicontinuous structures [56, 57]. Often, o/w systems are abbreviated as L1-phases, w/o as L2-phases, and bicontinuous structures often as L3-phases or sponge phases. Bicontinuous structures consist of networks of oil and water nanodomains separated and stabilised by a surfactant interfacial film. Their net curvature is close to zero. Mostly, they can be found at almost equal amounts of water and oil.

Another important phase classification was introduced by Winsor [42] who discovered four general types of phase equilibria:

- Winsor I : two phases in equilibrium, o/w structure and an almost pure upper oil phase

- Winsor II : two phases in equilibrium, an aqueous phase containing surfactant and an upper w/o phase

- Winsor III : three-phase system consisting of a surfactant poor water phase, a bicontinuous middle phase, and an almost pure upper oil phase

- Winsor IV : classical single phase microemulsions that can be L1, L2 or L3

I.2.3. Phase Diagrams

Mixing water, oil and surfactant produces at certain compositions areas of microemulsions. At all other compositions macroemulsions, liquid crystalline phases, precipitation of surfactant or undissolved surfactant can occur. A way to present the phase behaviour within a ternary or pseudo-ternary system is the *Gibbs triangle*. It is a equilateral triangle. Along the sidelines either the mass, volume, or mole fraction of the components are plotted. Every corner corresponds to the pure component. When the phase behaviour is investigated as a funtion of temperature as well, the triangle is extended to the *Gibbs Prism*. In this case the *Gibbs triangle* is the basis and temperature the ordinate. Usually, the effect of the pressure on the phase behaviour is very weak and neglected [58]. Figure I.5 is an illustration of a *Gibbs prism*. In these diagrams two important variables were defined to classify microemulsion: the oil-to-water ratio, α, and the amount of added surfactant γ.

$$\alpha = \frac{m_{oil}}{m_{oil} + m_{water}} \tag{I.1}$$

$$\gamma = \frac{m_{surfactant}}{m_{water} + m_{oil} + m_{surfactant}} \tag{I.2}$$

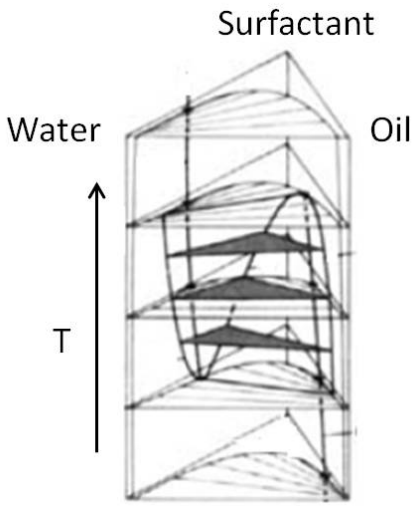

Figure I.5.: Illustration of a *Gibbs prism*.

But this three-dimensional representation is often not very descriptive, thus two-dimensional representations are preferred. A very common way is to "cut" the phase prism. In the following the most common cuts are presented:

Δ-Cut

The Δ-cut gives the common *Gibbs triangle* at a constant temperature and pressure. The two variables in these diagrams are the surfactant concentration and the oil-to-water ratio.

γ-Cut

In these diagram types, the oil-to-water ratio is kept constant. The total amount of surfactant is plotted against the temperature. This cut gives access to important parameters for applications. γ_0 is the minimum amount of surfactant needed to form a $WinsorIII$ phase. The lowest temperature required to obtain this three phase body is T_l. And the temperature above the three phase body disappears is T_u. The minimum amount of surfactant needed to form a single phase microemulsions

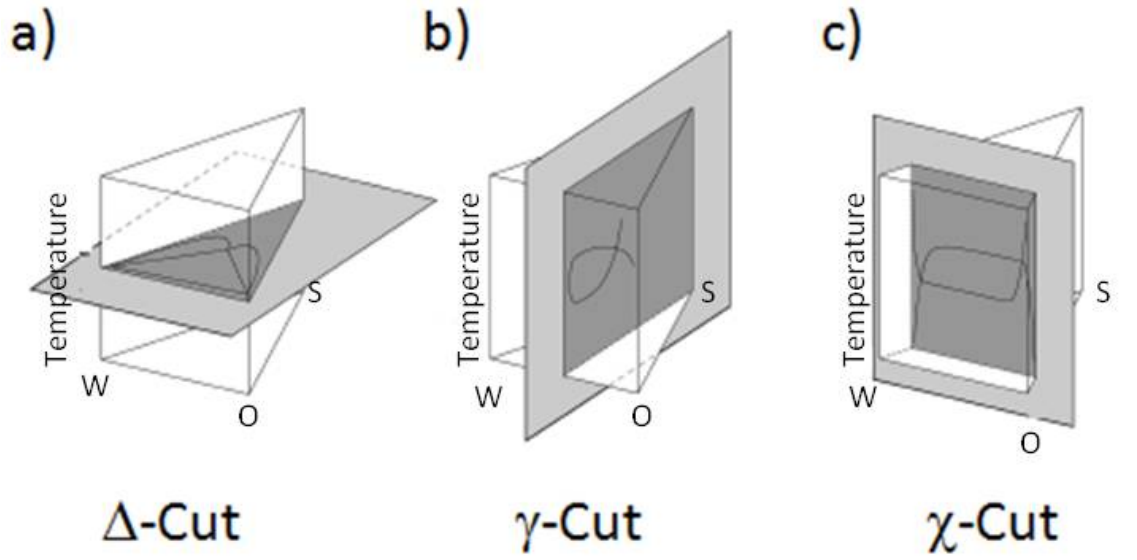

Figure I.6.: Illustration of a) the Δ-Cut, b) γ-Cut and c) χ-Cut. Redrawn from [59].

($WinsorIV$) is $\bar{\gamma}$. The corresponding temperature is $\bar{T}$, the so called phase inversion temperature (PIT).

χ-Cut

The last possibility is named χ-Cut. In this cut, the surfactant concentration γ is constant and the oil-to-water ratio α is a function of the temperature. It is the most appropriate way to locate the boundary between the o/w and w/o systems of microemulsions.

Figure I.6 shows an illustration of the above mentioned cuts.

I.3. Surfactant-less Microemulsions

I.3.1. The Beginnings

The concept of surfactant-less microemulsions has been known for a long time. Already in 1976 the group of Barden initiated a series of investigations to determine

the effect of an interfacial environment on the properties of metal-ligand complexes [60]. In this work the system water/hexane was used with hexadecyl-trimethyl-ammonium perchlorate as surfactant and 2-propanol as cosurfactant. The aim was to characterise the system in absence of metals and ligands. Already the ternary system water/2-propanol/hexane showed an area which had properties typical of microemulsions [61]. For a better understanding of this phenomenon in their following work the ternary diagram was screened with the help of ultracentrifugation and conductivity experiments. The obtained phase diagram is shown in Figure I.7 a). They were able to divide the single phase area of the phase diagram into five regions. Region A included turbid compositions which were refered to unstable macroemulsions. Region B was a transparent, stable oil-continuous microemulsion. In region C small aggregates of water and 2-propanol were present and region D is composed of a ternary solution. The fifth region E was described as a "metastable" microemulsion. It should be noted that this last region was no longer mentioned in the following articles. The way of characterising the different regions will be shown in Section I.3.2. In the same work, the influence of different alcohols on the single phase region was examined. They found that within a series of alcohols of the same carbon number, the formation of a microemulsion requires larger volumes of the branched alcohols than of the straight ones in the presence of hexadecyl-trimethyl-ammonium bromide. Further, monofunctional alcohols containing more than seven carbon atoms do not form microemulsions. The obtained data sets confirmed the trend found by other groups [62, 63]. Moreover, the addition of a surfactant, in their case hexadecylammonium perchlorate, does not lead to a significant change of the phase diagram (see Figure I.7 b)). So, not the surfactant but the cosurfactant was in charge of the structure in the system.

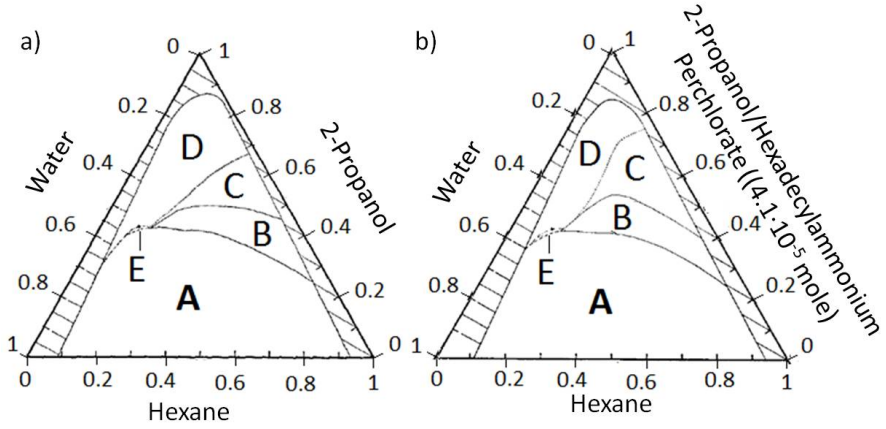

Figure I.7.: a) Ternary phase diagram for the ternary system water/2-propanol/hexane. The compositions are in mole fractions. The meaning of the several regions A-E is explained in the text. b) To the same system hexadecyl-trimethyl-ammonium perchlorate was added as surfactant. The figures are taken from [61].

For the interpretation of the obtained data the model of Prince was used [66, 67]. According to this model a microemulsion will form when the interfacial tension γ_i in the system becomes equal to zero:

$$\gamma_i = (\gamma_{o/w})_a - \pi \tag{I.3}$$

with $(\gamma_{o/w})_a$ as the oil/water interfacial tension in the presence of alcohol and π as two-dimensional pressure within the film which encapsulates a suspended droplet. In this theory the infinite miscibility of the alcohol in both phases is indispensable. This is the case for 2-propanol in the system water/hexane. Only alcohols fulfilling this requirement can reduce $(\gamma_{o/w})_a$ to very low values, because the partitioning of the alcohol will significantly decrease the difference in chemical potential between those two phases.

In a following work Keiser *et al.* investigated the same system (water/2-propanol/ hexane) with NMR measurements (results are shown in Section I.3.2) and the influence of added sodium chloride on the phase behaviour [64]. For the determination

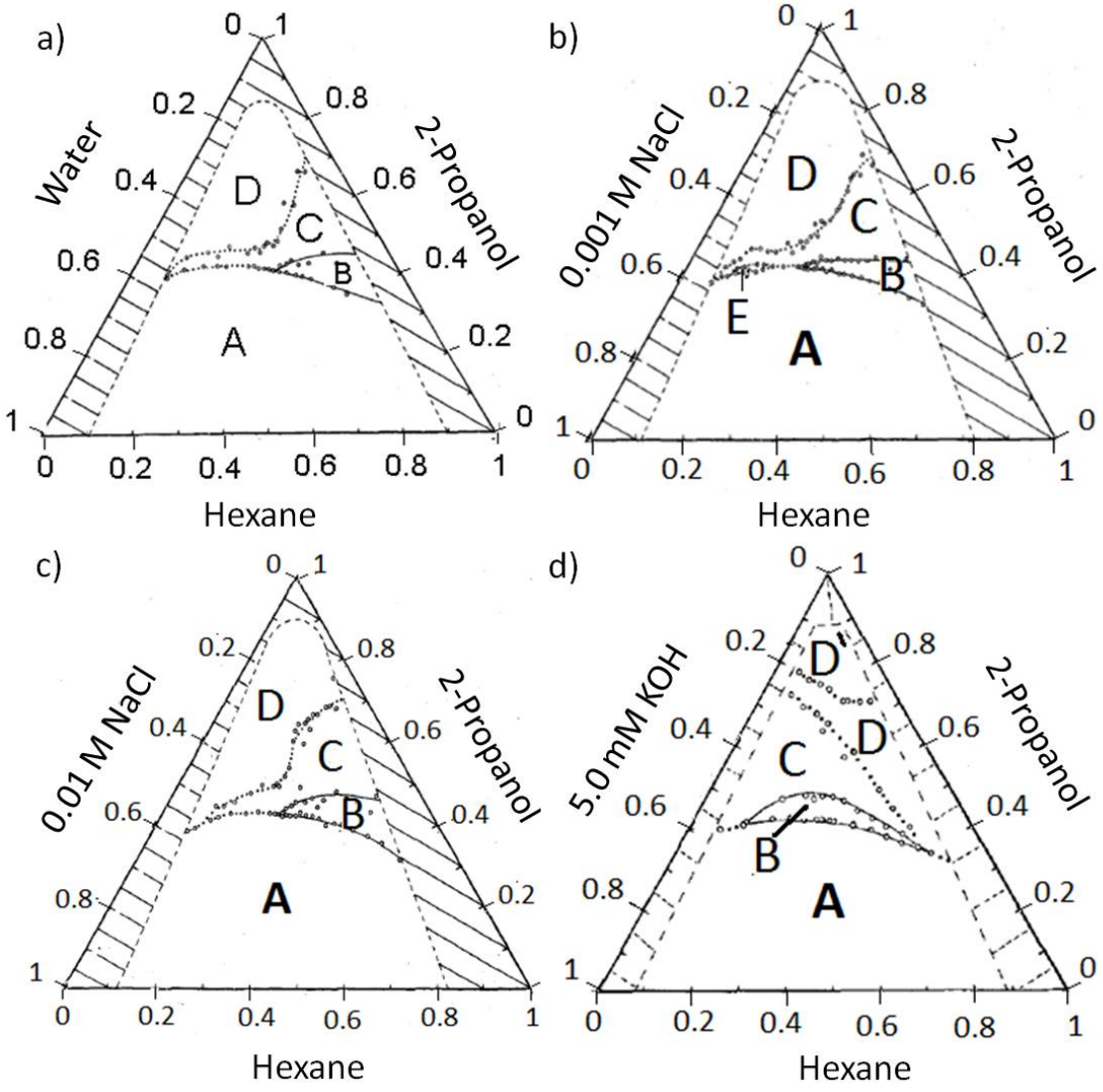

Figure I.8.: a) Ternary phase diagram for the ternary system water/2-propanol/hexane. The compositions are in mole fractions. The meaning of the several regions A-E are explained in the text. Compared to Figure I.7, slight changes in the phase behaviour were observed [64]. b) Sodium chloride was added, in this diagram 0.001 M and in c) 0.01 M. d) Also the influence of KOH (5 mM) was investigated. The figures are taken from [64, 65].

of the different regions within the ternary phase diagram again ultracentrifugation and conductivity measurements were used. For the effect of sodium chloride two phase diagrams were investigated with 0.001 M and 0.01 M of sodium chloride. The diagrams are shown in Figure I.7 c) and d). As a resume, the replacement of water by sodium chloride solutions results in an increase of region B and a decrease in C. The destabilisation of the small aggregates of water and 2-propanol in region C can be explained with the interruption of the H-bonding network due to sodium chloride. This effect of salt addition and the disruption of H-bonds has been already discussed by Schooley and Alder [68]. The stabilisation of region B was not so obvious. In the explanation of Keiser, again the model of Prince and the partition of the alcohol between the two solvents played an important role. Water is gradually transferred from the dispersed water droplets into the continuous oil-phase. H-bonding with 2-propanol will occur followed by a redistribution of the water into the droplet. With sodium chloride in the system the H-bonding will be disrupted. The transfer of water from the droplet to the oil phase is slowed down which causes a stabilisation of the microemulsion. In contrast to sodium chloride, potassium hydroxide shows a totally different behaviour [65]. The influence of potassium hydroxide was investigated in the case of microemulsions as reaction media. A closer look will be given in Section I.3.3. Here, only the difference in phase behaviour should be mentioned. Thus, sodium chloride increases region B and decreases C, for potassium hydroxide its vice versa (see Figure I.7). The critical effect of the hydroxide ions compared to chloride is the possibility to take part in the H-bond network. The explanation for the destabilisation of region C with sodium chloride is in this case the reason for the stabilisation with potassium hydroxide (the same counts for region B).

In another series of studies, the phase behaviour of the pseudo-ternary systems alcohol/hydrocarbon/brine was examined [63, 69, 70]. Again, the single phase areas were

similar to those observed with surfactants. Also the determined interfacial tensions of these systems were comparable to systems with surfactant-based microemulsion systems.

In 1981, Lara *et al.* examined the ternary system water/2-propanol/benzene with heat capacity measurements. Due to their results, the formation of systems similar to microemulsions were proposed. Also a bicontinuous structure could be suggested [71].

So, already in the late 1970s several groups independently from each other found the presence of structures similar to microemulsion in surfactant-free systems. But surprisingly, no further work was done to investigate such systems more into detail.

In the next section the different experimental ways are explained how the structures of surfactant-less microemulsions were determined so far and the particular results are discussed.

I.3.2. The Techniques

Conductivity measurements

Conductivity experiments are a very easy method to screen a large area in a ternary phase diagram. This was very often the method of choice, in addition with others, to distinguish the different regions [61, 64, 65, 72, 73]. In Figure I.9 representative evolutions of the conductivity as function of the 2-propanol content are shown with water and hexane. In these graphs, three different parts can be seen which can be attributed to the four regions. In the case of 2-propanol addition, the starting points of the curves are the amount of 2-propanol needed to produce a clear solution. With the addition of alcohol a linear increase of conductivity appears until point α. With

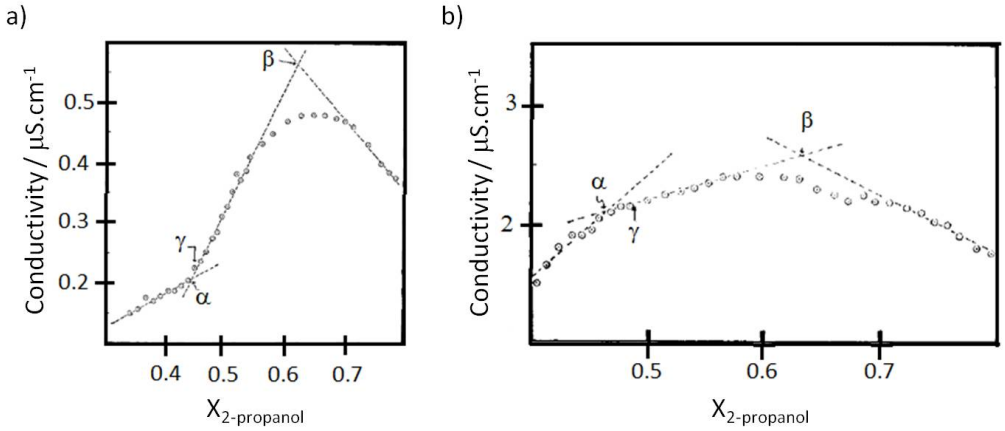

Figure I.9.: Conductivity curves as function of 2-propanol of the system water/2-propanol/ hexane a) with 10 mL hexane and 0.4 mL water and b) 10 mL hexane and 1.0 mL water. Point γ represents the transition point from region B to C determined with ultracentrifugation measurements. α is the transition point B to C and β C to D.

increasing amount of alcohol, the amount of dispersed water in the oil-continuous phase increases as well. This results in a rise in conductivity. Point α fits very well with the transition point γ of region B to C derived from ultracentrifugation experiments. Beyond point α, conductivity still increases linearly but with a different slope. By addition of alcohol, the size of the formed aggregates decreases, which results in an increase of conductivity. At a certain amount of alcohol a maximum is reached. After this point conductivity linearly decreases. The curve beyond point α can be divided into two linear parts. By plotting two straight lines through these parts one can extrapolate a crossing point β close to the maximum of the curve. This point was attributed to the transition of region C to D. At point β a ternary solution occurs which will be diluted with further addition of alcohol. This results in the decrease of conductivity. Similar results from conductivity measurements were obtained by Lund and Holt [72]. In their study, the ternary system water/ 2-propanol/toluene was investigated. They were able to determine the same regions using this technique in combination with ultracentrifugation experiments. Nevertheless, differences in the evolution of conductivity as function of alcohol content were

observed with the addition of salts. When hexadecyltrimethyl perchlorate was used additionally, the only influence on conductivity was a shift of the curve to higher values due to the presence of charged particles [60]. The same counts for sodium chloride [65].

Ultracentrifugation experiments

As already mentioned above, a combination of conductivity and ultracentrifugation experiments were typically used to determine the different regions in the ternary phase diagram of water/2-propanol/hexane [61, 64, 65, 72, 74]. In region B the sedimentation of water-rich droplets was observed, whereas in regions C and D no water droplets were included. Very often a water-soluble dye was added (e.g. Rhodamine 6G [60] or Rhodamine B [74]). In these centrifugation experiments a gradual distribution of the colour was observed. The solutions were less coloured at the top and more at the bottom of the cell, in the case of region B. In contrast, samples within regions C and D showed a uniform distribution of the dye after the same experimental treatment. Khmelinsky *et al.* were the first deriving a radius of the water-rich droplets with this technique [74]. They found an approximate radius of 1 nm with an accuracy of $\pm$ 5%. Moreover, it was possible to obtain the density of the droplets (ρ_d). Comparing these densities with the ones of water/2-propanol mixtures, a volume fraction of 0.2 of 2-propanol in the droplets was found. This corresponds to approximately 110-180 molecules of water and 20-30 molecules of 2-propanol in the droplets.

Nuclear Magnetic Resonance Spectroscopy

By using NMR measurements to investigate the nanostructure of the clear solutions, three variables are of great importance:

- Peak Width

- Chemical Shift
- Peak Shape.

Again, the focus was on the system water/2-propanol/hexane (Figure I.8). All discussed results were taken from ^{1}H-NMR measurements.

Peak Width

In Figure I.10 a) the half width at half height of the proton resonance of water and the hydroxyl and methine groups of 2-propanol are plotted as function of water content [64]. The starting point was in region D and the end point in region A crossing only region C. The hexane mole fraction was kept constant at 0.2. Two phenomena occurred: a broadening of the hydroxyl group of 2-propanol and water proton peaks and a narrowing of the methine group resonance. The shift to higher values implies a higher rate of proton exchange. The drop of the half width for the methine group can be explained due to a more rotational freedom in 2-propanol. This corresponds to a transition from an ordered (H-bond network) to a less ordered (macroemulsion) system. Another curve is obtained at conditions of constant mole fraction of water (0.1) (see Figure I.10 b)). Here the half peak widths have a maximum. These three maxima occur at the same mole fractions of alcohol as obtained with conductivity measurements for the transition points. The starting point of the experimental path in this case was region A, passing regions B and C and finishing in region D. Comparable results were found in the work of Lund and Holt [72] for the system water/2-propanol/toluene with ^{13}C-NMR measurements.

Chemical Shift

By investigating the evolution of the chemical shifts, a description of the environ-

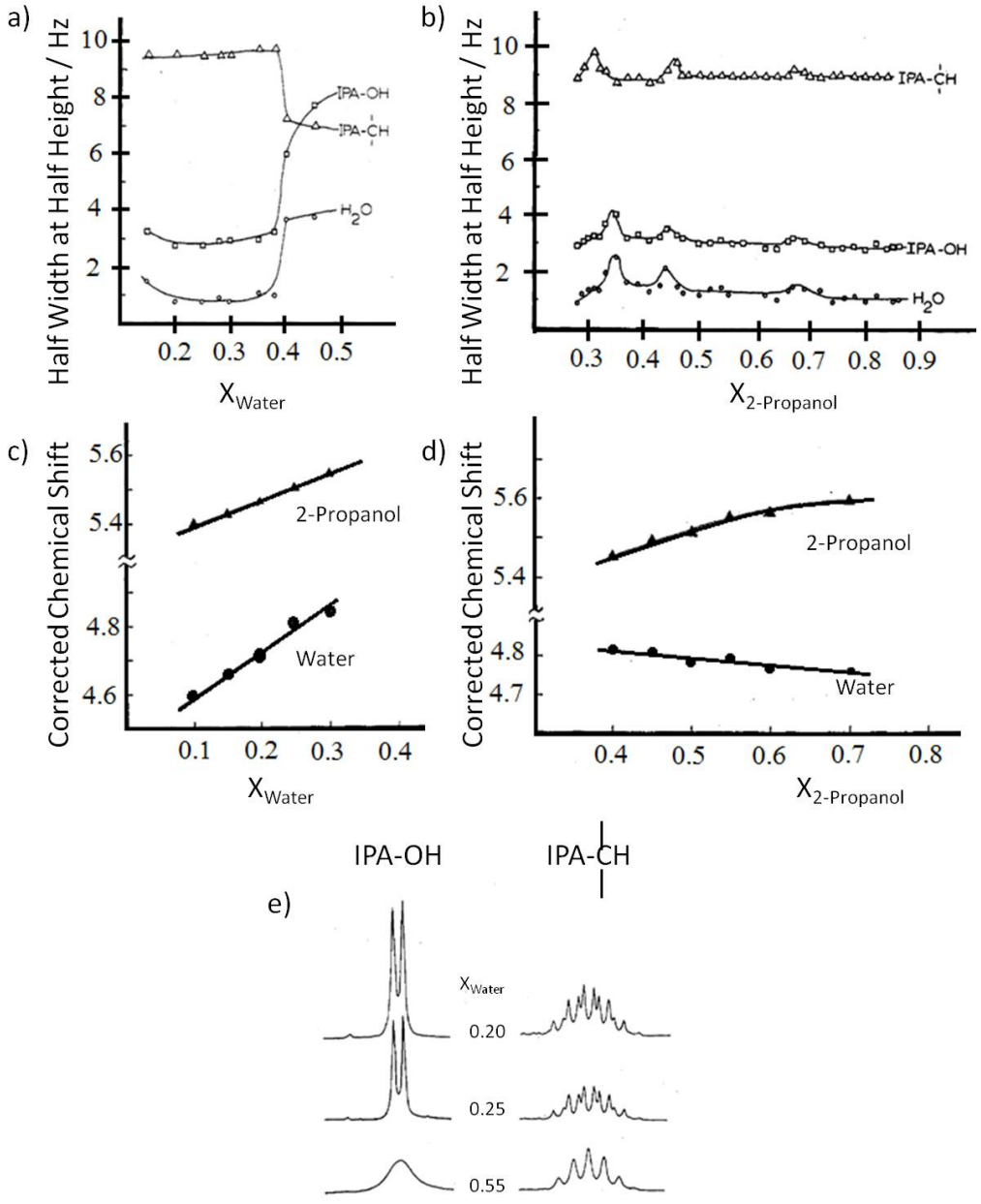

Figure I.10.: a) Half peak width as a function of mole fraction of water of the hydroxyl and methine group of 2-propanol and the water proton at a constant mole fraction of hexane of 0.2. b) Half peak width as a function of mole fraction of 2-propanol of the hydroxyl and methine group of 2-propanol and the water proton at a constant mole fraction of aqueous phase of 0.1 and 0.01 M of sodium chloride. c) Chemical shifts of the hydroxyl group of 2-propanol and water protons as function of the mole fractions of water at constant mole fraction of 2-propanol (0.5) and d) of 2-propanol at constant mole fraction of water (0.25). e) Changes in the proton signals of the hydroxyl and methine groups of 2-propanol with increasing amount of water. Figures are taken from [64].

ment of the protons can be given. An example of the interpretation of chemical shifts is given in Figure I.10 c) and d) for the system water/2-propanol/hexane. A downfield shift, as it can be seen for the hydroxyl group proton of 2-propanol and the water proton, was observed with increasing water content (Figure I.10 c)). This is due to a deshilding of the protons. In the case of water, more hydrogen bonds are built between the water molecules. Also the fraction of water 2-propanol hydrogen bonds increases. But the slope for the water protons is higher than for 2-propanol. The interpretation of Keiser *et al.* was that...

> *"...we may conclude that, at a constant mole fraction of 2-propanol, as the water content increases the "bulk" water character increases resulting in droplet size increases and more water-water interactions. At the same time, 2-propanol is being absorbed from the continuous phase into the interface to stabilise the droplet, bringing more alcohol into proximity with the water of the droplet and increasing the alcohol-water H bonding."*

In contrast, at constant water content and addition of 2-propanol, the behaviour of the change in chemical shift of these protons are different. The water proton is shifted upfield but the proton of the hydroxyl group is shifted downfield. In this case, the transition of water-rich droplets to aggregates bound via hydrogen bonds is observed. The amount of "bulk" water decreases, this results in a reduction of hydrogen bonds between water molecules, but the number of hydrogen bonds between water and 2-propanol increases (see Figure I.10 d)). In these experiments the overall trend of the phase behaviours can be seen and proof the concept of the present nanostructure. However, the transition points of the different regions can not be seen.

Peak Shape

As already described in the paragraph about chemical shifts, the peak shape delivers no information about the transition points but about the nanostructure in the system. In Figure I.10 e) the evolution of the hydroxyl and methine proton peak shape of 2-propanol with water addition is plotted. At the beginning, at low mole fraction of water, very distinct peaks can be seen, getting replaced by broader peaks at higher water concentration.

Light Scattering

Lund and Holt [72] were the first to estimate the "droplet" sizes in region B with DLS experiments in the system water/2-propanol/hexane. They found that the scattered light follows Rayleigh behaviour which indicates that the droplets have a radius of less than 1/15 of the incident light wavelength. Though it was not possible for them to perform meaningful particle size calculations because of the ternary nature of the system, rough estimation leads to a diameters range from a lower limit of 5 nm to an upper limit of 30 nm. Other DLS results dealing with surfactant-less microemulsions were presented by Drapeau *et al.* [75]. They investigated the system water/2-propanol/para-menthane-3,8-diol. Close to the phase separation boundary, significant auto-correlation functions were obtained and the calculated radius of the droplets was 10.5 nm.

Fluorescence Experiments

Khmelnitsky *et al.* adopted time-resolved fluorescence and fluorescence anisotropy decay studies to investigate the interior properties of these surfactant-free microemulsions [74]. The system was again water/2-propanol/hexane using Rhodamine B as probe molecule. From these measurements, on the one hand the microviscosities in-

side the droplets were obtained and on the other hand their polarities. By comparing the viscosities again with bulk mixtures of water and 2-propanol, a value of approximately 0.2 for the volume fraction of alcohol in the droplets was derived. This fits remarkably well with the value obtained from ultracentrifugation experiments (see Section I.3.2). From anisotropy decay experiments and the derived polarity a 2-propanol concentration between 60-70% was expected. This was explained by the fact, that the observed polarity in microemulsion droplets is known to be in many cases much lower than that of the liquid from which the droplets are formed.

Other fluorescence experiments were conducted by Zoumpaniot *et al.* [73]. With steady state fluorescence and fluorescence energy transfer techniques, they investigated the structural change in the system water/1-propanol/hexane containing enzymes. In these experiments, the protein tryptophan served as fluorescent spectral probe. In the first enzyme which was used (RmL) four tryptohan residues are present. In the "closed" formation of this enyzme only 15.1% of this residue are on the surface. Only in the "open" conformation this residue is completly exposed. In the second enzyme (CaL) five tryptophane residues are present, but only two of them are relatively close to the surface, whereas the other three residues are almost completely buried in the interior of the protein. This property makes the enzyme not sensitive to the microenvironmental changes. The fluorescence emission of this enzyme did not change with the addition of water. But an increase of emission was observed for RmL as the water content was increased. This indicates a change in the microenvironment of the fluorophore, indicating a higher polarity coming from an increase of the water barrier of the fluorophore. These results were conformed with fluorescence energy transfer experiments. The measurements were performed with PNA (cis-parinaric acid [9,11,13,15]-cis,trans,trans,cis-octadeca-tretaenoic acid) showing an overlap of its adsorption spectrum with the emission spectra of RmL. From these

experiments the donor-acceptor distance r was calculated as a function of water content. With increasing amount of water a slight increase of this r value was observed. This was explained with the occurrence of water microstructures in the organic phase. But, this increase is not as remarkable as it is for classic reversed microemulsions [76].

Electron Paramagnetic Resonance Spectroscopy

EPR is a technique to investigate the properties of interfaces due to the examination of the mobility of a EPR probe, here a fatty acid which is surface active, in the interface and the polarity of its microenvironment. In the studies of Zoumpaniot *et al.* in the ternary system water/1-propanol/hexane [73], this method was used to examine the interface of the aqueous phase and the organic solvent. A result of these experiments was that the mobility of the probe decreases with water addition. This indicates the formation of water droplets in the organic solvent. From EPR measurement the so called hyperfine coupling constant α_N can be obtained. This constant did not change with 1-propanol content at constant concentrations of water. This implies that 1-propanol is not located within the water-rich droplet and must be either in the interface or in the organic phase.

Freeze Fracture and Cryo-TEM

In a recent study by Xu *et al.*, the presence of the nanostructure in the ternary system water/1-propanol/oleic acid was confirmed with FF- and cryo-TEM images [77]. At first, the different nanostructures were determined with classical conductivity measurements described by Clausse [78]. The single phase area was divided into o/w, bicontinuous and w/o regions. In the w/o area as well as in the o/w region spherical droplets can be clearly observed. From these pictures a droplet radius of 20

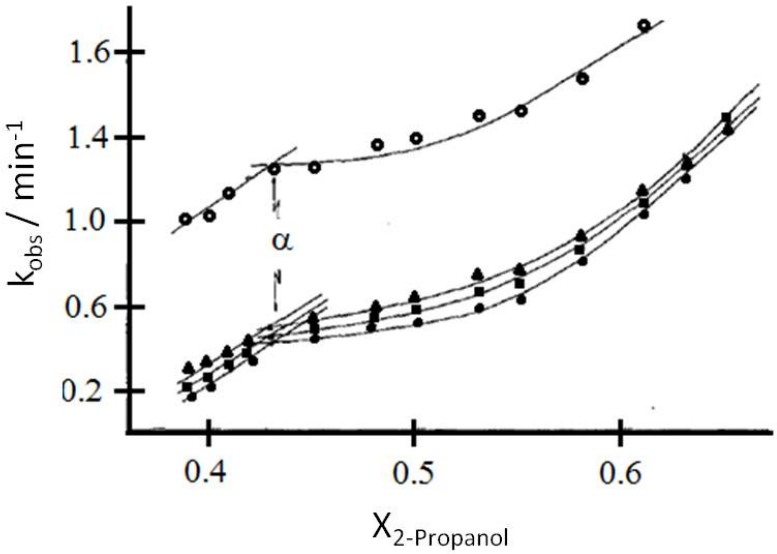

Figure I.11.: Plots of k_{obs} as function of 2-propanol mole fraction for p-nitrophenyl esters. Figure redrawn from [65].

nm in the o/w and approximately 7.5 nm in the w/o regions and in the bicontinuous area a network-like structure were obtained.

I.3.3. Reactions

Microemulsions are often used as reaction media, because they can solubilise both, ionic, water-soluble and organic, water-insoluble, reactants in a homogeneous reaction medium. The absence of a detergent is an advantage of the surfactant-less microemulsions. Usually, after a process the major problem is the removing of the surfactant from the reaction medium, when classic microemulsions are used. Thus, the isolation of a product is simpler in a system without surfactants. Several proposals can be found, where detergent-less microemulsions are applicable. One example is shown by Keiser *et al.*. In their work, the reaction rate of the basic hydrolysis of esters was investigated in the ternary system water(5 mM KOH)/2-propanol/hexane [65]. In Figure I.11 the obtained rate constant is plotted against the mole fraction of 2-propanol. The chosen experimental path started in region B, crossing region

C and ended in region D. In this diagram, two distinct zones can be distinguished. The transition point is denoted as α, which corresponds to the composition of the B/C boundary. In region B, a linear increase of k_{obs} with the addition of alcohol can be seen. At the beginning of region C, the rate constant remained more or less constant for a certain amount of 2-propanol. After a "threshold" was reached, k_{obs} increases rapidely. This correlates with the picture of large aggregates of water, 2-propanol, potassium and hydroxide ions that break up into individual ions at higher 2-propanol concentration. The reaction yield was in regions B and C approximately 98%.

Another example of reactions in surfactant-less microemulsions is the incorporation of Copper(II) into meso-Tetraphenylporphine ((TPP)H_2) [79]. Cupper (II) is soluble in aqueous solutions, whereas (TPP)H_2 in organic solvents. The used system was water/2-propanol/toluene. Additionally, in some experiments surfactants were added. Depending on the counterion, either no significant change in reactivity was found, or a behaviour as observed in "nonorganized" systems.

Further, relevant studies were the use of enzymes in such systems. This is of great importance, because the considered enzymes need interfaces. So the measurement of an enzyme activity could also refer to a detection method of the overall structure in surfactant-less systems. One of the first works on detergent-less microemulsions and their use in enzymatic reactions was presented by Khmelnitsky *et al.* [74, 80, 81]. They found that the maximum of enzyme activity is within region B, so the microemulsion area. Other works concerning the use of enzymes were made by O´Connor *et al.* [82]. The most astonishing result was that the enzyme retained its catalytic activity in region B with a water concentration less than two volume percent. But, in homogeneous mixtures of water and oil with such a low water

content, enzymes would usually become inactive.

Other works in the field of enzymatic reactions, which should be mentioned, were presented by Vulfson *et al.* [83] and Zoumpanioti *et al.* [73, 84].

I.3.4. State-of-the-Art

The research on surfactant-less microemulsions was more or less restricted to the studies mentioned above. Though, the concept is known now for almost 35 years, only few articles are available and the real structure and the mechanism of the formation of these regions is not well explained. Nevertheless, recent articles deal again with this phenomenon and try to give a reasonable explanation [75, 77, 85–88].

Pfennig and Schott presented a work concerning mass-transfer induced instabilities at liquid–liquid interfaces. With computer simulations they described the formation of nano-droplets in the close vicinity of the interface induced by mass transfer across these interfaces [85]. In the simulation they found areas in a ternary system where stable nano-droplets were formed or only fluctuations exist.

I.4. Ouzo-Effect

Though, the principle of surfactant-less microemulsions has already been known for 35 years, it was not forwarded to understand the mechanism behind. But, in the last 10 years another phenomenon was intesively examined which is related to it. The so called "ouzo-effect" [89–93]. Vitale and Katz were the first, who discovered the dispersion of liquid droplets by homogeneous liquid-liquid nucleation in the metastable spinodal decomposition region of a ternary phase diagram [89]. They termed this phenomenon "ouzo-effect" in relation to the Greek alcoholic beverage ouzo. By ad-

dition of water to ouzo, the anis oil dissolved in the ouzo forms spontaneously small oil droplets, which cause the drink to appear milky. Though, such emulsification processes have already been reported earlier [94, 95], Vitale and Katz were the first to analyse this effect in detail. The formation of these fine and time-stable emulsions occurs, when water is added above a certain concentration to a mixture of cosolvent and oil (for example divinyl benzen (DVB) [89], anethanol [90–92], polymethylmethacrylate (PMMA) [96]). The necessary condition for this phenomenon is the rapid addition of water (or any other solvent) to the mixture of cosolvent and oil. As already seen in the chapter of surfactant-less microemulsions, another condition is the different solubilities of the components. The cosolvent has to be soluble in the other two solvents, whereas the others must be insoluble in each other. These two conditions are necessary for the solution to be supersaturated in the components. If the supersaturation is high enough, homogeneous nucleation takes place. At first, local concentration fluctuations occur which are the starting point of spontanously formed nuclei. Around each nucleus there are not sufficient solute molecules left. So, further nucleation will take place as far as possible from already existing nuclei. A hint of this mechanism was the uniform distribution of the obtained droplets, which is expected by homogeneous nucleation [89]. Further growth of the particles seems to take place only due to Ostwald ripening [91]. After this growth, the size of the droplets remains more or less constant at approximately 1-4 μm [89–91]. There are some other important conditions for the long-time stability of the formed emulsion. Vitale and Katz used DVB as oil phase, because it has approximately the same density as water. If there is a great discrepancy, either creaming (lower density) or sedimentation (higher density) will occur [89]. Moreover, the partition of the cosolvent has an effect on the stability as well. Cosolvents which partition into the oil droplets will have an influence on the density within these droplets and the dropelts will be larger. This will accelerate creaming or sedimentation as well.

I.5. Characterisation Methods of Microemulsion

I.5.1. Conductivity

Water molecules of o/w microemulsion are concentrated in the continuous phase, whereas surfactant molecules are localised at the surface of micelles and oil molecules at the inner of the micelles. With the use of ionic surfactants, counter ions are present as well, which can be found exclusively in the water-rich domain. In this case, surfactant and oil molecules can move only in a constricted area. Water and counter ions can more or less move via the whole extension of the liquid. Due to their larger size, micelles move much slower than single molecules. So the diffusion coefficient of the molecules within the continuous phase will be much higher than the one of the micelle. In w/o microemulsions water plays the part of the oil and vice versa and so the diffusion coefficients of the species are reversed as well. Between these two states a gradual transition takes place. At this stage, the bicontinuous phase, the diffusion coefficient of the surfactant molecules has its maximum value because the interface extends over the whole space. So the knowledge of the diffusion coefficient gives deep insight in the nanostructure of the microemulsion. In principle, self-diffusion coefficients can only be determined with NMR relaxation experiments.

But, the diffusion coefficient is directly linked to the conductivity of an electrolyte in solution. So, the measurement of electrical conductivity is an adequate method to determine the nanostructure and the film rigidity of a microemulsion, especially with ionic surfactants and water as polar phase. Two phenomena can be distinguished: Anti-percolative and percolative behaviour. Systems with a flexible interfacial film show typically bell-shaped evolution of the specific conductivity κ with increasing amount of water (see Figure I.12). At the beginning of the curve a non-linear increase of κ can be observed, which converts to a linear one at point M_1. At M_2 the slope of the curve decreases and reaches a maximum at M_3. Afterwards the

conductivity decreases again in a non-linear way.

The first interpretations of the drastic conductivity increase with water addition were made by Lagues *et al.* [97, 98]. Starting from a w/o microemulsion, κ is close to zero. Only few water droplets are present but not enough for an exchange of charge. The system is an isolator. Due to the brownian motion the inverse micelles can collide to a certain extent. At a certain volume fraction of water the conductivity rises continuously up to a certain point, the percolation threshold ϕ_P [99]. At values below ϕ_P the water droplets start to form clusters that come sufficiently close to each other so that an undisturbed transport of charge carriers over the whole sample can take place. At ϕ_P, the first time an infinite path appears through the system which allows an unhindered flow of charge. For a three-dimensional system with spheres in a continuum the theoretical ϕ_P is 0.31 [100]. For infinite conducting spheres in an isolator κ, for regions $\phi \leq \phi^P$, can be written as

$$\kappa \propto (\phi^P - \phi)^{-s} \tag{I.4}$$

and for regions $\phi \geq \phi^P$

$$\kappa \propto (\phi - \phi^P)^t. \tag{I.5}$$

Here, s and t are critical exponents. They are independent of the composition of the systems, but characteristic for the dimensionality of the percolation [100]. After the percolation threshold is overcome, more and more channels are formed which are connected via side-channels. According to the "theory of the effective medium" κ is

$$\kappa \propto (\phi - \phi^c). \tag{I.6}$$

ϕ^c is the critical volume fraction which should be $\frac{1}{3}$ in theory. At higher water contents a maximum is reached followed by a decrease of the conductivity due to

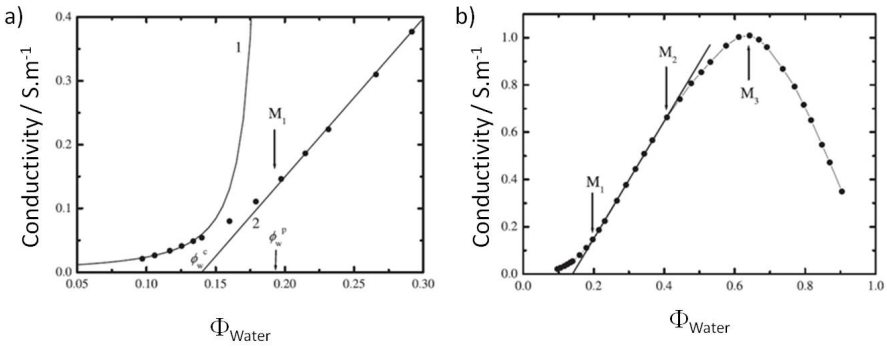

Figure I.12.: a) Magnification of the area of the percolation threshold. Curve shows the characteristic law of the aggregation of particles of an ideal conductor in a nonconducting medium with approaching the percolation threshold ϕ^P, according to equation I.4. Curve 2 corresponds to the theory of the effective medium, see equation I.6. b) Specific conductivity κ of a microemulsion system as function of the volume fraction of water.

dilution effects indicating the formation of an o/w system. Around the inflexion point bicontinuous structures appear. In contrast to this percolative behaviour, anti-percolative systems show a complete different evolution of the κ value. The rigid interface prevents the droplets to merge and so the values of κ are usually very low.

I.5.2. Light Scattering

Light scattering experiments are commonly used methods to characterise colloids in solution. The effect of scatterd light has already been known since 1868 and was mentioned by Tyndall in 1871 in literature. Farady and Tyndall observed bluish scattered light by irradiating a gold brine with polychromatic light. The Farady-Tyndall effect was and is a powerful method to characterise colloids. Besides colloid particles with a diameter of only few nanometers, polymers, macromolecules and micelles can be investigated. One of the first light scattering theories was introduced by Lord Rayleigh in 1871. He stated that the light scattering occures when irradiated light induces an oscillation of the electrons of the outer atomic shell.

There are different theories of light scattering depending on the wavelength of the incident beam and the size of the origin of the scattering (Compon-, Rayleigh, Mie-, Brillouin-, and Raman-Theory). Only the most important for this work, Rayleigh Theory, should be shortly mentioned.

I.5.2.1. Rayleigh Scattering

The elastic scattering of light at molecules with the size of $\frac{1}{1000}$ to $\frac{1}{20}$ of the wavelength of the incident beam is called Rayleigh scattering. During this process, the wavelength does not change. The intensity I is the non-polarised light, scattered at small particles with a diameter d, is

$$I = I_0 \cdot \frac{1 + cos^2\theta}{2 \cdot R^2} \cdot (\frac{2\pi}{\lambda})^4 \cdot (\frac{n^2 - 1}{n^2 + 2})^4 \cdot (\frac{d}{2})^6. \tag{I.7}$$

I_0 is the intensity of the incident light, θ the scattering angle, R the distance of the particles and n the refractive index. The intensity of the scattered light can be increased by increasing the wavelength, but as shown by the term $(\frac{d}{2})^6$ big particles scatter one to the power of times more. So scattered light of small particles can be easily suppressed by the scattered light of bigger ones.

I.5.2.2. Dynamic Light Scattering

Dynamic light scattering (DLS) (also known as photon correlation spectroscopy (PCS) or quasi-elastic light scattering (QELS)) is a powerful technique to measure in situ the size of particles. DLS is a standard routine widely used in colloid and polymer laboratories, where it is applied for the characterisation of particles as well as to study the nature of interactions of molecules and particles in liquid dispersions. Usually, particles in the sub-micron size range can be measured. DLS counts to the so called "hydrodynamic" experiments because only hydrodynamic quantities like the translational diffusion coefficient can be measured. The obtained diffusion

coefficient can be transformed into information about the hydrodynamic radius R_h. This relation is described with the Stokes-Einstein equation:

$$R_h = \frac{k_B \cdot T}{6 \cdot \pi \cdot \eta \cdot D} \tag{I.8}$$

k_B is the Boltzmann constant, T the absolute temperature, η the dispersant viscosity and D the diffusion coefficient. The obtained radius contains the hydration shell of the molecule. One of the greates problems of DLS is to distinguish spherical and non-spherical particles. Due to equation I.8 non-spherical particles are treated as spherical ones. If the change of the shape has any influence on the diffusion speed, the hydrodynamic diameter will change as well. For example the sphere-to-rod transition of micelles. Small changes in the length of a rod-like particle has a great impact on the calculated size, but changes in the rod's diameter, which hardly affects the diffusion speed, is difficult to detect.

DLS measures time-dependent fluctuations in the scattering intensity arising from particles undergoing Brownian motion [101–103]. These fluctuations in the intensity of the scattered light can be analysed with an autocorrelator.

In general, a correlator is an apparaturs comparing signals. It measures the degree of similarity between two signals or one signal with itself at varying time intervals. If the intensity of a signal for a randomly fluctuating signal is compared with itself at a time t_0 and t_1, there will be no correlation between these signals. This is true for any random process, like diffusion of particles in solution. But, if the intensity of a singal at t_0 is compared to the intensity $t_0 + \tau$, whereas τ is the sample time of the correlator in ns or μs, there will be a strong correlation between these intensities. At a point $t_0 + 2\tau$, there is still a reasonable correlation, but not as good as before. The correlation reduces with time. The signal compared to

itself at t_0 has a perfect correlation as the signals are identical. Such behaviour is expressed by 1.0 and no correlation is indicated with 0.0. The correlation decreases with $t_0 + 2\tau$, $t_0 + 3\tau$, $t_0 + 4\tau$, etc. until no correlation can be seen any more at t_∞. The evolution of the correlation with time depends on the particle size present in solution. This dependency of time is plotted in a so called correlogram and the function of time is called auto-correlation function. These correlograms comprehend a lot of informations concering particle size and polydispersity. For small particles, the decrease will occur earlier or faster then for large particles. A steep decay of the function indicates monodisperse samples, whereas the more extend the decay the greater the polydispersity. The correlation function, g^2, declines exponentially depending on the diffusion coefficient [101–103]. The auto-correlation function can be written as

$$g^2(\tau) = \langle I(t) \cdot I(t+\tau) \rangle \tag{I.9}$$

with the intensity signal $I(t)$ and the function of the delay time $I(t+\tau)$. The normalised form is

$$g^2(\tau) = \frac{\langle I(t) \cdot I(t+\tau) \rangle}{\langle |I|^2 \rangle}. \tag{I.10}$$

From the particle's correlation curve the diffusion coefficient can be measured indirectly. Since the signal statistics is Gaussian, the Siegert relation holds for the auto-correlation function and gives a correlation between g^2 and g^1 [104]:

$$g^2 = a_0 + a_1 \cdot (\left|g^1(\tau)\right|)^2 \tag{I.11}$$

a_0 and a_1 are experimental constants. $g^1(\tau)$ is the auto-correlation function of the electric field and can be written as

$$g^1(\tau) = \int_0^\infty c(a_2) \cdot \exp(-a_2 \cdot \tau) da_2. \tag{I.12}$$

$c(a_2)$ is the normalised intensity weighted distribution function of decay rates. a_2 is the decay rate which can be expressed as

$$a_2 = D \cdot q^2 \tag{I.13}$$

with D as translational diffusion coefficient and q as scattering vector. q is defined as

$$q = \frac{4\pi n}{\lambda} \cdot sin\frac{\theta}{2}. \tag{I.14}$$

In this equation n is the refractive index of the dispersant, λ the wavelength of the laser and θ the scattering angle. In the case of monodisperse samples $g^1(\tau)$ can be expressed as a simple exponential function which decreases with a single decay constant:

$$g^1(\tau) = \exp(-q^2 \cdot D \cdot \tau) \tag{I.15}$$

For polydisperse samples $g^2(\tau)$ is the sum of all exponential declines contained in the correlation function [105]. There are common approaches to extract the size distribution. First, non-trivial Laplace transformations of $g^1(\tau)$ can be performed. Several approximate solutions have been proposed such as exponential sampling, non-negatively constrained least squares (NNLS) [106], CONTIN [107], etc. Second, a rough estimation of size distribition can be made to adjust the variables to get the best fit to the experimental data. This often gives ambiguous results, given ill-conceived initial assumptions. Third, the method of cumulants can be used [108]. With the cumulants analysis a single exponential is fitted to the correlation function. Actually, the cumulants analysis means a polynomial to the logarithm of the correlation function g^1:

$$ln(g^1) = a + b\tau + c\tau^2 + d\tau^3 + e\tau^4 + ... \tag{I.16}$$

Value b is known as second order cumulant or z-average. The z-average is an intensity mean. It is neither correlated to mass nor to number mean because it is calculated from the signal intensity. Only the first three terms a, b, c are used in the standard analysis in order to avoid over-resolving the data. The coefficient of the squared term c, when scaled as $\frac{2c}{b^2}$, is known as the polydispersity or polydispersity index (PDI). For very poor or noisy data, when the count rate is low or when very small particles are present, it may be useful to choose fewer points to fit. In this case a second order fit might be preferred as it is difficult to get a reliable second moment here. The following equation is used traditionally in cumulants analysis

$$ln(g^1(\tau)) = \ln(B) - a_2 \cdot \tau + \frac{\mu_2}{2} \cdot \tau^2. \tag{I.17}$$

B is the back ground and μ the variance. The ratio of variance to the square of the mean is a measure of the polydispersity of the diffusion coefficient and this is very often represented as PDI.

Chapter II.

II Experimental

II.1. Chemicals

Chemicals used in Section III.1.1

Sodium dodecylsulfate (purity≥99.0%), 1-pentanol (≥98%) and R-(+)-limonene (≥94%) were purchased from Merck KGaA (Darmstadt, Germany). The FAME-rapeseed biodiesel and the TBK rapeseed biodiesel were generous gifts respectively of Tecosol (Ochsenfurt, Germany) and Mr. János Thész (Hungary), and the FAME-cuphea biodiesel was kindly prepared for us by Dr. Gerhard Knothe from the National Center for Agricultural Utilization Research (Peoria, Illinois, USA). Rapeseed oil was purchased from VOG AG (Linz, Austria).

Chemicals used in Section III.1.2

All dibasic esters were purchased from Sigma Aldrich (Steinheim, Germany) and have the following purities: DMS 98%, DES≥99%, DMG99%, DEG≥99%, DMA≥ 99% and DEA99%. Sodium oleate (≥82%) and 1,5-pentanediol (≥97%) were also purchased from Sigma-Aldrich (Steinheim, Germany), ethanol (≥99.9%) from Baker (Deventer, Netherlands), sodium dodecylsulphate (ultrapure) from AppliChem (Darmstadt, Germany) and 1-pentanol (≥98%) from Merck (Hohenbrunn, Germany).

Chemicals used in Section III.1.3 R-(+)-limonene (≥94%)and citronellol (≥97%) were purchased from Merck (Hohenbrunn, Germany). Sodium oleate (≥82%) was purchased from Sigma-Aldrich Chemie GmbH (Steinheim, Germany) and ethanol (≥99.9%) from Baker (Deventer, Netherlands).

Chemicals used in Section III.1.4

Sodium oleate (purity≥82%), 1-heptanol (≥98%) and 1-dodecanol (≥98%) were purchased from Sigma-Aldrich Chemie GmbH (Steinheim, Germany), ethanol (purity≥ 99.9%) from Baker (Deventer, Netherlands), and 1-pentanol (purity≥98%) from Merck KGaA (Darmstadt, Germany). The FAME-rapeseed biodiesel was a generous gift of Tecosol (Ochsenfurt, Germany). Isofol®12, 14T, 16 and 20P were obtained by Sasol Germany GmbH (Hamburg, Germany). The alcohol compositions of these four chemicals are: Isofol 12 (≥97% 2-Butyloctanol), 14T (10-20% 2-Butyloctanol, a mix of 45-55% 2-Butyldecanol and 2-Hexyloctanol, and 25-35% 2-Hexyldecanol), 16 (≥97% 2-Hexyldecanol), and 20P (≥97% 2-Octyldodecanol).

Chemicals used in Section III.2.1 and III.2.2

Ethanol (≥99.9%) was purchased from Baker (Deventer, Netherlands), n-octanol (≥99%) and n-hexanol (≥99%) from Merck (Hohenbrunn, Germany) and Disperse Red 13 (DR-13, dye content95%) from Sigma-Aldrich (Steinheim, Germany).

Chemicals used in Section III.2.3

Ethyl lactate (98%), γ-valerolactone (99%), and Disperse Red 13 (DR-13, dye content 95%) were provided from Sigma-Aldrich (Steinheim, Germany). Ethanol (≥ 99.9%) was purchased from Baker (Deventer, Netherlands) and benzyl alcohol (≥

99%) from Merck (Hohenbrunn, Germany).

All chemicals were used without further purification. All solutions and microemulsions were prepared using water with a resistivity of 18 MΩ.cm.

II.2. Methodes

II.2.1. Phase diagrams

Pseudo-ternary phase diagrams (PTPDs) were established by using a dynamic and static process according to Clausse *et al.* [78]. An illustration of such a PTPD is shown in Figure II.1 a). In screwable tubes blends of the emulsifying agents (surfactants, cosurfactants and cosolvents) were filled in appropriate proportions and melted with oil or water at various weight ratios to obtain a starting weight of 3 g. Water (oil) was successively added with Eppendorf pipettes until a change in the phase occurred. Further to microemulsions, liquid crystalline (LC) phases, "classical" emulsions and homogeneous solutions in equilibrium with undissolved surfactant were observed. The phase transitions were determined with the naked eye and through cross polarized filters in order to differentiate between LC and microemulsion phases. Between polarizing filters most of the liquid crystalline phases appear birefringent. The weight fractions of water and oil at which transparency-to-turbidity occurred were derived from precise weight measurements. The composition of the solution was then calculated from the masses of all components. It was estimated that the accuracy of the measurements for the transparency-to-turbidity transition was better than 2wt%. The temperature was kept constant at 25 °C with a temperature controlled test tube rack. In pseudo-ternary systems the surfactant-to-cosurfactant mass ration is called ζ. The mass fraction of the surfactant/cosurfaction mixture-to-oil ($R_{S/O}$) is defined as

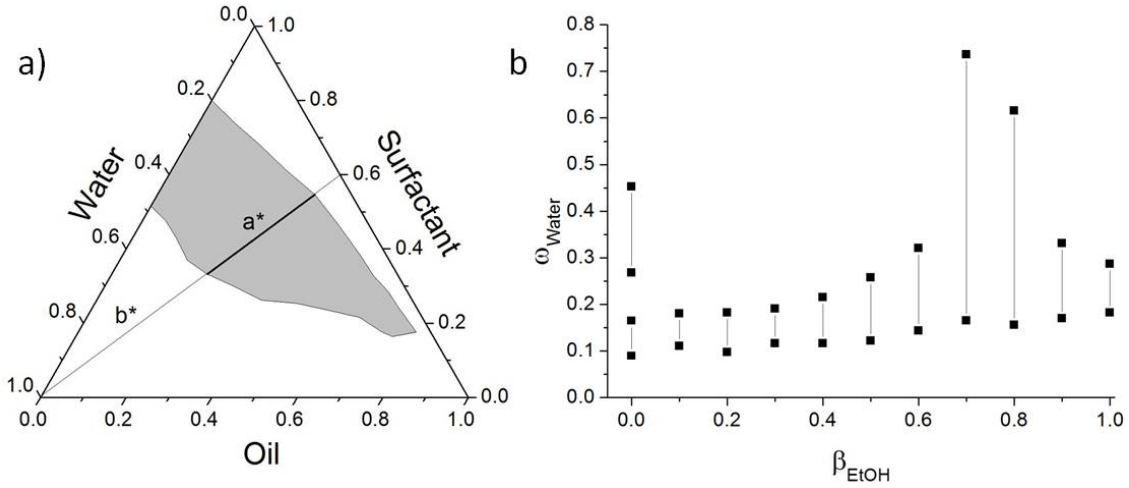

Figure II.1.: a) Illlustration of a ternary phase diagram composed of water/oil/surfactant. Line b* is the experimental path where the solubilisation experiments with the different co-surfactants were carried out. Line a* represents the part of path b* being within the single phase area. $R_{S/O}$ is equal to 3:2. b) Histogram showing the incorporation of water in the single phase area as a function of EtOH in the surfactant-EtOH blend. With this diagram the optimal β_{EtOH} respectively the longest a* was determined.

$$R_{S/O} = \frac{m(surfactant) + m(cosurfactant)}{m(oil)}. \tag{II.1}$$

In Section III.1.3 and III.1.4 a short-chain alcohol was used as cosolvent. The influence of the cosolvent mixed with a cosurfactant on the microemulsion area was examined. The representation of these multi-component systems in a ternary phase diagram is not adequate. This three-dimensional system was transformed into a two-dimensional one. An experimental path, b*, with a constant $R_{S/O}$ was chosen (see Figure II.1 a)). a* is the part of b* within the single phase region. The representation of a* in a histogram was chosen. On the abscissa the percentage of EtOH in the cosurfactant/cosolvent blend (β_{EtOH}) is plotted and on the ordinate the percentage of added water (ω_{water}). The black bars represent a*. For systems with the longest paths a* PTPDs were recorded. With this method a fast screening of the countless possibilities of mixing five components with several cosurfactants was possible.

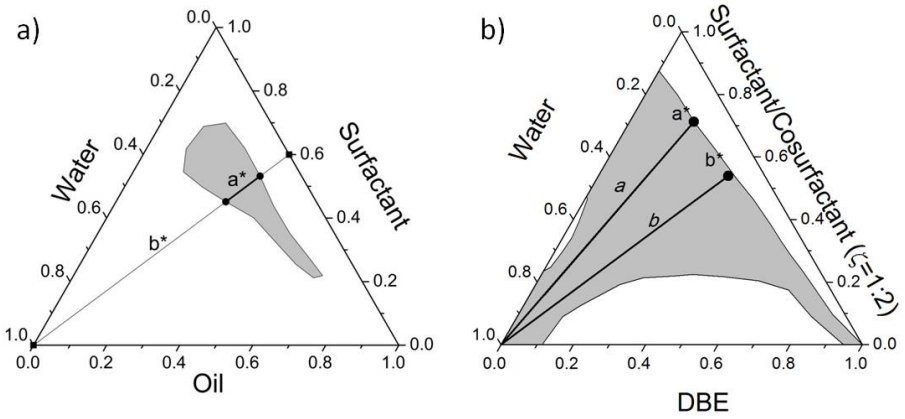

Figure II.2.: a) Illustration of a representative (pseudo-)ternary phase diagram with water/ surfactant/oil. The grey area represents the microemulsion region. Additionally, two experimental paths are shown. b* is the path with a fixed $R_{S/O}$=3:2. Path a* is the part of b* within the microemulsion area. This path was used in Section III.1.1, III.1.3 and III.1.4. b) Representation of experimental paths *a* and *b*, starting from the compositions a* and b* in a classical PTPD. $R_{S/O}$ is equal to 3:2 (path *b*) or 4 (path *a*). These paths were used in Section III.1.2.

II.2.2. Conductivity

Conductivity measurements were carried out at 25 °C with the *inoLab*® *Vario Cond 730* Conductometer. The temperature was controlled by a thermostated cell. All measurements were conducted twice. The experimental error is approximately 2.5 %. w/o mEs were prepared as described above whereas the content of water was as low as possible. Water was then progressively added with an Eppendorf pipette and the volume and the corresponding specific conductivity κ were recorded. The measurement was finished when the turbid area was reached. The experimental paths for the conductivity measurements are shown in Figure II.2

II.2.3. Light scattering experiments

II.2.3.1. Dynamic Light Scattering

Dynamic light scattering (DLS) experiments were performed with a goniometer CGS-II from ALV (Langen, Germany). The goniometer was equipped with an ALV-

7004/Fast Multiple Tau digital correlator and a vertical-polarised 22mW HeNe-laser (wavelength λ=632.8 nm). All measurements were done at a scattering angle of 90 ° after thermostating to 25 °C. Before the measurements, all solutions were filtered with a 0.2 μm PTFE membrane filter to remove all dust particles. Then, the samples were transferred to a cylindrical light-scattering cell of 10 mm outer diameter. The measurement time was 300 s. The obtained correlation functions were fitted with the software TableCurve 2D v5.01 by a monomodal equation. This function can be described as followed:

$$y = a_0 + (a_1 \cdot e^{-a_2 \cdot X})^2 \tag{II.2}$$

a_0 is a constant base value, usually 1, a_1 refers to the dynamic part of the amplitude and a_2 is the decay rate linked to the diffusion coefficient D:

$$a_2 = D \cdot q^2 \tag{II.3}$$

q is the scattering vector which is defined as

$$q = \frac{4\pi n}{\lambda} \cdot sin\frac{\theta}{2}. \tag{II.4}$$

In this equation, n is the refractive index, λ the wavelength of the irradiated light, and θ the detection angle. The hydrodynamic radius R_h can be derived from the Stokes-Einstein equation:

$$D = \frac{k_b \cdot T}{6\pi \cdot \eta \cdot R_h} \tag{II.5}$$

For the precise calculation of the hydrodynamic radius R_h the knowledge of the dynamic viscosities (η), the densities (ρ) and the refractive indices (n) of the solutions is indispensable (see eq. (II.5)). These measurements are explained later in section II.2.4.

II.2.3.2. Static light scattering

Static light scattering experiments were performed with the same apparatus as described above. Measurements were conducted at 25 °C and at scattering angles of 45 °, 90 ° and 135 °. Before the measurements the samples were treated in the same way as for DLS experiments. The apparent molar mass obtained from SLS via the Rayleigh relation is

$$\frac{\Re}{K \cdot C} = M \cdot S(q) = M_{app}, \tag{II.6}$$

where $\Re$ is the Rayleigh ratio in m^{-1} (Rayleigh ratio standard taken from [109, 110]), $S(q)$ is the structure factor which expresses the influence of micelle-micelle (or more general object-object) interactions on the scattering, C is the concentration in g/L, M the molar mass of the micelles and M_{app} the corresponding apparent mass. K is defined as

$$K = 4 \cdot \pi^2 \cdot n^2 \cdot (\frac{dn}{dc})^2 \cdot \lambda^{-4} \cdot N_A^{-1}. \tag{II.7}$$

In this equation n is again the refractive index, $\frac{dn}{dc}$ the refractive index increment in L/g, which was obtained by precise refractive index measurements as described above, λ the wavelength in m and N_A is the Avogadro number. The Rayleigh ratio of particles in solution can be calculated with the following equation:

$$\Re_{solution} = \frac{I^0_{solution} - I^0_{solvent}}{I^0_{standard}} \cdot \Re_{standard} \cdot (\frac{n_{solvent}}{n_{standard}})^2 \tag{II.8}$$

with I^0 being the scattered intensity of the solvent, solution or the used standard (in our case toluene). $(\frac{n_{solvent}}{n_{standard}})^2$ a correction factor of the scattered volume , which is often introduced due to different diffraction effects between sample and standard [111]. In first approximation we set this term equal to one. The spherical volume

(V_{sphere}) can be obtained from M_{app} according to eq. II.9.

$$V_{Sphere} = \frac{M_{app}}{N_A \cdot \rho_{particle}} = \frac{4}{3} \cdot \pi \cdot r^3 \tag{II.9}$$

The problem was to find an expression for $\rho_{particle}$. Due to the similarity of the densities of the involved fluids, the density of the oil for the corresponding system was used.

II.2.4. Density, viscosity and refractive index

Density measurements were performed on a vibrating tube densimeter DMA 5000 M equipped with a precision thermostat from Anton Paar (Graz, Austria) at 25 °C with a temperature uncertainty ≥0.01 K. The uncertainty in densities is ± 0.005 kg.m^{-3}. Densities were used for calculations of dynamic viscosities from measured kinematic viscosities. The viscosities were measured with an automated rolling-ball viscometer from Anton Paar AMVn (Graz, Austria). The stated relative uncertinaty of the instrument is ≥0.005 s, though overall errors were probably slightly higher. The dynamic viscosities were then calculated with the following equation:

$$\eta = k \cdot (\rho_{ball} - \rho_{solution}) \cdot t \tag{II.10}$$

k is a constant, t the measured time the ball required to roll the distance in the capillary, ρ_{ball} is the density of the ball and $\rho_{solution}$ the denisty of the investigated solutions. The third value important for the precise calculation of R_h is the refractive index. The refractive indices were measured with an Abbemat WR-MW refractometer from Anton Paar (Graz, Austria). The apparatus has a resolution of Δ n = 10^{-6} (accuracy $\pm 4 \cdot 10^{-5}$).

II.2.5. Thermo Gravimetric Analysis

The volatilities of the components in the microemulsions in Section III.1.2 were investigated with thermogravimetric experiments. Samples of microemulsions of 13 mg were subjected to thermogravimetric analysis in an air atmosphere. A TGA7 instrument (Perkin-Elmer, Norwalk, CT, USA) was used. An isothermal heating program was set up at 32 °C. In order to obtain a low-noise TG signal, a constant gas flow of 45 ml/min was set for all tests. The precision of temperature measurements for the thermobalance was ± 1 °C. Continuous records of weight loss and temperature were obtained and used to determine the evaporation rates (weight loss %/min). The experimental time was 24 h.

Chapter III.

III Results and Discussion

III.1. Green and sustainable microemulsions

III.1.1. Microemulsions with renewable feedstock oils

III.1.1.1. Abstract

In this section the influence of chemical structures of renewable feedstock oils (RFOs) on the domains of existence and the nanostructures of microemulsions are investigated. The results were compared to those of classical microemulsions containing n-alkanes. First, the domains of microemulsions obtained from the melt of water, sodium dodecylsulfate (SDS) as surfactant, 1-pentanol as cosurfactant and different RFOs (or RFO melts) in PTPD are presented. ζ was kept constant at 1:2 and the RFO (or RFO melt) is considered as a pseudo constituent. Two different fatty methyl ester (FAME) biodiesels from rapeseed and cuphea oils, rapeseed oil, "TBK" biodiesel from rapeseed oil, limonene, and different mixtures limonene-to-FAME-rapeseed biodiesel and FAME-rapeseed biodiesel-to-FAME-cuphea biodiesel are used as RFOs or RFO melts. Second, conductivity data are shown along an experimental path having a constant RFO or RFO melt:(surfactant:cosurfactant) mass ratio, whereas the water content is varied. All obtained data are then compared to data from anterior studies with a series of n-alkanes (from n-hexane to n-hexadecane). As main conclusion it is found that RFOs or RFO melts can sub-

stitute easily n-alkanes. From the chemical structure of the oils, it appears that not only the polarity of the oil plays an important role but also the absolute size of the oil molecules. In all cases, microemulsion systems exhibit a percolative behaviour.

III.1.1.2. Introduction

Microemulsions have attracted attention in science and industry since a long time. They show thermodynamic stability, optical clarity and high solubilisation capacity [112], and they are isotropic with ultralow interfacial tensions [113, 114]. Usually, microemulsions are mixtures of non-polar solvents with polar liquids like water stabilised by a surfactant [115, 116], frequently in combination with a cosurfactant - often a short or medium chain alcohol [51] - forming an interfacial film which separates the two, in principle immiscible, solvents [117]. Though they are macroscopically homogeneous solutions, an ordered structure can be found on the nanoscopic scale such as oil-in-water (o/w) or water-in-oil (w/o) droplets, similar to the structures of micelles [41, 55, 118], but with droplet sizes of 100 nm [114]. Beside droplets, lamellar [119–121], random [122, 123] or bicontinuous [56, 57, 114] microstructures, a network of water tubes in an oil matrix or a network of oil tubes in a water matrix, have been identified. Various experimental methods like small angle neutron scattering (SANS) [49, 124], neutron spin echo [125], NMR [126, 127], freeze fracture electron microscopy (FFEM) [128], cryo-scanning electron microscopy [129], and conductivity measurements [130] have been used to investigate these microstructures.

However, for a first screening, such sophisticated experiments are not necessary. The measurement of electrical conductivity is a very efficient method to study the global structure of microemulsions, especially in the case of w/o systems [131, 132]. The electrical conductivity undergoes a significant change over many orders of magni-

tude when the volume fraction of the dispersed aqueous pseudo-phase is increased above a certain value. The sharp increase is the consequence of the percolative behaviour of formed nanostructures in the system [132]. The percolation is induced when droplets in the microemulsion come close enough for an ion exchange from one to another or when the droplets coalesce and form clusters leading to an exchange of material [133]. This phenomenon can be observed when the specific conductivity of the polar phase is some orders of magnitude higher than the one of the oil. Sometimes, an anti-percolative behaviour is observed. Then, only a small increase or even decrease of conductivity is reported when increasing the water content. An anti-percolative behaviour is associated to the formation of droplets having rigid interfacial films thus preventing the reversed micelles to merge [134].

Microemulsions have been intensively studied during the last few years by many scientists and technologists. The applications investigated at present range from classical fields like solubilisation media in food, cosmetic [135–138] and pharmaceutical industry [139–142], oil recovery [143], ground water remediation [117, 144], soil cleanup [145] and organic chemistry to new subjects like improvement of fuels [116] or the use as decontamination media [146]. The use of microemulsions is not only advantageous due to the facile and low cost preparation, but also because of the improved bioavailability [115, 147].

Due to the consumer lifestyle of health and sustainability (LOHAS) requiring bio-based concepts, it is a must to formulate and characterise microemulsions based on biological amphiphiles [148] and different kinds of renewable feedstock oils (RFOs) [116, 142, 149, 150]. Nowadays, green microemulsions are already on the market [137, 147, 148, 151]. Especially, mono-alkyl esters made from renewable biological sources such as vegetable oils or animal fats have been investigated, and the physical

properties of microemulsions with these compounds as the oil phase are of growing interest [148, 152–154].

Biodiesel is obtained by transesterification of vegetable oils with monohydric alcohols, commonly methanol, to give the corresponding mono-alkyl esters (FAME) [155, 156]. Besides sunflower, rapeseed, palm and soybean oil [152, 157, 158] sources such as used cooking oils, Jatropha [159] and algae [160] oils are receiving increasing attention. Already as early as in the 1960s, Cuphea, with its vast diversity of fatty acids [161, 162], was proposed as a source of fatty acids with medium chain lengths [163]. In recent years, biodiesel gained importance in a great number of research and industrial processes, for example as green solvent [164–166], in cleaning and degreasing agents [167] or cleaning up of oil spills [168], as polymerization solvent [169], in pesticides [148, 151, 170] or as an alternative to organic solvents in liquid-liquid extractions [171] and last but not least as biofuels. Biodiesel based microemulsions have already been made and tested [146] and the produced bicontinuous microemulsion-fuels are effective fuels with low emissions [172–174]. It was shown that biodiesel from cuphea oil had improved fuel properties due to the composition of triglycerides [175], a relatively high cetane number and a low cloud point [162]. Other advantages of biodiesel are the absence of aromatic hydrocarbons, low or no sulfur content and a positive energy balance. Some advantages in the use of FAME as green solvent in the formulation of microemulsions are their lower toxicity [176–178], rapid biodegradability in soil [179], low vapour pressure and non-inflammability [180]. The problems due to the over-production of glycerol induced by the classical processes of transesterification can be avoided by the production of "TBK" biodiesel. In this process triglycerides react with ethyl acetate to give TBK-biodiesel associated with partially acetylated triglycerides [181].

Another class of molecules widely used as solvents, and as a promising substitute for the oil compound in microemulsions, are monoterpenes. These are inexpensive monocyclic, monoterpenic hydrocarbons produced from renewable feedstock and the major constituents of citrus oils [182]. Limonene itself is among the most commonly used fragrance additives or active substances in technical and fine products, for example in defatting agents [183], cleaners [184], in perfumes, soaps, foods and beverages, with a typical concentration between 50 ppm and 2300 ppm [183] and it can be used as a fuel or fuel additive [185, 186] as well. Microemulsions based on limonene are of great importance for the formulation, for example of pharmaceuticals [115, 187], cleaning agents [188, 189], and flavouring vectors in foods and beverages [190] etc. The anti-carcinogenic properties [191] have been shown and limonene is considered as a skin irritant and a sensitizer in high concentration [192], but not allergenic [193].

In the following paragraph the influence of the use of RFOs and non renewable feedstock oils (NRFOs) in order to formulate microemulsions is shown. The domain of existence and the nano-structures of microemulsions with different RFOs or RFO melts, and NRFOs ranging from n-hexane to n-hexadecane are then compared using PTPDs and conductivity measurements; sodium dodecyl sulfate (SDS) and 1-pentanol are used respectively as surfactant and cosurfactant. The used RFOs or RFO melts are two different FAME biodiesels from rapeseed and cuphea oil, TBK biodiesel from rapeseed oil, limonene, and mixtures of limonene and FAME-rapeseed biodiesel as well as FAME-rapeseed and FAME-cuphea biodiesel. The biodiesels essentially differ in the carbon chain length and proportion of unsaturations of the fatty methyl esters and the amounts of tri-, di- and mono-glycerides.

III.1.1.3. Results and discussion

III.1.1.3.1. Phase diagrams

FAME-rapeseed biodiesel and limonene - two "green" solvents

At first, FAME-rapeseed biodiesel, limonene and afterwards melts of those RFOs were used as oil phase. For this purpose, the phase diagrams for the limonene-to-biodiesel melt with biodiesel-to-limonene mass ratios of 1:3, 1:1 and 3:1 were also determined. The resulting phase diagrams are illustrated in Figure III.1 a). The grey areas represent the clear and homogeneous single phase regions without liquid crystals. These areas can be assimilated to the domain of existence of microemulsions [78].

The use of limonene gives a phase diagram with two domains of existence of microemulsions, L1 and L2, as in the case where n-hexane or n-heptane are used, see Figure III.2. L1 is constituted of a/w droplets for the compositions having the highest proportions of water. In L1, the microemulsions can have a high content of oil. Then, they can be bicontinuous or still form oil-in-water droplets. The exact determination of the structure of these microemulsions remains a matter of discussion, and is not discussed. L2 is formed by reversed w/o droplets at low water contents. L1 and L2 are generally separated by clear, or unclear, or homogeneous or not homogeneous media showing liquid crystalline phases. The area between L1 and L2 generally contains liquid crystals (LC).

The domain of existence of the microemulsions obtained using FAME-rapeseed biodiesel is more like the one observed in the presence of n-hexadecane. The phase diagram shows a microemulsion domain that consists of a large single realm of ex-

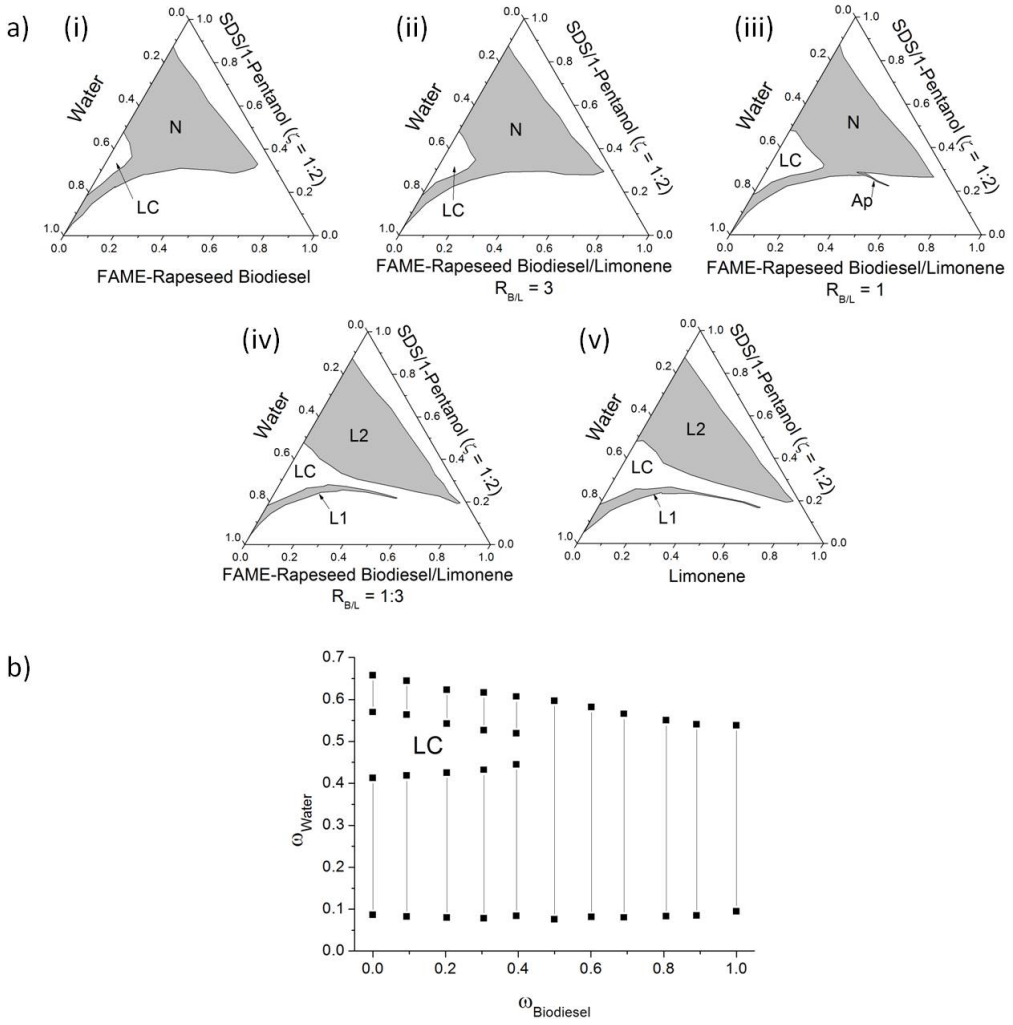

Figure III.1.: a) PTPDs for the system water/SDS/1-Pentanol/RFO at 25 °C and constant weight ratio of SDS-to-1-Pentanol (ζ=1:2) with (i) FAME-rapeseed biodiesel, (ii) FAME-rapeseed biodiesel/limonene 3:1, (iii) FAME-rapeseed biodiesel/limonene 1:1, (iv) FAME-rapeseed biodiesel/limonene 1:3 and (v) limonene as RFO phase. Compositions are in weight fraction. b) Histogram showing the incorporation of water in the single phase area as a function of FAME-rapeseed biodiesel mass fraction ($\omega_{Biodiesel}$ in the biodiesel-limonene mixture. The black bars represent path a* (see Figure II.1 a)).

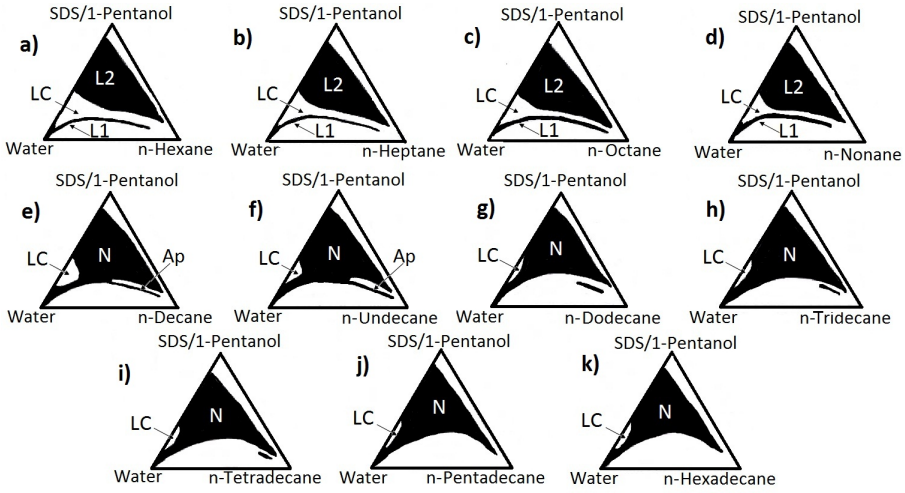

Figure III.2.: Homologous series of PTPDs for the water/SDS/1-Pentanol/n-alkanes systems. The domains of existence of the microemulsions are represented in black. All these phase diagrams were determined during an anterior work [194] using the same method as described in the chapter "methods and techniques". Temperature was kept constant at 25 °C and the weight ratio of SDS-to-1-Pentanol (ζ=1:2) as well.

istence comparable to the domains obtained with long-chain n-alkanes, see Figure III.2. In this case, the w/o droplets obtained at low water contents can be converted into oil-in-water droplets by adding water along some well-defined paths that do not pass through the LC area. The structure of the microemulsions between the water in oil and the oil-in-water droplets is then bicontinuous. By mixing both RFOs, it is possible to screen roughly the whole spectrum of PTPDs with conventional alkanes, beginning with n-octane and ending with n-hexadecane. For the mixtures of both RFOs however, slight differences of phase behaviours in comparison to the ones obtained with n-alkanes are apparent. The main difference appears for the domains of existence of microemulsions obtained with the weight ratio 1:1 of limonene-to-FAME-rapeseed biodiesel. In particular, the appendix (noted Ap in Figure III.1 a) diagram (iii)) appears less extended than in the case of the use of n-decane or n-undecane (Figure III.2, diagrams (d) and (e)). The loss of this appendix can be explained by the formation of microemulsions due to the increased flexibility of the n-alkane molecules. Nevertheless, the main microemulsion domains are similar to

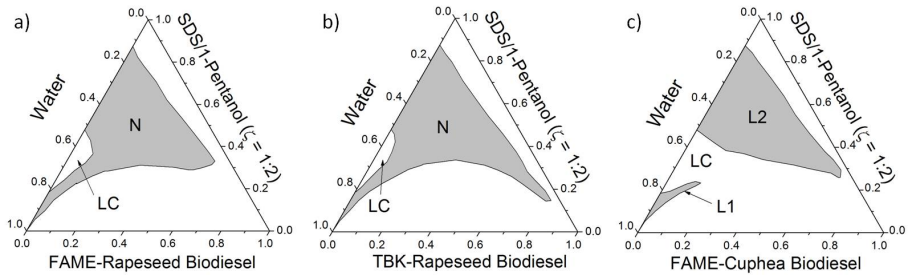

Figure III.3.: Influence of different types of biodiesel on the domain of existence of microemulsions for the system water/SDS/1-pentanol/ (a) FAME-rapeseed biodiesel, (b) TBK-rapeseed biodiesel and (c) FAME-cuphea biodiesel. Temperature was kept constant at 25 °Cand the weight ratio of SDS-to-1-pentanol as well (ζ=1:2).

those found for the homologous series of the n-alkanes (Figure III.2) considering an increase of the average number of carbon atoms or an increase of the average volume per RFO and n-alkane molecules from limonene to FAME-rapeseed biodiesel and from n-hexane to n-hexadecane.

FAME, TBK-rapeseed biodiesel, FAME-cuphea biodiesel and rapeseed oil - a comparison

In the next step, the domains of existence of microemulsions using as RFOs TBK-rapeseed biodiesel and FAME-cuphea biodiesel are determined. Figure III.3 shows the resulting phase diagrams. For a better comparison, the diagram water/SDS/ 1-pentanol/FAME-rapeseed biodiesel (Figure III.1(i)) is reported again.

For TBK-rapeseed biodiesel, a large single realm of existence N is observed and the topology of the phase diagram is similar to that observed with n-hexadecane (Figure III.2 k). In the case of the FAME-rapeseed diagram, the extent of the homogeneous transparent N phase into the oil-rich region is less pronounced. This may be explained by the lack of mono- and diglycerides, which are widely present in the TBK-rapeseed system and wich exhibit a much stronger propensity to the interface

than triglycerides.

Biodiesel derived from cuphea oil leads to two separate domains, L1 and L2, but the extent of L1 towards the oil area is more limited in comparison to the ones obtained using short-chain n-alkanes or limonene. Nevertheless, the presence of the two domains, L1 and L2, is in agreement with the fact that the molecular structures of the fatty acid mono alkyl esters of the FAME-cuphea biodiesel have a number of carbon atoms and a molecular volume closer to short-chain n-alkanes than to long-chain ones. From cuphea seed, especially saturated fatty acids with medium chain length of C8-C16 are achieved with decanoic acid being one of the main fatty acids (about 60 % of total fatty acids contents in most cuphea species [161, 162, 191]). The reduction of the L1 domain of microemulsions could be due to a reduction of the flexibility of the FAME-cuphea biodiesel molecules. This can be attributed to a slight cosurfactant behaviour of the ester-group leading to a greater interaction with 1-pentanol/SDS bilayer.

Now, the phase diagram obtained with pure rapeseed oil is compared with the phase diagram based on FAME-rapeseed biodiesel in order to investigate the influence of the transesterification reaction on the extent of the domain of existence of microemulsions, see Figure III.4.

The used FAME-biodiesel was produced by transesterification of rapeseed oil with methanol, to give the corresponding mono-alkyl esters (FAME). It appears that this reaction is largely favourable to the formation of microemulsions. As the fatty acids are also linked to the glycerol by ester-functions, the polarities of the rapeseed oil molecules and of the FAME molecules should be comparable. So, it seems that the number of carbon atoms per molecule or of the molecular volume is the decisive

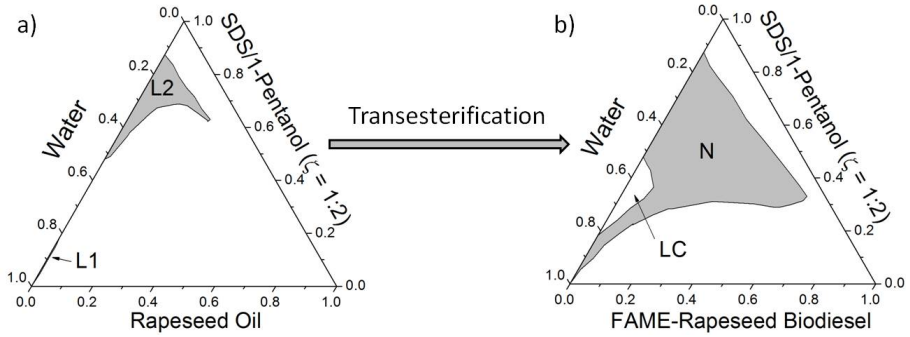

Figure III.4.: Influence of the production of FAME on the solubilisation of the renewable carbon coming from the rapeseed oil: a) PTPD of the system water/SDS/1-pentanol/rapeseed oil and b) PTPD of the system water/SDS/1-pentanol/FAME-rapeseed biodiesel at 25 °C and at constant weight ratio of SDS-to-1-pentanol (ζ=1:2).

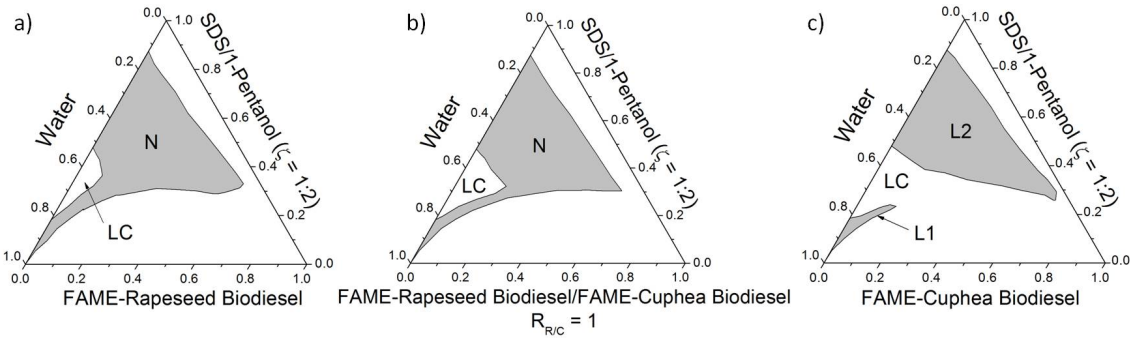

Figure III.5.: PTPDs for the system water/SDS/1-Pentanol/RFO at 25 °C and constant weight ratio of SDS-to-1-Pentanol (ζ=1:2) with (a) FAME-rapeseed biodiesel, (b) FAME-rapeseed biodiesel/FAME-cuphea biodiesel 1:1, (c) FAME-cuphea biodiesel as RFO phase.

parameter which makes the difference in the phase behaviours and not the polarity of the oil molecules. Figure III.5 shows that similar to limonene, FAME-cuphea biodiesel can roughly yield the whole spectrum of PTPDs known from alkanes beginning with n-octane and ending with n-hexadecane, by mixing it with appropriate amounts of FAME-rapeseed biodiesel.

III.1.1.3.2. Conductivity

The experimental path of the conductivity measurements is the same as already shown and explained in Section II.2.2. Independently of the oil components, all the microemulsion systems exhibit a similar general dependence of the electrical conductivity on the amount of water (see Figure III.6). At low water content, the electrical conductivity of the samples is close to zero, which can be attributed to the fact that the oils forming the initial continuous pseudo-phase constitute an excellent insulator to the first reversed w/o droplets formed. Then, there is a progressive increase in electrical conductivity with increasing amount of water.

This well-known behaviour can be explained with a percolation model [131, 195]. At the percolation threshold, the w/o droplets form nano-clusters favourable to the SDS counter-ion mobility. The deviation from the linearity observed for higher water content in the presence of certain oils has been ascribed to the formation of bicontinuous structures, generally observed before the pseudo-phase inversion. The percolation threshold (value of the water content where a large increase of the conductivity value starts) appears to be dependent on the chemical nature of the oil. The more the oils have molecules with a high average number of carbon atoms (or a high molecular volume), the lower is the value of the percolation threshold. In Figure III.6 it can be seen that the curves obtained in the presence of n-hexadecane and n-hexane are the upper and lower boundaries, respectively, and the other curves

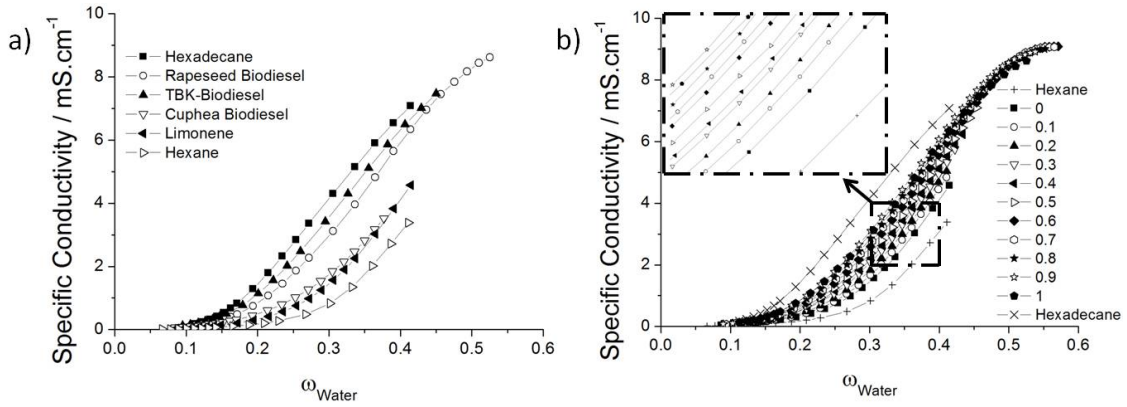

Figure III.6.: a) The specific conductivity of the microemulsions as a function of water weight ratio for the pseudo-ternary system water/SDS/1-pentanol/oil with a constant weight ratio of SDS-to-1-pentanol (ζ=1:2) is shown. As oil phase either hexadecane, or hexane, or limonene, or FAME-rapeseed, or TBK-rapeseed, or FAME-cuphea biodiesels were used. All experiments followed path a* (see Figure II.2 a)). b) The specific conductivity of the microemulsions as a function of water content for the pseudo-ternary system water/SDS/1-pentanol/oil with a constant weight ratio of SDS-to-1-pentanol (ζ=1:2) is shown. As oil phase, mixtures of FAME-rapeseed biodiesel and limonene were used. The experimental path of the conductivity measurements is the same as already shown and explained in Figure II.2 a). All experiments were recorded at 25 °C

are situated in between. The conductivity curves obtained using TBK- and FAME-rapeseed biodiesel are close to the one obtained with n-hexadecane whereas those obtained using FAME-cuphea biodiesel or limonene are in the vicinity of the one recorded in the presence of n-hexane. This result is in line with the observations concerning the domains of existence of microemulsions in the PTPDs (previous section). The conductivity curves obtained from melts of FAME-rapeseed biodiesel and limonene show the same trend (see Figure III.6 (b)). With increasing amount of FAME-rapeseed biodiesel, there is a shift of the percolation towards lower values. The curves obtained using the FAME-rapeseed biodiesel only (oil with a higher average number of carbons per molecule) and the limonene (oil with a lower number of carbons per molecule) are the lower and upper curves and all the other curves are in between, in the expected order.

III.1.1.4. Conclusion

This study shows the possibility of replacing classical n-alkanes as oil phase in common microemulsions by green RFOs, whether RFOs are "pure" or a mixture of RFOs of different origins. Limonene and Cuphea biodiesel can replace short-chain alkanes whereas TBK- and FAME-rapeseed biodiesel can substitute long-chain ones. The extent of the microemulsion domains and the organisation of the nano-droplets can be predicted by the average number of carbon atoms per molecules (or the average molecular volume) of the RFO or RFO mixtures. The presented results may be used to formulate more environmentally friendly industrial products, e.g. "green" cutting fluids, pesticids [148], cosmetics [136, 137] or pharmaceuticals [146]. Furthermore, from the phase diagrams shown in the present work (Figure III.1 (ii, iii), Figure III.5 (b)) the formulation of a potential bicontinuous microemulsion-fuel of FAME-rapeseed biodiesel and FAME-cuphea biodiesel (or limonene) mixtures appears possible. By addition of cuphea biodiesel (or limonene), a lower cloud point of the system and a positive influence on the combustion could be expected. All these systems show percolative behaviour, whatever the molecular volume or the polarity of the oil. This result is in agreement with the fact that the passage to an anti-percolative system depends rather on the nature of the alcohol used as cosurfactant than on the nature of the oil; the longer chain alcohols are responsible of the appearance of an anti-percolative behaviour [78].

III.1.2. Highly and fully water dilutable sustainable microemulsions with dibasic esters as oil phase

III.1.2.1. Abstract

In the previous section, the formulation of microemulsions with RFOs was presented. In this part, a strategy of formulating highly and fully water dilutable sustainable microemulsions with dibasic esters as oil pseudo-phase is shown. First, dimethyl- or diethyl dibasic esters with different numbers of carbon atoms between the ester functions (succinate C2, glutarate C3 and adipate C4) or ester blends and a surfactant-cosurfactant melt consisting of sodium dodecyl sulfate and 1-pentanol with a constant weight ratio of 1:2 are used. The extent of the realms of existence of homogeneous single phases were investigated and represented with pseudo-ternary phase diagrams. It is possible to formulate fully water dilutable oil-rich single phase solutions with all dimethyl dibasic esterss but not with the diethyl ones. By mixing the most hydrophilic dibasic ester with the most hydrophobic one with a mass ratio of 3:2, a fully water dilutable oil-rich single phase can also be obtained. The presence of w/o, bicontinuous and o/w microemulsions is checked with conductivity and dynamic light scattering measurements. A percolative behaviour is observed for all systems. Secondly, to formulate green and sustainable microemulsions, sodium dodecyl sulfate was successively replaced by sodium oleate and 1-pentanol by EtOH or 1,5-pentanediol. With sodium oleate highly water dilutable microemulsions were obtained. Homogeneous and translucid samples in the very diluted area turned bluish after several days. Longtime pH measurements of systems containing sodium oleate show no degradation of dibasic esters at low and a rapid hydrolysis at high water content with 1-pentanol as cosurfactant. Always in presence of sodium oleate, the substitution of 1-pentanol by EtOH or 1,5-pentanediol drives the system to microemulsions showing an instability of the ester at any water concentrations. Ther-

mal gravimetric analysis measurements at 32 °C for 24 h confirm a rapid evaporation of EtOH and water and negligible evaporation of 1,5-pentanediol.

III.1.2.2. Introduction

Due to the high quantities of solvents in our environment, the quest and the need of finding and developing green alternatives are evident. Solvents should be environmentally friendly, have low costs, low toxicity, high stability, and rather high boiling temperatures. One group of solvents fulfilling most of these requirements are dibasic esters (DBEs). Moreover, they have viscosities and densities close to water. DBEs are oxygenated organic compounds of the diester type with the formula $CH_3(CH_2)_mOC(O)(CH_2)_nC(O)O(CH_2)_mCH_3$ were n is an integer and m is zero for dimethyl- or one for diethyl-esters. Starting from dibasic acids, DBEs can be synthesised via esterification with alcohols, produced in most instances from renewable feedstock or also available from caprolactam plants in which the dibasic acids are considered as waste compounds. They have excellent properties in industrial applications where especially aromatic hydrocarbons and chlorocarbons have to be replaced [196]. Many patents can be found in the fields of industrial cleaning applications [197–200], paint [201, 202], coating [202–204] and polymer industry [205–207]. In these industries, DBEs are even recycled by vacuum distillation [208]. The diesters of succinic, glutaric and adipic acids are the most promising DBEs in terms of green chemistry. Between 20,000 to 30,000 t/a of succinic acid, also known as amber or butanedioic acid, are produced worldwide [209]. It can be used as a precursor for many important chemicals in industry, such as N-methylpyrrolidone, 1,4-butanediol, γ-butyrolactone, adioic acid, tetrahydrofuran and linear aliphatic esters [210, 211]. Today, the starting material of succinic acid production is often liquefied petroleum gas or petroleum oil via maleic anhydrid which has to be oxydised afterwards. This last synthesis step is a serious limitation that explaines why

the global market and the production of maleic anhydrid is much larger than for succinic acid [212, 213].

In the last years, scientists have screened and studied many different microorganisms, like fungi [214, 215] or bacteria [216, 217] for succinic acid production. A fermentative process using *E. coli* bacteria and a large amount of renewable feedstock, including glucose, ligno-cellulosic sugars (mixed C5 and C6) and glycerol, was scaled up by the company ARD (Pomacle, France) to 2,000-3,000 t/a [218]. This quantity is already around 10 % of the total succinic acid production worldwide. A mentionable side-effect is that CO_2 is fixed into the succinic acid during fermentation. In theory, one mole of CO_2 is needed per mole of succinate produced.

Commercial glutaric acid is a side product of the chemical adipic acid production, but glutaric acid can be obtained from bacteria as well [219]. The starting material for adipic acid is currently benzene from crude oil. Hydrogenation of benzene to produce cyclohexane is followed by air oxidation to yield a mixture of cyclohexanol and cyclohexanone [220, 221]. Rennovia (Menlo Park, CA, US) has recently shown a strategy to transform d-glucose from biomass to adipic acid [222] and Verdezyne [223] has opened in Carlsbad, California, a pilot plant to produce adipic acid from renewable resources. For the moment, the adipic acid production by fermentation remains still "homeopathic" in front of the chemical one.

The use of DBEs in microemulsion systems for industrial applications has already been described in several patents [198–200, 224]. Until now, to the best of my knowledge, no studies have shown a coherent comparison of the influence of different carbon chainlength between the ester functions, different carbon chainlength of the alcohol or on the stability of the diesters against hydrolysis in the water-rich

area. In this work, it was focused on microemulsions with dimethyl- and diethyl diesters with succinic, glutaric and adipic acids as oil pseudo-phase.

PTPDs are presented and the realms of existence of microemulsions in the model system water/SDS/1-pentanol/DBEs, where the surfactant-to-cosurfactant mass ratio (ζ) is kept constant at 1:2. In order to make the system more sustainable, SDS is then replaced by sodium oleate and 1-pentanol by either EtOH or 1,5-pentanediol. The world production of bioethanol is estimated to be 22,000 millions of U.S. liquid gallons per year [225]. 1,5-pentanediol can be obtained by hydrogenation of glutaric acid [226] or using furfural as starting material [227, 228]. These ways of synthesising give the possibility to get sustainable 1,5-pentanediol from renewable feedstock. Compared to the use of EtOH a lower vapour pressure and an increase of the boiling point of the formulations can be expected. The nanostructures of the systems were investigated with conductivity and DLSexperiments, the long-time stability of the esters was checked with pH-measurements and the volatile stability of the formulations was observed with TGA measurements.

III.1.2.3. Results and discussion

III.1.2.3.1. Phase diagrams with DBEs

In the first step, the phase behaviours of the system water/SDS/1-pentanol/DBE with six different DBEs, dimethyl-/diethyl-succinate (DMS, DES), glutarate (DMG, DEG) and adipate (DMA, DEA) were investigated. In Figure III.7 a) the structures of the six molecules are shown. These components differ by the number of carbon atoms between the two ester functions (succinate C2, glutarate C3 and adipate C4) and the alcohol used in the esterification process (methanol or EtOH). In this ordering DMS is the most "hydrophilic" and DEA the most "hydrophobic"

DBE. Figure III.7 b) illustrates the resulting PTPDs of the systems water/SDS/ 1-pentanol/DBE. The grey areas represent the clear and homogeneous single phase regions. All dimethyl esters form large areas of single phase regions that are fully water dilutable. In the case of DMS, the single phase area stretches even to the oil-rich corner, but this region was not in the field of interest of this study and was not examined in details. In contrast, the extent of the single phase area for diethylesters is restricted to the oil- and surfactant-rich area. They have a small channel to the water-rich zone for well-defined paths, but this type of microemulsion is not fully water dilutable. A detailed study of the nanostructure of the systems will be given later. In all the described systems LC phases occur near the water-surfactant binary.

As already shown in a previous section (SectionIII.1.1), by mixing two oils an intermediate behaviour of the resulting mixture can be expected. Therefore, in the next step, the most "hydrophobic" diester, DEA, which produces only a relatively thin monophasic area in the water-rich region is mixed with the most hydrophilic one, DMS, which gives the largest area of homogeneous single phase (see Figure III.7 b)). The "best" mixing ratio of these two DBEs is defined as a compromise of a high concentration of DEA in the melt and a high water solubility. In Figure III.8 a) the water solubility of this DBE melt, $\omega_{DBE,added}$, of these solutions is plotted against the weight ratio of DMS, $R_{DMS/DEA}$, in the DBE blend. With the ratio $R_{DMS/DEA}$=3:2 a good solubility in water was kept. Again, a fully water dilutable microemulsion was obtained.

III.1.2.3.2. Towards sustainable microemulsions

The mixture of SDS and 1-pentanol as amphiphilic pseudo-phase is still a drawback in the formulation of sustainable microemulsions. To overcome this obstacle, sodium oleate was used as alternative surfactant and EtOH or 1,5-pentanediol as cosurfac-

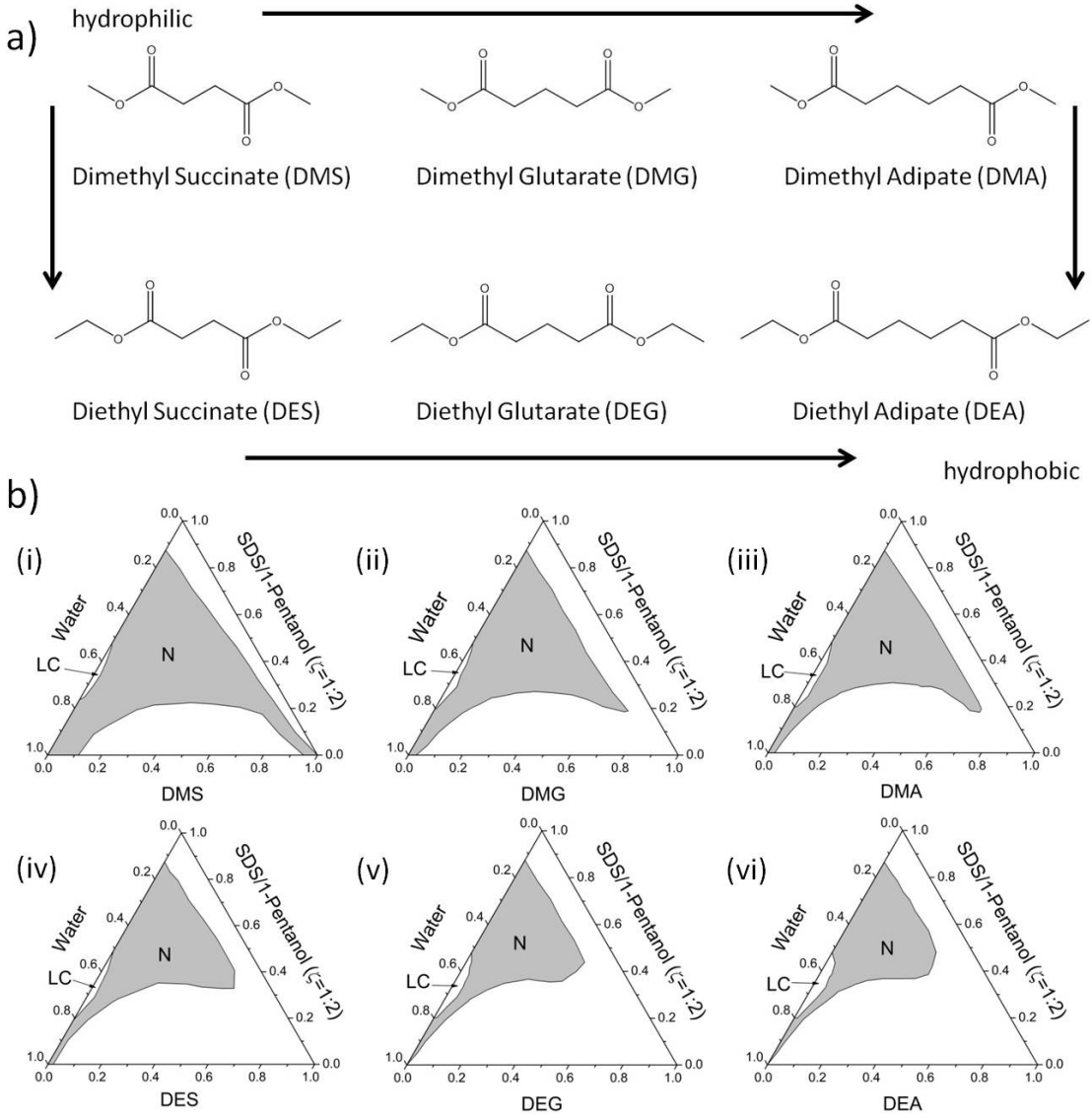

Figure III.7.: a) Molecular structure of the six DBEs used in this study ordered by hydrophobicity. b) PTPDs of the systems water/SDS/1-pentanol/(i) DMS, (ii) DMG, (iii) DMA, (iv) DES, (v) DEG and (vi) DEA at 25 °C and with ζ=1:2. The grey areas represent the homogeneous single phase regions (N). All compositions are in weight fractions.

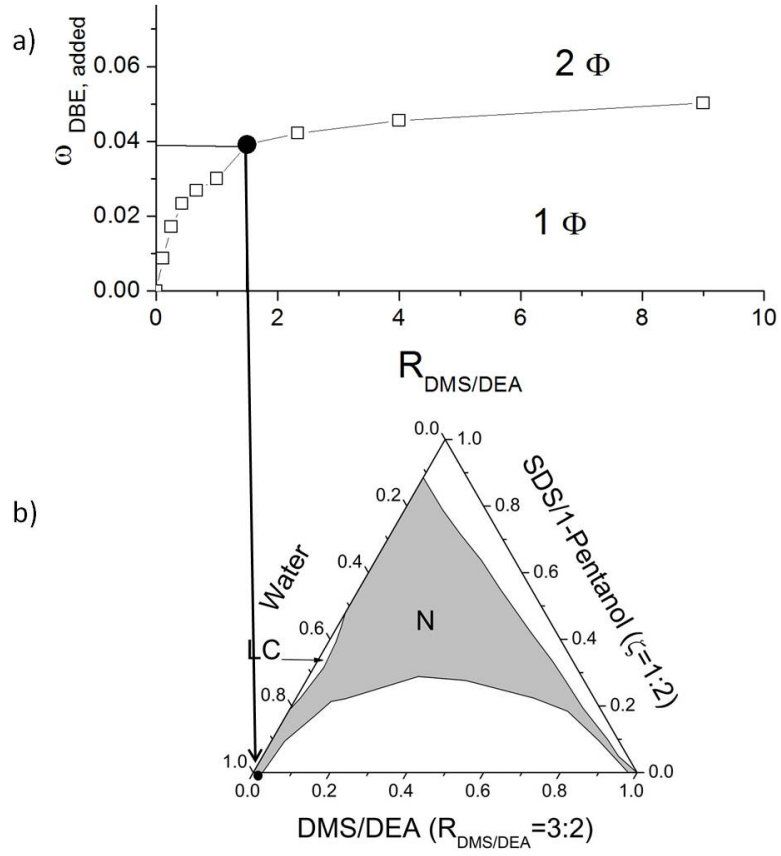

Figure III.8.: a) Phase diagram of the water solubility of different DMS/DEA blends. The mass fraction of DBE blend, possible to dissolve in water, $\omega_{DBE,added}$, is plotted as a function of the weight ratio of DMS, $R_{DMS/DEA}$, in the DBE blend. b) PTPD of the system water/ SDS/1-pentanol/DMS/DEA with ζ=1:2 and $R_{DMS/DEA}$=3:2 at 25 °C.

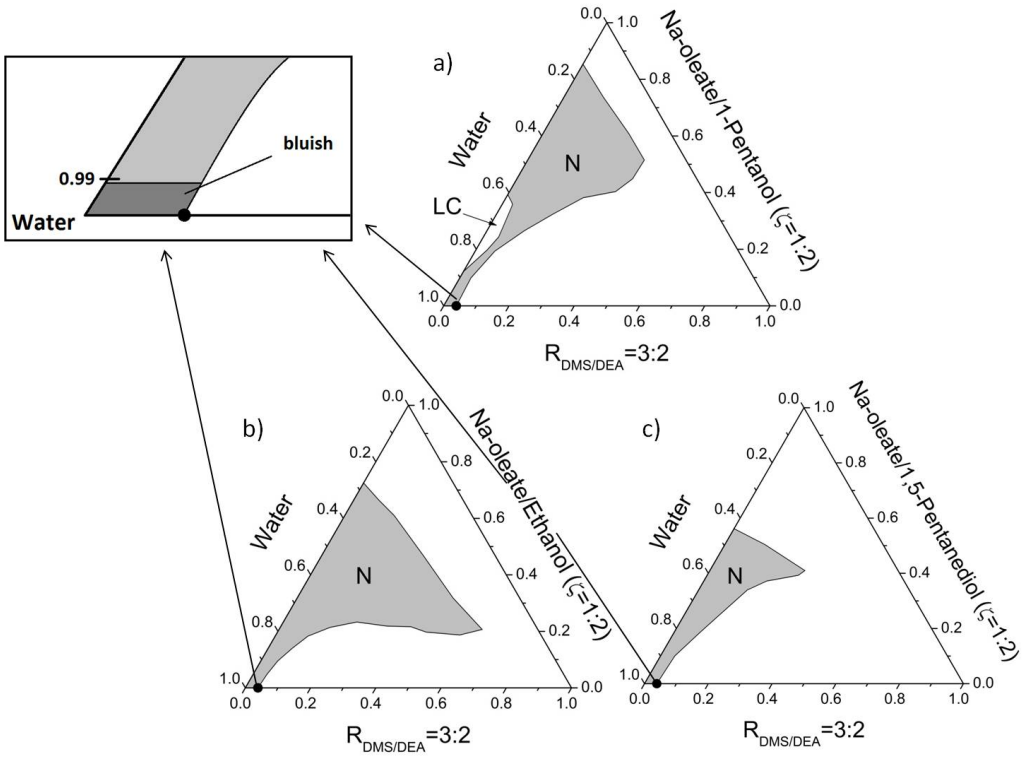

Figure III.9.: a) The phase diagram of the pseudo-ternary system water/sodium oleate/ 1-pentanol/DMS/DEA with $R_{DMS/DEA}$=3:2 and ζ = 1:2 was recorded at 25 °C. b) In this system 1-pentanol was replaced by EtOH and c) EtOH was replaced by 1,5-pentanediol.

tant. The components were progressively replaced for a better understanding of the influence of each ingredient on the formulation. In Figure III.9 the resulting PTPDs of the systems water/sodium oleate/DMS/DEA/ a) 1-pentanol, b) EtOH and c) 1,5-pentanediol with $R_{DMS/DEA}$=3:2 and ζ = 1:2 are shown. In the system shown in Figure III.9 a), still a highly dilutable microemulsion can be obtained, though the connection to the water-rich corner is diminished and only distinct dilution paths remain compared to Figure III.8. None of these systems containing sodium oleate as surfactant are fully dilutable. Over 99 wt% of water, the solutions get a bluish appearance and turn turbid with time. This phenomenon will be discussed in another section (III.1.3). Figure III.9 b) and c) present systems with alternative non-toxic sustainable cosurfactants. Replacing 1-pentanol by EtOH or 1,5-pentanediol, no

LC phases could be found. As a positive result, the area of highly water dilutable microemulsion was increased, but the overall single phase area for the system with 1,5-pentanediol was reduced. Using EtOH as cosurfactant had one striking disadvantage, which is the high vapour pressure even at ambient temperature leading to a steady change of the composition and the risk of producing combustible emissions. The challenge was to find another non-toxic cosurfactant with comparable properties which is less hazardous. As discussed later on, 1,5-pentanediol was a good choice for that. A drawback is the relatively high viscosity of the resulting microemulsion in the oil-and surfactant-rich area, which is less pronounced in the water-rich region.

It should also be mentioned that using sodium oleate had a significant drawback in combination with DBEs due to its high pKa value. In literature the apparent pKa value of oleic acid is reported to be between 8.0 and 8.5 by Cistola *et al.* [229] and 9.25 by Kanicky *et al.* [230]. The resulting high pH will accelarate the hydrolysis of the diesters. The stability aspect of these systems will be presented later.

III.1.2.3.3. Investigation of the nanostructure of the systems

In the next step, the nanostructures of the systems were investigated. Conductivity and DLS measurements were performed. In Figure III.10 the results for the systems containing DMS and DEA are shown as examples, because they are the most and the least hydrophilic DBEs. The complete results of all DBEs are presented in the Appendix. Conductivity experiments were performed following paths *a* and *b* (Figure III.10 a) and d)). The conductivity curves (see Figure III.10 b) and e)) show always a percolative behaviour. At very low water concentrations the specific conductivity κ is almost zero. With increasing water content, κ starts slowly to increase until a linear correlation between the two parameters can be seen. From the extrapolation of the linear part of the curve, the so called percolation point, P_c,

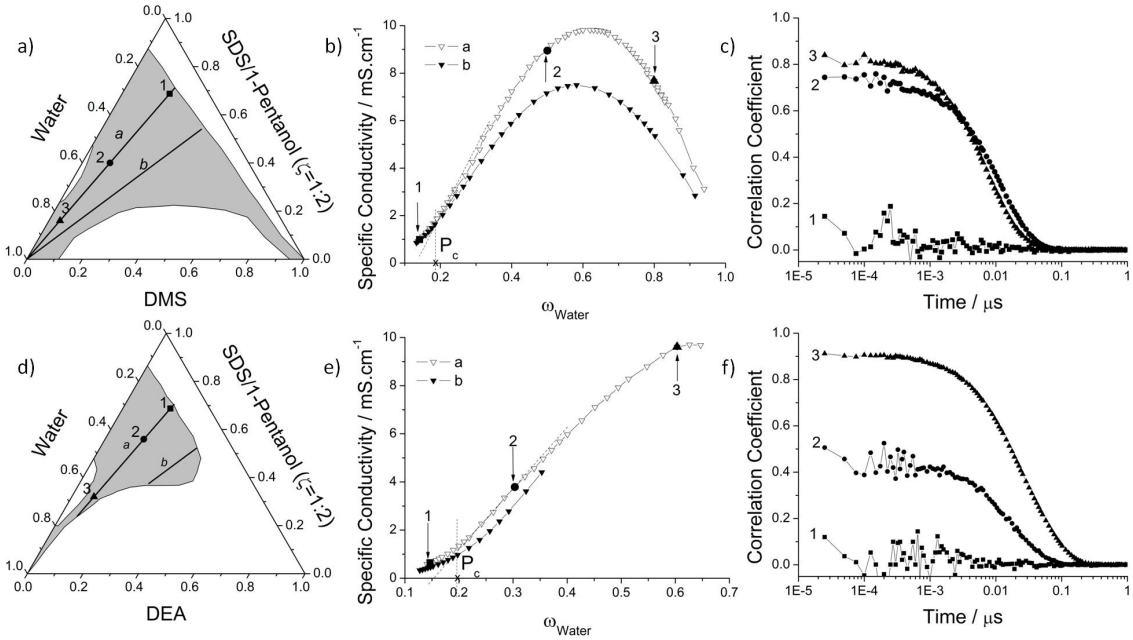

Figure III.10.: In this figure the PTPDs obtained using a) DMS and d) DEA respectively as oils are shown again in order to associate the topology of the realms of existence of the single phase to conductivity and DLS measurements. Paths *a* and *b* are the two lines were the conductivity experiments were performed (see also Figure II.2 b)). The three different points located on path *a* are the three corresponding compositions investigated with DLS. Curves b) and e) show the results of conductivity measurements following path *a* (▼) and *b* (▽). P_c is the percolation threshold. The three arrows give the compositions investigated by DLS. Curves c) and f) show the correlation functions obtained by DLS measurements for the three points. The symbols of the DLS curves correspond to the same symbols as shown in a) and d).

can be derived. At a certain amount of water the curve deviates again from linearity and reaches a maximum (slope = 0). With further increase of water, κ decreases. This behaviour is linked to the different structures in the systems. For systems with the hydrophobic DBEs only the first part of the curves can be obtained due to the smaller area of microemulsions. The same evolution of κ can be seen for the systems with sodium oleate, EtOH and 1,5-pentanediol. At water contents below P_c, the water molecules are bound to the surfactant headgroups and a true solution is obtained. No defined structures can be observed in the systems by DLS measurements (see Figure III.10 c) and f)). Above this threshold, the structures in the systems become more pronounced with the addition of water as the evolution of the correlation functions shows. Now, enough water is in the system to form inverse micelles with a water core. This was observed for all investigated systems. Like in common percolative or U-type systems the appearence of well-defined nano-droplets occurs when sufficient water is added to pass the percolation threshold P_c.

III.1.2.3.4. Stability experiments

Chemical stability of DBEs in the formulations

To investigate the stability of the DBEs in the systems, pH-measurements were performed. For sure, the measured pH does not correspond to the real pH in the system, especially for samples with very little amount of water. When the term "pH" is used, always the apparent pH is meant. The longtime stability of two systems water/SDS/1-pentanol/DMS and water/sodium oleate/1-pentanol/DMS/DEA with $R_{DMS/DEA}$=3:2 and ζ=1:2 was compared. The compositions correspond to the experimental path *a* shown in Figure II.2 b). Figure III.11 shows the evolution of the pH as a function of time for different water contents. For SDS samples no significant change can be observed with time. The evolution of the pH value is linear and the

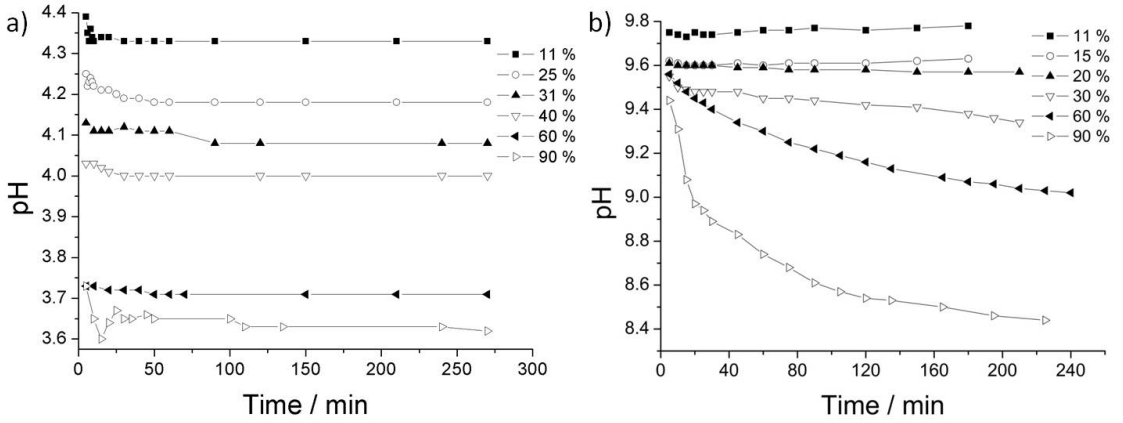

Figure III.11.: pH values as a function of time for the systems a) water/SDS/1-pentanol/ DMS and b) water/sodium oleate/1-pentanol/DMS/DEA with $R_{DMS/DEA}$=3:2 and ζ=1:2 at 25 °C. Every curve corresponds to one composition in the PTPDs. The percentages in the legends refer to the mass fraction of water in %.

resulting solutions are acidic, see Figure III.11 a). Long chain fatty acids have a high pKa and so, as expected, the resulting aqueous solutions have relatively high pH values. So, in systems with sodium oleate esters should be hydrolised very easily. From the curves of Figure III.11 b) it is obvious that for sodium oleate two different regions have to be distinguished. The pH value for samples with percentages of water $\leq P_c$, but still in the single phase area, were remarkably stable. Formulations in the region of bicontinuous structures and direct microemulsions show a drop of pH value of several orders after a few minutes. An observation which can be made with the naked eye was the transition from a clear to a turbid solution after several days for samples with $\omega_{water} \geq 0.9$. So the conductivity, DLS and pH experiments can be directly compared. The instability is linked to the formation of water nano-droplets and perhaps to the appearance of free water which is not completely bound by the surfactant ion-pair. Non-structured systems were stable in terms of hydrolysis and these areas occured before P_c. At very distinct structures (pronounced correlation functions) the hydrolysis was more rapid.

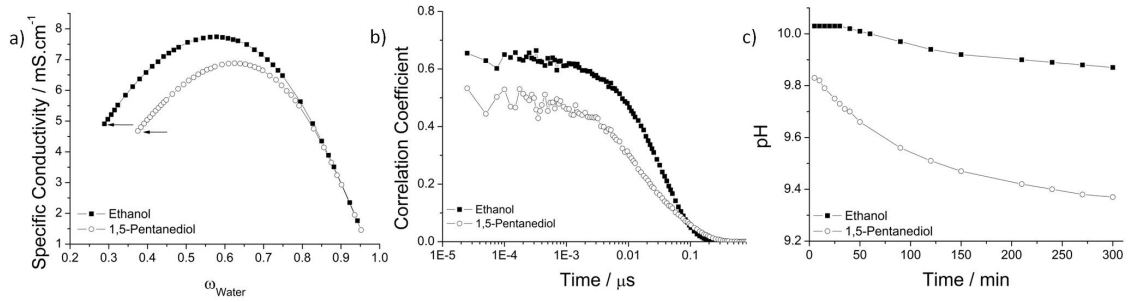

Figure III.12.: a) Conductivity curves along path *a* of Figure II.2 b) for the systems water/ sodium oleate/EtOH (■) or 1,5-pentanediol (○)/DMS/DEA with $R_{DMS/DEA}$=3:2. In these systems, no P_c is observed. The black arrows indicate the compositions studied with DLS (b) and where the pH stability (DBEs) was examined (c).

In a further study, the stability of the two sustainable microemulsions with EtOH or 1,5-pentanediol were investigated. They showed the same behaviour as described above. Even samples with very low amount of water showed a significant drop of pH after short times. Comparing the conductivity and DLS measurements of these two systems, the same trend can be found concerning the formation of structures. In these two systems, no percolation thresholds could be detected and significant correlation functions were obtained by DLS for all water contents. The κ value was always increasing until reaching a maximum at high concentrations of water (which is not the case in an anti-percolative system). This marks the point of phase inversion. It can be deduced that water nano-droplets exist from the beginning of the appearance of the single phase at low water content (see Figure III.12). The results show the possibility to formulate concentrated clear single phase solutions which can evolve during an industrial process towards w/o, bicontinuous and o/w microemulsions adding water with a decelerated hydrolysis of DBEs in the starting formulation even at basic pH values. The condition for this is the presence of a percolation threshold P_c and a quantity of water in the storage formulation below P_c. This is not the case using sodium oleate and EtOH or 1,5-pentanediol as cosurfactant. For these systems, fresh formulations have to be used in technical processes.

Volatile stability of the formulations

In the sustainable microemulions, 1-pentanol was first replaced by EtOH. As described above, EtOH has a high vapor pressure even at room temperature, i.e. 5.760 kPa [231]. This is not only a problem because of the permanent change of the compositions during evaporation but also because of the formation of dangerous flammable EtOH vapour. The flash point of EtOH is even less than ambient temperature ($16 - 17\,^{\circ}C$). To avoid this problem, 1,5-pentanediol was used in replacement, which has a very low vapour pressure, i.e. $5.5 \cdot 10^{-4}$ kPa [232]. For a better visualisation of the evaporation, thermogravimetric measurements were performed. The mass of samples with the same compositions differing only by the cosurfactant (EtOH or 1,5-pentanediol) was recorded over 24 h at $32\,^{\circ}C$. In Figure III.13 the evolution of the mass as function of time is shown. Substracting the masses of water, DBE and EtOH from the total mass, corresponds to a loss of weight of 85 %. This correlates very well with the 15 % of total mass left in the sample derived from TG measurements. A different picture occurs for the system with 1,5-pentanediol. From the TG experiment 40 % of the original mass remains. The calculated loss of mass, assuming that only water and the DBE evaporate, is 44 %. This value is again in good agreement with the experiment.

III.1.2.4. Conclusion

In this chapter, the possibility of formulating fully and highly water dilutable microemulsions is shown. DBEs were used as apolar phase, SDS or sodium oleate as surfactant and 1-pentanol, EtOH or 1,5-pentanediol as cosurfactant. Using SDS, the acidic pH value prevents the degradation of the DBEs in the systems at any water content.

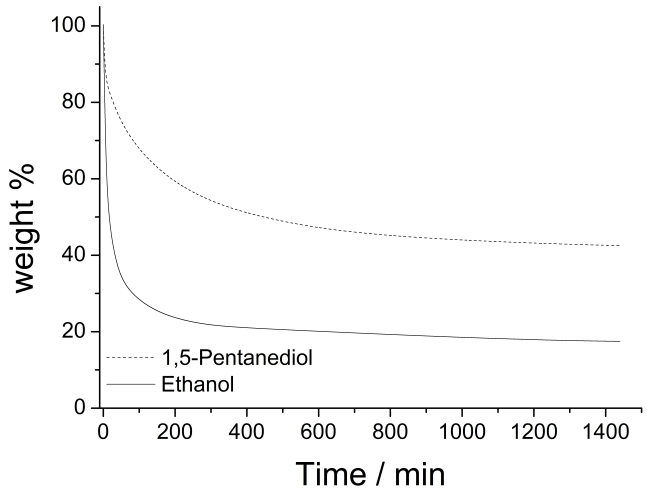

Figure III.13.: Loss of mass of single phase formulations obtained with TGA at constant temperature of 32 °C. The two samples have the same compositions except the nature of the cosurfactant and are chosen to be on path *a* in Figure II.2 b) with a water mass fraction of 0.4. The surfactant was sodium oleate and the DBE was a melt of DMS and DEA with $R_{DMS/DEA}$=3:2.

In the presence of sodium oleate and 1-pentanol, the stability of DBEs is only favoured at water concentrations lower than P_c. By contrast, an instability of the DBEs was observed even at the lowest possible water concentration to obtain single phase areas in the systems water/sodium oleate/EtOH or 1,5-pentanediol/DBE. This instability can be linked to the nearly immediate formation of water nano-droplets. It can be inferred that a significant amount of free water molecules, i.e. not involved in hydration processes, drives the systems to the formation of water clusters responsible for the hydrolysis of the esters. On the other hand, the use of 1,5-pentanediol as cosurfactant gives a better thermical stability of the formulation because of its lower volatility compared to EtOH.

III.1.3. Highly water dilutable green microemulsions

III.1.3.1. Abstract

In the last two sections, it was possible to replace sodium dodecyl sulfate as surfactant by sodium oleate and several possibilities for green and/or sustainable oils were given to formulate microemulsions. In the following part, the first time highly water dilutable completely green microemulsions are presented. For the investigations, the model system water/sodium oleate/citronellol/limonene was used. Herein, sodium oleate is the surfactant and citronellol the cosurfactant. The optimal surfactant-to-cosurfactant mass ratio is found to be 1:1. By replacing successively citronellol with EtOH the homogeneous single phase can be extended. At first, an anti-percolative behaviour of the system was obtained that could be converted into a percolative one. For low EtOH content microemulsions remain of w/o type. With increasing EtOH, between 30 and 90 wt% of EtOH in the blend, the monophasic region is diminished whereas liquid crystalline phases (lamellar and mixed lamellar and cubic ones) extend in the water-rich area. Above 90 wt% the realms of existence of microemulsions are increased again and bicontinuous structures and oil-in-water (o/w) microemulsions were found. For a certain percentage of EtOH (92.5 wt%) in the blend with citronellol and a surfactant+cosurfactant-to-oil ratio equal to or higher than 4:1 a highly water dilutable concentrated microemulsion is formed which can incorporate 99 wt% of water. By adding water rapidly to the water-rich areas of this system, thermodynamically unstable translucid nanoemulsions can occur, which turn into transparent microemulsions with time.

III.1.3.2. Introduction

Applications of microemulsions can be found in several industrial fields, e.g. in cosmetic [135, 136], pharmaceutical [139–141], food [233–235], etc., due to the high solubilisation capacity of hydrophilic and lipophilic compounds [112]. Especially

flavours and perfumes are important active-ingredients in cosmetics, pharmaceutics and foods and beverages, where the behaviour of fragrance molecules and the potential interaction with surfactants in mE systems is important. Only a few articles deal with the distribution of the perfume molecules between the aqueous and micellar phase [236] or with the distribution within micelles [237]. Recently, Tchakalova *et al.* investigated the formation of mixed surfactant-cosurfactant films of fragrances using the hydrophilic-lipophilic deviation (HLD) quantified with the Equivalent Alkane Carbon Number (ECAN) [238]. They found a classification of the chemicals using their property of forming mixed surfactant-cosurfactant films according to their chemical functionalities following the order alcohols $\geq$ aldehydes $\geq$ terpenes $\geq$ aromatics $\geq$ alkanes. Further, it could be confirmed that primary alcohols have a high interfacial solubility and play the role of cosurfactants.

Flavours and perfumes have already been extensively used in the formation of biocompatible microemulsions [239–248]. Especially microemulsions with the citrus oil limonene can be found in literature [243, 247, 249, 250].

In the following the realms of existence of the microemulsions in the system water/sodium oleate/citronellol/limonene are studied by making pseudo ternary phase diagrams (PTPD) and through conductivity measurements. The long time stability of the system is checked with dynamic light scattering experiments. All used components are either from natural origin or are derived from natural sources. Citronellol, found in the oils of roses or geraniums, is an acyclic oxidised terpene, and as a primary long alcohol it can be considered as cosurfactant. Limonene is a cyclic monoterpene produced from renewable feedstock and the major constituents of citrus oils [182]. Limonene itself is one of the most commonly used perfume molecules or active substances in technical and fine products [183, 184]. Sodium oleate, a

colour- and odourless classical soap from animal and vegetable fats and oils, classified by the Food and Drugs Administration (FDA) as food additive (E470) [251], is used as surfactant. Further, the effect of adding a short chain alcohol (EtOH) to the system is investigated. The addition of alcohols or glycols to surfactant systems is frequently used to influence the extent and the internal structures of microemulsions [252–256]. The aim is to formulate a fully or at least highly water dilutable microemulsion where water can be added in any amounts without phase transition [257–260]. The great advantage of fully or highly water dilutable microemulsions is the fact that they allow a very good dispersion of active in a huge volume of water. Though several papers can be found dealing with solubilising essential oils in microemulsions or micellar systems [233, 261–263] fully dilutable systems with fragrances are rarely reported. For the first time, low toxic and highly water dilutable microemulsions are presented using a long chain natural alcohol like citronellol as cosurfactant and a short chain natural one like EtOH.

III.1.3.3. Results and discussion

III.1.3.3.1. Phase diagrams

At first, a mass ratio surfactant-to-cosurfactant, called ζ, was determined to obtain the largest area of microemulsion. For this purpose, experiments were carried out following path b* (denoted in Figure II.2 a)) of the PTPD of the system water/ sodium oleate/citronellol/limonene. As mentioned before, path a* represents the part of path b* within the microemulsion area. The starting point was a mixture of sodium oleate, citronellol as amphiphilic pseudo-phase and limonene with $R_{S/O}$=3:2. Water was then added progressively. The results for the different ζs (1:2, 1:3, 1:4 and 1) are shown in Figure III.14 a). The largest area is obtained with ζ=1 with approx. 35 wt% of water solubilised in the system. The PTPD was recorded with

this ratio. As shown in Figure III.14 b), the realms of existence of the microemulsion are restricted to the oil-rich and surfactant/cosurfactant-rich area.
In the next step, instead of pure citronellol as cosurfactant a melt of citronellol and EtOH was used to enlarge the microemulsion area and to increase the water solubility. The percentage of EtOH in the EtOH-citronellol mixture (cosurfactant blend) is called β_{EtOH}. Experiments were again carried out following path b* from Figure II.1 a) with ζ=1. The results are shown in Figure III.14 c). The first boundary is always between 10 and 15 wt% of added water. A possible explanation is that this is the minimal amount of water which is necessary to hydrate sodium oleate. The weight fraction of sodium oleate is the only constant in every experiment. At around 10 wt% of water, sodium oleate is dissolved and a homogeneous single phase is formed. In Figure III.14 c) three parts can be discerned with respect to the amount of EtOH in the cosurfactant melt. In the region with low content of EtOH, $0 \leq \beta_{EtOH} \leq 0.25$, a continuous enlargement of a* is observed with increasing percentage of EtOH. In presence of an intermediate percentage of EtOH, $0.3 \leq \beta_{EtOH} \leq 0.9$, a* is again very limited and large zones of liquid crystals (LC) appear. The presence of LC can be attributed to a greater hydration of the interfacial film. This prevents the penetration of the surfactant headgroup into the oil phase. Another aspect is the insufficient amount of EtOH to separate the citronellol and sodium oleate molecules to make the interfacial film more flexible. At β_{EtOH}=0.925, a* has its largest extent. At even higher values of β_{EtOH}, the path a* shrinks again. At β_{EtOH}=0.925 enough EtOH is in the system to reduce the interfacial rigidity and to favour the formation of bicontinuous microemulsions. With this β_{EtOH} it is possible to formulate a highly water dilutable microemulsion using another experimental path (see Section III.1.3.3.3). To confirm the "expected" formation of microemulsions DLS measurements were performed. Already at the lowest amount of water necessary to form

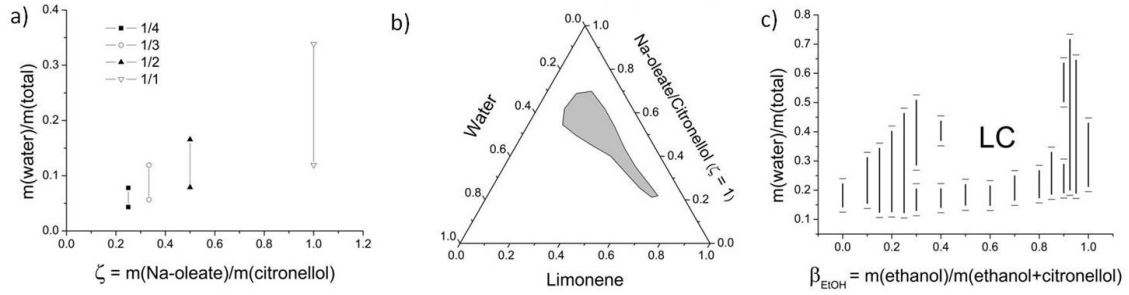

Figure III.14.: a) 2-dimensional representation of path b* of the system water/sodium oleate/citronellol/limonene with different ζ values. The black lines correspond to the extension of a*. The longest line is obtained for a 1:1 mixture of sodium oleate-to-citronellol. b) With ζ=1 a PTPD was recorded. The microemulsion is situated only in the oil- and surfactant/cosurfactant-rich area. The microemulsion region is presented in grey. c) The water solubility in the system water/sodium oleate/EtOH/citronellol/limonene (ζ=1) for different β_{EtOH} is plotted. The black lines represent again a*.

single phases correlation functions were obtained. They become more significant with the addition of more water. The results are presented in the Appendix.

III.1.3.3.2. Conductivity

Depending on β_{EtOH}, the microemulsions show different behaviours of the specific conductivity κ with increasing amount of water (see Figure III.15). Again, three areas can be distinguished, as already shown in Section III.1.3.3.1, namely for low, intermediate and high amounts of EtOH. For pure citronellol κ does not change at all and stays at almost 0 mS.cm^{-1}. The interfacial film is too rigid and prevents the micelles to merge. The solution consists of discrete water droplets within a continuous oil phase. This well-known behaviour can be explained with an anti-percolation model [134]. For β_{EtOH}=0.25 a bell-shaped curve is observed. But the values are still very low and do not exceed 0.3 mS.cm^{-1}. At low water content κ starts to increase with water addition showing a percolative behaviour. After reaching a maximum, at higher amounts of water, κ drops down to almost 0 mS.cm^{-1} again, indicating an anti-percolative behaviour. At intermediate concentration of water a certain contri-

bution of EtOH molecules to the interfacial film can be assumed. With the addition of water nearly no EtOH molecules participate in the interfacial film.

In the second region with intermediate amounts of EtOH, $0.3 \leq \beta_{EtOH} \leq 0.7$, there is a progressive increase in specific conductivity with increasing amounts of water. At the percolation, the w/o droplets form nano-clusters favourable to the sodium ion mobility, which is an indication for a more flexible interfacial film. In the last area , $\beta_{EtOH} \geq 0.9$ a deviation from the linearity is observed for higher water content. This has been ascribed to the formation of bicontinuous structures, generally observed before the pseudo-phase inversion [131, 195]. After reaching a maximum with the slope equal to 0, the slope becomes negative, which is related to a phase inversion and the presence of an o/w microemulsion. The decrease of the conductivity is related to further dilution of the charge in the water pseudo-phase. In Figure III.15 b) a schematic representation of the appearing microstructures as inferred from the conductivity results is shown. Only in the EtOH-rich area the formation of bicontinuous structures and o/w microemulsion is possible, which can be explained by the less rigid interfacial film due to the intercalation of EtOH.

III.1.3.3.3. Towards a highly water dilutable microemulsion

From Figure III.14 c) it can be deduced that the largest a* zone can be obtained with β_{EtOH}=0.925 with a maximum amount of 73 wt% of solubilised water in the system. In Figure III.16 the PTPD of this system water/sodium oleate/citronellol/EtOH/ limonene is plotted with ζ=1 and β_{EtOH}=0.925. In comparison to Figure III.14 b) the microemulsion area is largely extended, with a small LC region inside. A realm of existence of the microemulsion can be denoted starting at very low water concentrations, not crossing LCs and ending up in the water corner. Line A is comprised in that area starting from very low water content with a surfactant-to-cosurfactant

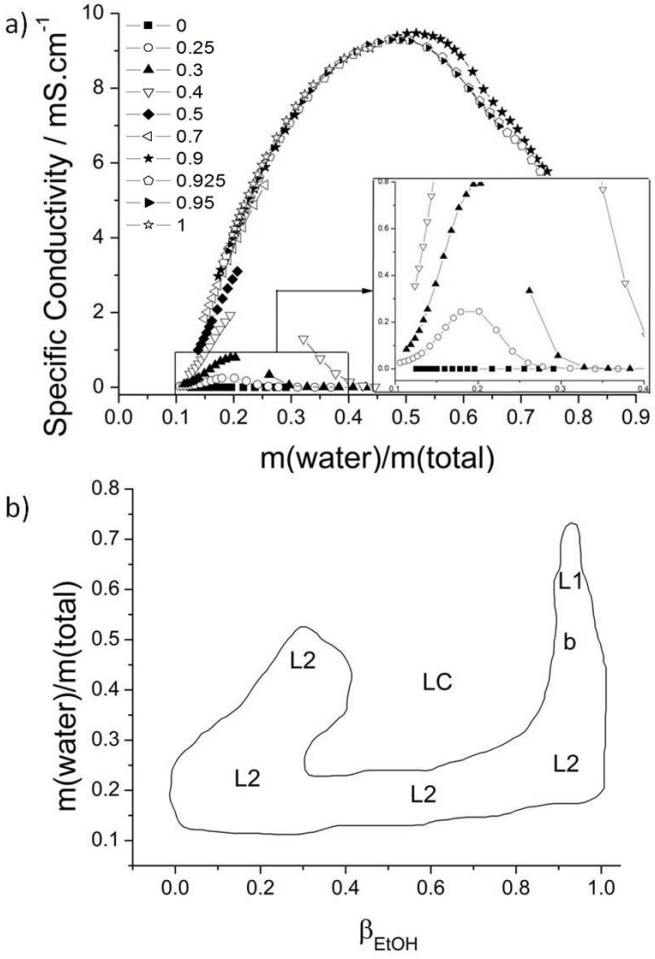

Figure III.15.: a) The specific conductivity κ of the microemulsion is plotted against the amount of added water for several β_{EtOH} values in the system water/sodium oleate/EtOH/ citronellol/limonene with ζ=1. All experiments were recorded at 25 °C. b) Schematic representation of the results of the conductivity measurements. The microstructures of the microemulsion at different β_{EtOH} values are shown. L2 corresponds to a w/o, L1 to an o/w microemulsion, and b to bicontinuous structures.

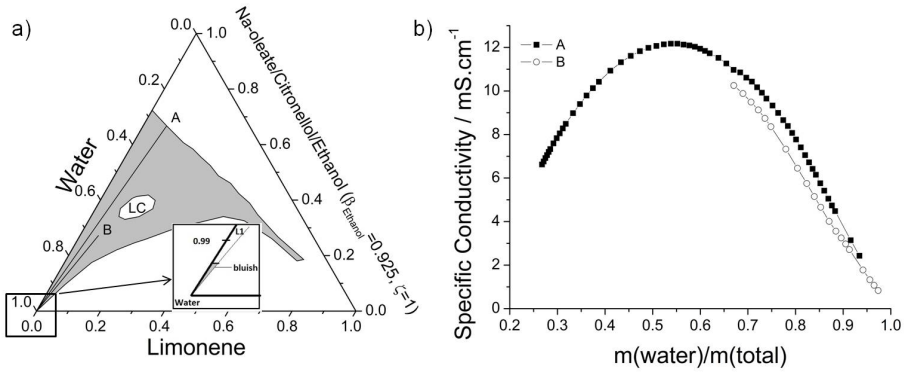

Figure III.16.: a) PTPD of the system water/sodium oleate/EtOH/citronellol/limonene (ζ=1, β_{EtOH}=0.925) at 25 °C. A highly water dilutable microemulsion is obtained for a surfactant+cosurfactant-to-oil mass ratio larger than 4:1. The magnification shows the water-rich area where the solutions are no longer clear but turn bluish. b) Specific conductivity as a function of added water for experimental paths A and B.

mass ratio of 9:1. The specific conductivity along this line is shown in Figure III.16 b). The system shows a percolative behaviour. The w/o microemulsion passes into an o/w microemulsion crossing a bicontinuous structure. In order to analyse the highly water dilutable area another experimental path was studied. In Figure III.16 a) line B is represented within the water-rich region. As in the experiment of path A, the conductivity was measured as a function of water content (Figure III.16 b)). As κ is monotonously decreasing with increasing amount of water, the microemulsion can be attributed to the o/w type. Two phenomena were observed when diluting samples along path B. When water is added slowly, no phase transition occurs and the solutions remain homogeneous and clear. In contrast, by adding water rapidly, the solutions become opalescent. After a long time period the solutions return to the initial clear and homogeneous state. For a better understanding of this behaviour the droplet sizes as a function of time and preparation method were measured using DLS. The two processes of dilution, (1) one-time dilution and (2) progressive dilution, are shown in Figure III.17 a). In process (1) the starting droplet size was approx. 3 nm. After the addition of water it raised up to more than 100 nm and remained almost stable for 90 min. After 2 h a sharp decrease appeared down to an

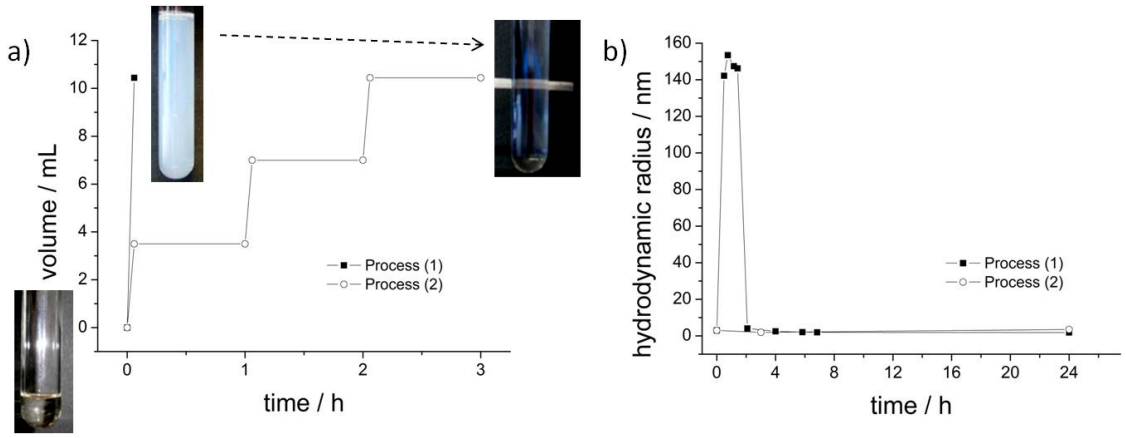

Figure III.17.: a) The two processes of dilution are presented. (1) stands for a rapid addition of water and (2) for a slow and progressive one. The experimental path B is shown in Figure III.16. b) Hydrodynamic radii as a function of relaxation time after dilution. (1) shows a drastic increase of the droplet size after water addition. After approx. 4 h a sharp decrease occurs ending up at the initial radius. For process (2) no change in size can be obtained.

average size of 4 nm. Finally, an overall size of 1.8 nm was obtained after more than 24 h. In contrast, at process (2) the same amount of water was added in distinct proportions after waiting 1 h between each addition. The final size of the droplets was 1.9 nm in this case, which was more or less the same as in process (1). This difference between the two processes was observable with the naked eye as well. In process (1) the clear and homogeneous solution turned bluish with a white appearance after the addition of water. With time, it became more and more transparent ending up with a completely clear solution. On the contrary, the sample following process (2) was clear during the whole period of time.

Two different stability phenomena face each other. On the one hand process (1) is first kinetically stabilised due to a slow setting up of the thermodynamic equilibrium which is attained after several hours. The different solubility of the two cosurfactants has a significant effect. With the quick addition of water EtOH molecules from the interfacial film will be dissolved preferentially in the water phase. Cit-

ronellol with its relatively low water solubility stays in the film. This results in a super-saturation of the water continuum with EtOH. In this non-equilibrium state, EtOH molecules are missing at the interface corresponding to a smaller β_{EtOH}. The droplets start to merge ending up at sizes comparable to nanoemulsion systems. No phase separation occurs due to a kinetic stability of these nanoemulsions. After a certain period of time, EtOH molecules start to equilibrate between the water phase and the interfacial film. As a result, the system comes back to more or less the original concentration of EtOH molecules in the interface and the microemulsions form again. By contrast, the thermodynamic equilibrium is reached faster with slow and progressive addition of water to the system, because less EtOH molecules are dissolved in the water continuum. A comparable phenomenon was observed by Gutiérrez *et al.*, where different dilution procedures were investigated in order to form nanoemulsions [264].

A total percentage of over 99 wt% of water can be incorporated before it turns bluish. Even after several days it did not come back to complete translucence. The formation of vesicles is assumed. This behaviour has already be shown in literature for systems containing fatty acids [265, 266]. With DLS a hydrodynamic radius of approx. 120 nm is obtained.

III.1.3.4. Conclusions

The addition of a short chain cosurfactant like EtOH has significant effects on the formulation of microemulsions. It is possible to transform an anti-percolative system with a rigid interfacial film with only a minor ability of solubilising water in the microemulsion into a highly water dilutable percolative system with a flexible film. This observation allows to formulate a green highly water dilutable microemulsion. All components are either natural products or can be obtained from natural re-

sources. In contrast to the huge literature about mixed surfactant systems, only few papers contain information about mixed cosurfactants. EtOH has the particularity to partition between the three occurring pseudo-phases: the water-rich, oil-rich and the surfactant/cosurfactant-rich one. This behaviour of EtOH results in a higher sensitivity of the systems to external influences, like the rapid or slow addition of water. The optimised choice of the presented ingredients makes these microemulsions directly applicable in the flavour and perfumery industries. With citronellol as often used fragrance, not only the oil phase (limonene) but even the cosurfactant can be considered as active material. What is more, EtOH is often used as basis in cosmetic industry. So except sodium oleate, all ingredients can be considered as active materials.

III.1.4. The extension of microemulsion regions by combining EtOH with other cosurfactants

III.1.4.1. Abstract

In the previous section, the extension of the microemulsion area towards highly or fully water dilutable systems by adding a short chain alcohol as cosolvent, like EtOH, to the system water/sodium oleate/citronellol/limonene was shown. It was possible to convert an anti-percolative system to a percolative one by making the interfacial film more flexible. The question arises if this is a general concept. For this reason, pseudo-ternary systems water/surfactant/cosurfactant/EtOH/oil with different cosurfactants (1-pentanol, 1-heptanol, dodecanol, Guerbet alcohols) and FAME-rapeseed biodiesel as oil phase were investigated. Sodium oleate was used as surfactant. EtOH was added as cosolvent to enhance the film flexibility and so to increase the microemulsion area. With increasing hydrophobicity of the cosurfactants and the oil and without further addition of EtOH, only very restricted single phase areas were obtained. However, with a certain amount of EtOH, sodium oleate, and 1-heptanol a distinct path towards the water-rich corner was found. By replacing 1-heptanol by Guerbet alcohols this extension was lost and monophasic areas only in the surfactant-rich region were preserved. For all systems a limited "optimal" formulation was obtained for a specific percentage of EtOH in the EtOH-cosurfactant blend. With dynamic light scattering the homogeneous single phase areas were checked to distinguish real solutions from microemulsions. The nano-structure and film flexibility was investigated using electrical conductivity measurements. In the choice of the solvents, sustainable ones were used.

III.1.4.2. Introduction

Already in 1955, Bowcott and Schulman stated that their microemulsions needed alcohols (often short or mid-chain ones [53]) as cosurfactants [54]. A short chain

cosurfactant/cosolvent helps to avoid rigid structures such as gels, precipitates, and liquid crystals (LC), and to extend the microemulsion area [267], and can be considered as hydrotrope. In other words hydrotropes are included to fluidise the interfacial surfactant film and to provide further reduction in surface tension [268]. It is well-known that this effect can expand the area of existence of microemulsion systems [53, 269]. The influence of different alcohols on microemulsions has been studied intensively [270]. Healy and Reed [271] showed that the addition of alcohols causes dramatic changes in phase behaviour and reduces the system viscosity significantly, but the authors did not give a reasonable explanation. Stilbs and Lindman [53, 272] investigated the effect of alcohol length on microemulsion systems with NMR by determining self-diffusion coefficients. Bourrell *et al.* discussed in details the impact of alcohols as cosurfactants on the solubilisation by amphiphilic systems and concluded that the separation or at least the perturbation of the surfactant molecules at the interface is a method to achieve a reduction of the surfactant molecular interactions [273]. A thermodynamical study of droplet-type microemulsions containing cosurfactants was presented by Overbeek *et al.* [274]. He stated that the surfactant and cosurfactant are both adsorbed to saturation, and reduce the interfacial tension nearly to zero.

In the last section, a concept for the use of alcohols as cosurfactants in formulating microemulsions with ionic surfactants was presented and the investigation of the phase behaviour was studied in details. The addition of a short chain alcohol as cosolvent in presence of a long chain cosurfactant (citronellol) offered a way of extending the single phase area to obtain fully or highly water dilutable microemulsions. In this part, an illustration and analysis of the reason of the limitations of this concept with several cosurfactants in presence of a hydrophobic FAME-rapeseed biodiesel is reported. Further, a guideline for formulating a multiple component mi-

croemulsion containing water, biodiesel, a surfactant and cosurfactant mixture and a cosolvent is given. As short chain cosurfactant 1-pentanol was used and as long chain cosurfactants hydrophobic alcohols, 1-heptanol, dodecanol and the so called Guerbet alcohols, were used. In the Guerbet reaction primary aliphatic alcohols are converted into their β-alkylated dimer alcohols with loss of one equivalent of water. Because Guerbet alcohols are primary branched alcohols with a high molecular weight, they exhibit several advantageous properties. They are low in volatility, useful as superfatting agents, good lubricants and have low irritation potential [275]. But the preeminent advantage of Guerbet alcohols is their low melting point compared to linear saturated and unsaturated alcohols with the same carbon chain length [276].

III.1.4.3. Results and discussion

III.1.4.3.1. Phase diagrams

It has already been shown that n-alkanes can be easily replaced by more sustainable and less toxic alternatives (see Section III.1.1). SDS was used as surfactant and 1-pentanol as cosurfactant with a surfactant-to-cosurfactant mass ratio, called ζ, of 1:2. In the preceding section, SDS has already been replaced by sodium oleate and 1-pentanol by citronellol with limonene as oil phase. The extension of the microemulsion area by addition of EtOH was shown. Here, a general the concept of extending the homogeneous single phase by reducing the interfacial film rigidity with the addition of EtOH is given. The hydrophobicity of the cosurfactant was increased and a more hydrophobic oil (biodiesel) was used. Figure III.18 shows the results for the system water/sodium oleate/biodiesel and the most hydrophilic cosurfactant used, 1-pentanol. For a better understanding of the role of the cosurfactant, the value of ζ was varied (Figure III.18 a) ζ=1:2, Figure III.18 b) ζ=1:1). The higher

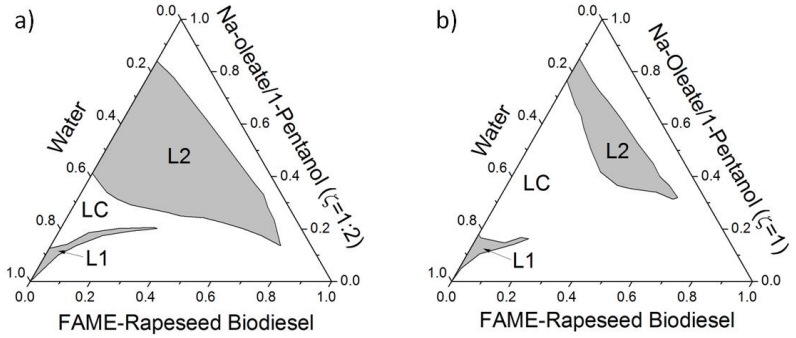

Figure III.18.: PTPDs of the system water/sodium oleate/1-pentanol/biodiesel with a) ζ=1:2 and b) ζ=1 at 25 °C. The grey areas represent the homogeneous single phase regions. The white ones consists of liquid crystals (LC), emulsions or not fully dissolved surfactant.

amount of 1-pentanol, which is a short chain alcohol and hence very flexible, makes the interfacial film itself more flexible and increases the single phase area. This allows the water droplets to merge and to incorporate/solubilise more water. In the next step the cosurfactant was replaced by 1-heptanol which is a more hydrophobic and rigid one. For a faster screening of ζ a two-dimensional representation was chosen as described in the experimental section. The longest a* was obtained for ζ=1. With this "optimal" ratio the PTPD was recorded. This formulation produced only two small single phase areas in the surfactant-rich region. That can be explained by the fact that 1-heptanol is a longer alcohol and may not be as efficient as cosurfactant as 1-pentanol. Further, the flexibility of the interfacial film is not low enough to let the droplets merge. To extend this region the concept of adding EtOH was adpted. Again, the best value for β_{EtOH} (the mass fraction of EtOH in the EtOH-cosurfactant blend), which means the longest a*, was determined as described above. β_{EtOH} values from 0 to 1 were used. From 0 to 0.4 the length of a* did not increase and only around 8 wt% of water can be solubilised. At around 0.5 the length of a* started to increase until 0.7. Only for β_{EtOH} values of approximately 0.7 highly dilutable systems were found. For values higher than 0.7, the a* value started to decrease again. The measurements were performed following path b*

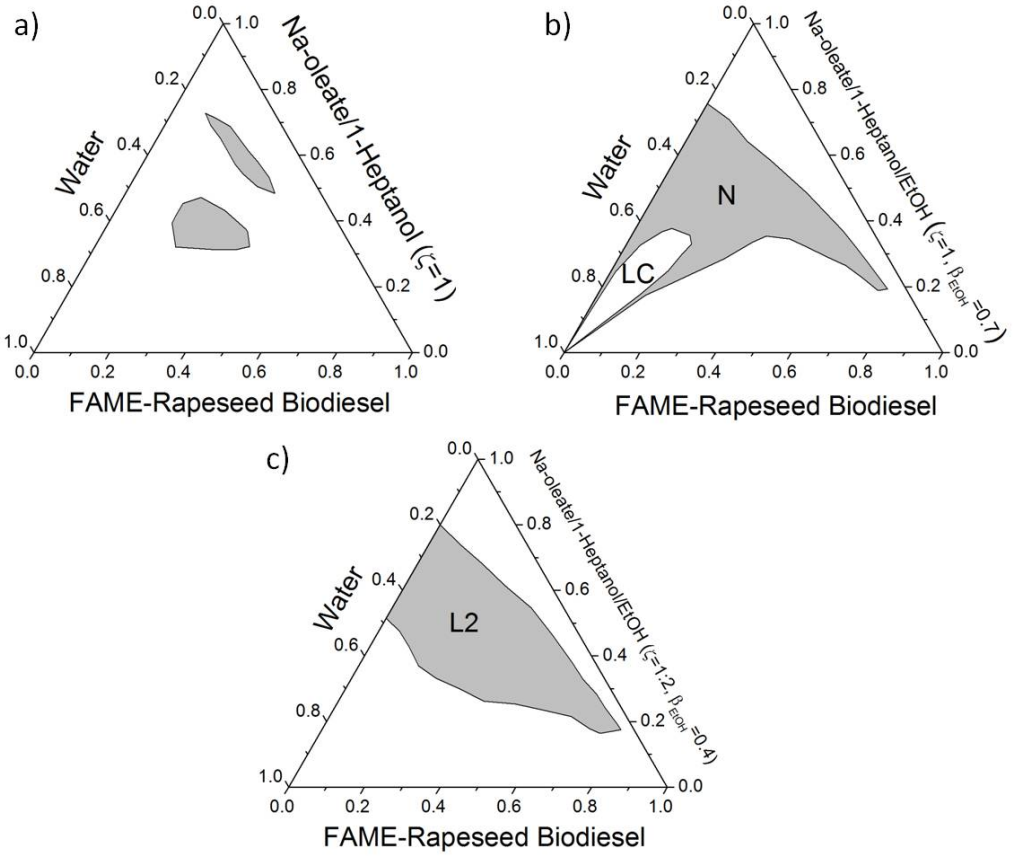

Figure III.19.: PTPDs for the systems water/sodium oleate/cosurfactant/biodiesel with a) 1-heptanol (ζ=1) b) a mixture of 1-heptanol and EtOH (ζ=1, β_{EtOH}=0.7) and c) a mixture of 1-heptanol and EtOH (ζ=1:2, β_{EtOH}=0.4) as cosurfactant recorded at 25 °C. The homogeneous areas are represented in grey. The white ones can correspond to emulsions, LCs, undissolved surfactant etc.

(Figure II.2 a)). With ζ=1 and β_{EtOH}=0.7 a PTPD was recorded and a highly water dilutable system was obtained. However, the very distinct path stretching to the water-rich corner is very narrow. For this reason and because of the technical grade of the surfactant and biodiesel the reproducibility was poor according to be batch of the used products. Figure III.19 a) and b) show the described PTPDs. Figure III.19 shows another PTPD for the system water/sodium oleate/1-heptanol/EtOH/ biodiesel with ζ=1:2, and β_{EtOH}=0.4. A principle known for a long time and stated and proven in Section III.1.1 is that the mixture of two oils with different numbers of

carbon atoms will produce an oil analogue with a number of carbon atoms being the average of the two oils used as mixtures. By mixing 1-heptanol and EtOH at a ratio of β_{EtOH}=0.4 an average carbon atom number of five is produced. When the PTPD obtained with 1-pentanol as cosurfactant (see Figure III.18 a)) is compared with the one in Figure III.19 c), they look very similar. The only difference is the loss of the small appendix in the water-corner. This can be attributed to the partition of the components in the pseudo-phases due to their hydrophobicity. As described above, 1-pentanol is hydrophilic and flexible enough to allow the solubilisation of a high amount of water. On the other hand, though the mixture of 1-heptanol and EtOH mimics 1-pentanol, 1-heptanol is too hydrophobic and rigid to form the L1 phase at high water content.

In the next step, the pharmaceutically acceptable dodecanol was used to substitute 1-heptanol in the formulation of environmentally acceptable microemulsions. Only for the β_{EtOH} values 0 and 0.4 homogeneous single phase systems were obtained. But due to the relatively high melting point of dodecanol, precipitation occurred after few days. To avoid this precipitation but still to use long chain alcohols as cosurfactant the so called Guerbet alcohols were used. These alcohols are low toxic and green cosurfactants with relatively low melting points. For this reason Isofol 12, 14T, 16 and 20P were used as cosurfactants in the system water/sodium oleate/ cosurfactant/EtOH/biodiesel with ζ=1. The same procedures were applied as described above. First the best β_{EtOH} value was determined and then the PTPDs were recorded. In Figure III.20 the results are shown. Again, only at the oil and surfactant-rich area a single phase region was obtained. The same explanation holds for the heptanol system. At high water content the different partition of the two alcohols limited the extention of the microemulsion area.

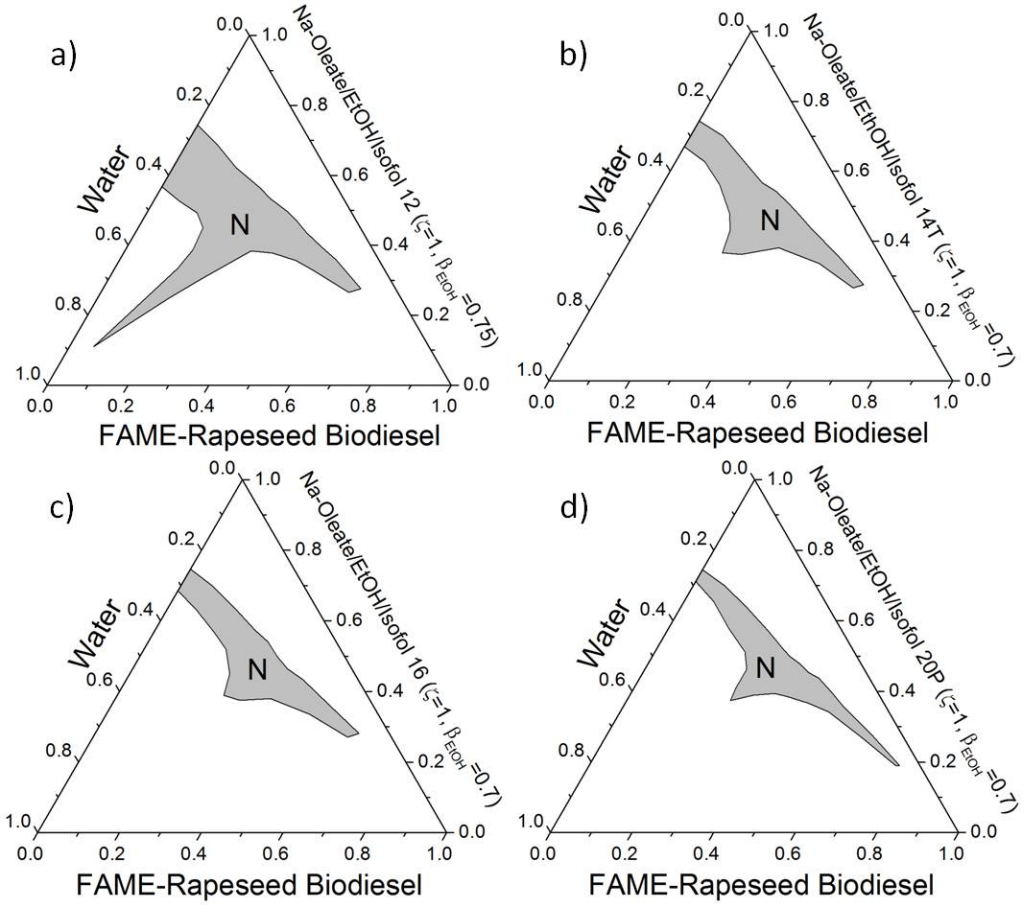

Figure III.20.: Influence on the phase behaviour of the systems water/sodium oleate/ cosurfactant/EtOH/biodiesel by using longer chain cosurfactants like Isofol a) 12, b) 14T, c) 16 or d) 20P. The diagrams were recorded at 25 °C. The grey areas represent the homogeneous single phase regions. The white ones can correspond to emulsions, LCs, undissolved surfactant etc.

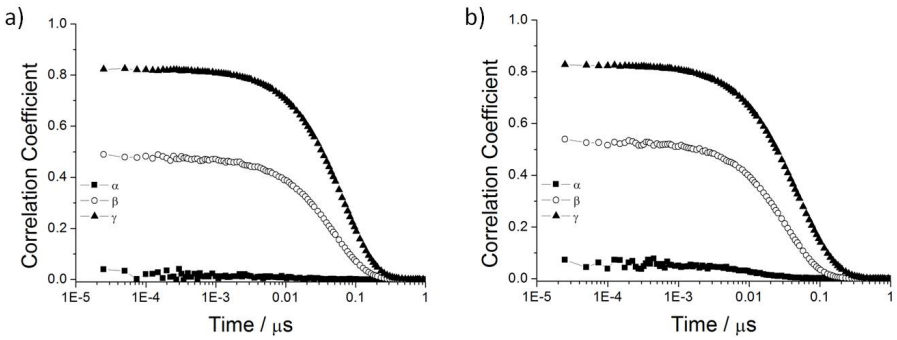

Figure III.21.: Time-dependent self-correlation functions as obtained by DLS of the systems a) water/sodium oleate/1-pentanol/biodiesel with ζ=1:2 and b) water/sodium oleate/EtOH/ 1-heptanol/biodiesel with ζ=1:2 and β=0.4. The experimental path was a* from Figure II.2. The points α, β and γ have always the same mass fractions of water (0.10, 0.25, and 0.42 respectively).

III.1.4.3.2. Dynamic light scattering

The overall structure of the homogeneous single phase areas was investigated with DLS measurements. In Figure III.21 a representative example of the results is shown. The correlation functions of compositions on path a* (Figure II.2) are presented for the systems water/sodium oleate/1-pentanol/biodiesel with ζ=1:2 and water/ sodium oleate/EtOH/1-heptanol/biodiesel with ζ=1:2 and β_{EtOH}=0.4 can be seen. The correlation functions get more significant the more water is added. This was also the case for all the other systems investigated in the present study. A significant amount of water has to be added before structures are formed. As already stated above these two systems look very similar at the macroscopic scale. From the DLS measurements the structure seems to be similar as well. In the next part further investigations concerning the nano-structure are shown.

III.1.4.3.3. Conductivity

In this paragraph the nano-structure and the film rigidity of the systems mentioned

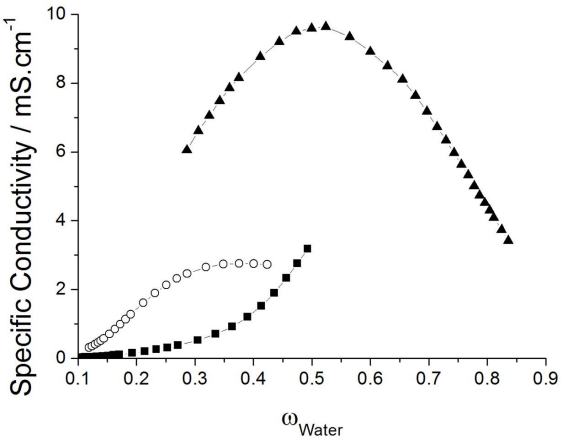

Figure III.22.: Specific conductivity as function of the water content ω_{Water} for the systems water/sodium oleate/1-pentanol/biodiesel (ζ=1:2) (■), water/sodium oleate/1-heptanol/ EtOH/biodiesel (ζ=1:2, β_{EtOH} = 0.4) (○) and water/sodium oleate/1-heptanol/EtOH/ biodiesel (ζ=1, β_{EtOH} = 0.7) (▲) at 25 °C.

above were investigated with the help of conductivity measurements. Figure III.22 shows the results for the systems water/sodium oleate/1-pentanol/biodiesel ζ=1:2, water/sodium oleate/1-heptanol/EtOH/biodiesel (ζ=1:2, β_{EtOH} = 0.4) and water/ sodium oleate/1-heptanol/EtOH/biodiesel (ζ=1, β_{EtOH} = 0.7). The system water/ sodium oleate/1-pentanol/biodiesel ζ=1:2 (■) shows a significant increase of the κ value typical of a percolative behaviour. The curve is only interrupted by the occurrence of liquid crystalline (LC) phases. As described above, 1-pentanol is a short chain alcohol that can form flexible interfacial films. With increasing amount of water the droplets can merge and form clusters with an undisturbed transport of charge carriers. In contrast, when 1-pentanol is replaced by the "pseudo-component" EtOH and 1-heptanol with β_{EtOH} = 0.4 with an average number of carbon atoms of five, which produces a similar PTPD (see Figures III.19 and III.20), conductivity shows a completely different behaviour. It is more anti-percolative. At first, the conductivity increases with the addition of water but reaches a maximum very quickly. Again, the curve is interrupted by the formation of LCs. But at very high water concentration no L1 phase appeared. This behaviour shows the limitation of

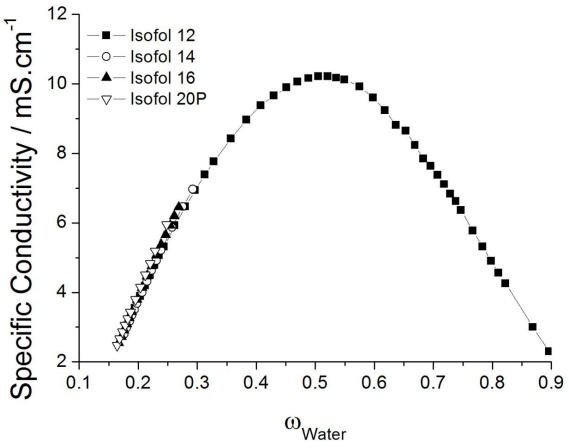

Figure III.23.: Conductivity curves for the systems water/sodium oleate/EtOH/biodiesel and Isofol 12 (■), 14T (○), 16 (▲) and 20P (△) at 25 °C.

the concept. The mixing of two components to obtain an intermediate behaviour, as shown in previous sections, works only to a certain extent. In a macroscopic way, by comparing the overall shape of the diagrams, it works quite well. But when two components are used with a large difference in hydrophobicity the different distribution of the two molecules plays an important role. At high water concentration the partition of EtOH and 1-heptanol in the polar and apolar phase is the crucial factor. EtOH is more dissolved in water now than in the interfacial film which makes it more rigid. The third curve (▲) corresponds to the system water/sodium oleate/ 1-heptanol/EtOH/biodiesel (ζ=1, β_{EtOH} = 0.7). Here, a percolative behaviour is observed. The amount of EtOH is high enough to form a highly water dilutable microemulsion with a flexible film. Though, EtOH is dissolved in the water phase at high water concentrations, still EtOH molecules are left to insert in the interfacial film. This system transforms from an inverse system via a bicontinuous area to a direct microemulsion. In Figure III.23 the conductivity curves of the systems with Isofol 12 to 20P are shown. It is obvious that these systems are again percolative.

III.1.4.4. Conclusions

In this section a closer look at the concept of adding a short chain alcohol as cosolvent to extend the homogeneous single phase area in ternary or pseudo-ternary systems is presented. As shown in Section III.1.3, this concept seems to be promising. However, as shown in the present paragraph, it seems not to be general enough to obtain always fully or highly dilutable microemulsions. The hydrophobicity of the used components is of great importance. The smaller the gap between cosurfactant and cosolvent, the better the concept works. This is probably related to the different partitions of these two components in the different pseudo-phases (polar-pseudo phase and amphiphilic one). Also the influence of the rigidity and fluidity of the interface is obvious, although the film rigidity is a disputed concept in the scientific community.

III.2. Surfactant-less microemulsions

III.2.1. Structure and solubility in surfactant-free microemulsions

III.2.1.1. Abstract

In this section, the concept of surfactant-less microemulsions is introduced. The system water/EtOH/n-octanol was investigated. At first, the ternary phase diagram was established. In the next step, the structure of the single phase area near the phase boundary was examined with light scattering experiments. With DLS measurements, significant correlation functions were obtained. But, such correlation functions could occur for critical fluctuations as well. So, the results were compared to the ones obtained from static light scattering. From both techniques similar particle sizes were derived. It was possible to prove the occurrence of well defined droplets. Further, visible light experiments were performed to investigate the solubilisation properties of this system.

III.2.1.2. Introduction

Microemulsions are transparent, macroscopically homogeneous, low-viscous one-phase systems consisting of a surfactant component in the form of a molecular film separating a polar from an apolar fluid [39, 40]. Four types of microemulsions were identified by Schulmann (Winsor I, II, III, IV) [42, 46, 51, 116]. Often, also a cosurfactant is necessary. Microemulsions separated by a rigid or fluid interfacial film have profound differences [52]. All these systems are microscopically structured in terms of domains of well defined size, named "swollen micelles". They can be connected and lead to bicontinuous structures, understood as coalesced droplets, connected cylinders or bi-liquid foams. Although they are excellent solubilisers, the drawback is that usually a high amount of surfactant (> 10 wt%) is required to achieve a single Winsor IV phase (microemulsions). Solubilisation is related to

Winsor I and Winsor III equilibria, where oil-rich or water-rich phases separate.

In contrast, over the last three decades and among the more than 10.000 papers dealing with microemulsions, only few papers deal with so-called surfactant-free microemulsions [61, 64, 65, 72–75, 79, 82, 84, 277–281]. However, to the best of our knowledge, there is no direct experimental proof of the presence of domains with well defined size below the optical microscopy resolution. Instead, indirect hints were taken as arguments, for example, the fact that enzymes that normally require interfaces work well in such systems [73, 82, 84, 280, 281] or an unexpected salt specific solubility when used in hydrometallurgy [282].
In the present study, we demonstrate that the combination of SLS and DLS delivers an unambiguous proof that, indeed, well-defined domains of two fluids of clearly different composition can exist in surfactant-free ternary mixtures.

The motivation for this study was initially different. The understanding of the so-called Ouzo effect [89, 91–93, 96] was in the focus of interest. This effect is related to the finding of remarkable fine and time-stable emulsions when water is added above a certain content to a mixture of EtOH and a longer-chain molecule, such as anethole. It was found that the necessary condition for such a phenomenon is the rapid addition of water (or any other solvent) to a second solvent (e.g. EtOH), which is highly or entirely miscible with the first solvent, and a third component (e.g. anethole), that is highly soluble in the second solvent, but not in the first.

During the study of the phase diagrams of such systems, it was discovered that even before the phase separation through the addition of water to a mixture of components 2 and 3 intriguing phenomena occur. In particular, close to the phase separation border, but still within the monophasic region, a remarkable light scat-

tering signal is observed in the single phase domain appearing as a clear solution to the naked eye. Since this is not the well-known Ouzo effect in the two-phase region, which appears as a stable milky emulsion, it is proposed to call this effect "pre-Ouzo" effect, expressing its occurrence before enough water is added to induce the phase separation.

III.2.1.3. Results and discussion

Figure III.24 presents the phase diagram of the ternary system water/EtOH/n-octanol and selected self-correlation functions from DLS with increasing water content. As can be seen in Figure III.24 b) the correlations become more and more pronounced the closer the composition of the ternary system is to the phase separation line. Assuming a spherical symmetry, the deduced radii of the micelles grow with increasing water content, from below 1 nm far away from the decomposition line up to tens of nanometres close to it. It should be noted that this is not a critical phenomenon with large fluctuations close to a critical point. Even relatively far away structures clearly occur, such as points 2 and 3 in Figures III.24 a) and b). DLS results taken alone are not a definitive argument, because only fluctuations in local concentrations are detected and the interpretation of spherical un-connected domains is arbitrary [64, 72, 75]. Therefore, SLS was also performed.

From M_{App} one can deduce a spherical volume (V_{Sphere}), assuming that the density of the micelles is equal to the one of pure octanol (see eq. III.1).

$$V_{Sphere} = \frac{M_{App}}{N_A \cdot \rho_{octanol}} = \frac{4}{3} \cdot \pi \cdot r^3 \tag{III.1}$$

If the assumption of spherical micelles leads to radii in agreement with those inferred from DLS, this is a strong hint to the validity of the presence of well-defined

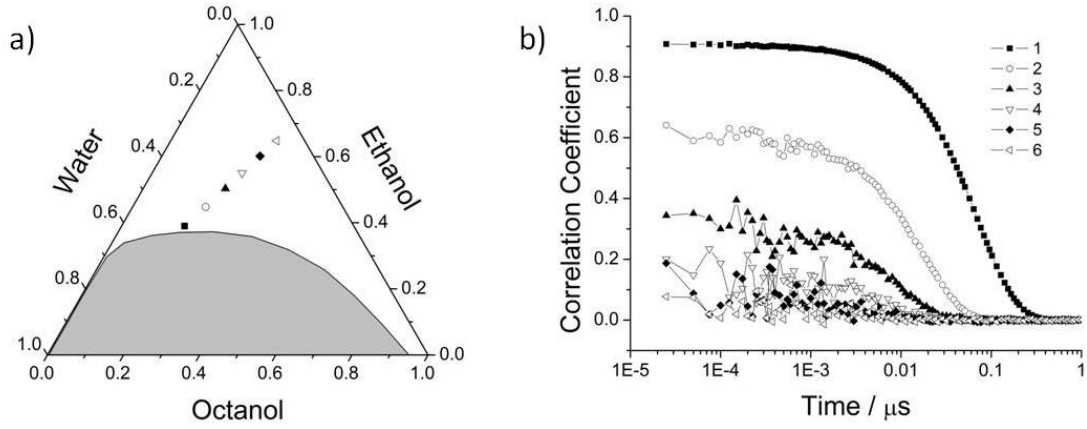

Figure III.24.: a) Ternary phase diagram of water/EtOH/n-octanol mixtures at 25 °C. The white region represents compositions of monophasic, clear, macroscopically homogeneous mixtures (pre-Ouzo region), the dark region compositions of two-phase systems (Ouzo region). Since the tie-lines point towards the water-corner, the grey area is a Winsor-II equilibrium, if the pre-Ouzo region is a structured microemulsion. b) Time-dependent self-correlation functions obtained by DLS. The symbols correspond to the compositions in a).

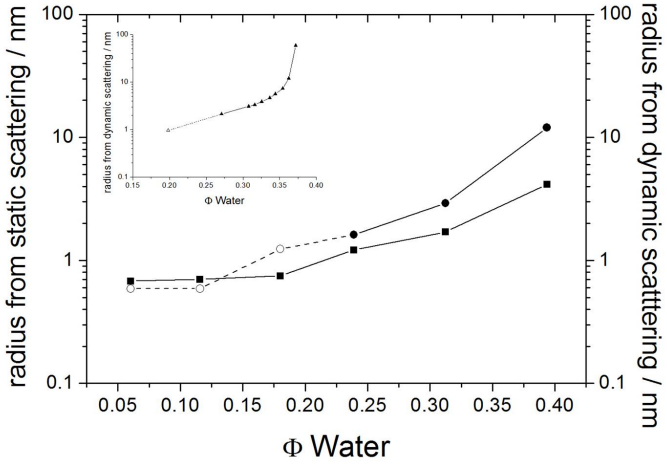

Figure III.25.: Estimated radii of scattering micelles inferred from SLS (■) and DLS (○, ●) assuming spherical geometry. The open circles (○) correspond to the compositions with bad time-correlation signals (curves 4 to 6 in Figure III.24 b)), the black circles to curves 1 to 3 in Figure III.24 b). The inset shows the evolution of the radii along a different path up to water volume fractions very close to the binodal line.

droplets. This procedure has identified micelles of defined sizes [283] as well as pre-micelles with strongly concentration dependent aggregation numbers for short chain surfactants (see [284]). The comparison of radii as derived from DLS and SLS is shown in Figure III.25. Especially in the region where clear self-correlation functions are detected, there is a satisfactory agreement between the radii deduced from both techniques. Moreover, the radii as derived from Rayleigh scattering at 45°, 90°, and 135° do not differ by more than 1%, in contrast to Ornstein-Zernicke scattering (scattering due to critical fluctuations) which would give a strong angle dependence. To make this important point clear, in the inset of Figure III.25 the results obtained from a dilution line towards the alcohol corner is shown. The mass as derived from scattering clearly diverges near the critical point. But the constant mass of microemulsion domains far from the critical point (as shown in this inset) is an unambiguous sign of the existence of aggregates of 2 nm radius. In addition, the inset of Figure III.25 shows that at the highest water content the hydrodynamic radius is, as expected, larger than the radius deduced from the mass. At lower water content, no detailed comparison can be drawn for such compositions, because of the uncertainties of the dynamic scattering. In any case, these results show that there must be domains of defined size that can be taken as "EtOH-swollen" octanol micelles in equilibrium with a solvent. The concept of pseudo-phases as developed by Charles Tanford applies also in the case of surfactant-free microemulsions [285]. Another important question that was just mentioned in this work is whether an interfacial film exists or not. It should be noted that the two constituents of the micelles are surface-active [232] and used as cosurfactant. Therefore, the surface of the domains is expected to be covered with hydroxyl groups at saturation, that is, a weakly associated interfacial surfactant film must exist. The theory explaining the stability of these domains for a given size requires the knowledge of the equation of state of this interfacial film, i.e. the cost in free energy of a cosurfactant to leave

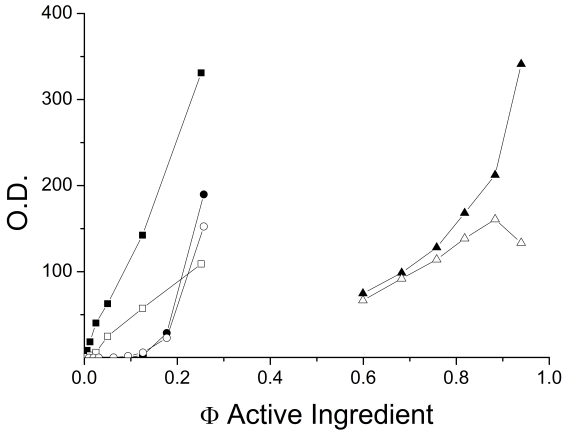

Figure III.26.: Optical densities of the dye Quinoline Yellow SS (open symbols) and of the dye Disperse Red 13 (full black symbols) in aqueous solutions of SDS (□, ■), of sodium xylene sulfonate (SXS) (○, ●), and a mixture of 7:3 (mass fraction) EtOH:n-octanol (△, ▲) as a function of the volume fraction of the organic component (either pure surfactant or hydrotrope or the sum of EtOH and n-octanol) at 25 °C.

the interfacial film [270].

Hierin, the solubility behaviour of such surfactant-free microemulsions is shown. In Figure III.26 the optical densities of two different hydrophobic dyes are shown, dissolved in three different systems.

The two hydrophobic dyes are Quinoline Yellow SS (octanol-water distribution log p = 4.9 [286]) and Disperse Red 13 (octanol–water distribution log p = 5.2 [287]). The results of solubilisation at saturation obtained with surfactant-free microemulsions are compared in Figure III.26 to aqueous solutions of the widely used reference surfactant sodium dodecylsulfate (SDS), and to a typical hydrotrope, sodium xylene sulfonate (SXS) [288], along the line shown in Figure III.24 a).

The ternary surfactant-less microemulsion system require a large amount of organic material to dissolve the hydrophobic dyes. This comes from the fact that the inte-

rior of the octanol rich domains of 2-3 nm radius, that is four times the maximum length of a stretched octanol molecule, is not as hydrophobic as in the case of classical surfactant-based micelles and microemulsions. The surfactant-less microemulsions are characterised by a "core" that contains a significant amount of OH-groups, stemming both from EtOH and from water bound to EtOH (the EtOH–water binding is 10 kT per molecule).

Although the hydrotrope SXS does not form any detectable aggregates in water, but only shows a weak band in the wideangle neutron scattering [289], it has a solubilisation efficiency between those of the surfactant-free microemulsions and typical SDS micelles.

In this sections, microemulsion results obtained by mixtures of water/EtOH/n-octanol are presented. However, it should be noted that several other ternary systems were investigated, all showing similar results, provided that the same conditions are fulfilled as for the Ouzo effect. These are first that solvent 1 is miscible with solvent 2, and the additional component 3 is highly soluble in solvent 2, but not in solvent 1. When the additional component is a solid salt consisting of "antagonistic" ions, that is, one showing a significant propensity to the polar phase whereas the other one tends to the unpolar phase, a similar phenomenon as described here occurs. However, in this case the individual droplets are now clearly visible by microscopy. They are thermodynamically stable and could be called surfactant-free microemulsions, but are called emulsions for historical reasons [290, 291]. The domain volumes are nine orders of magnitude larger than the swollen micelles described in the present section.

III.2.1.4. Conclusion

As a conclusion, it can be stated that well-defined domains (alias swollen micellar aggregagtes considered as a dispersed pseudo-phase) are clearly characterised in the "pre-Ouzo" region of appropriate ternary systems fulfilling the conditions of the Ouzo effect. These micelles have a core region that is less hydrophobic than in the case of classical microemulsions made of surfactants.

III.2.2. Pre-Ouzo effect

III.2.2.1. Abstract

In the previous section, the first experimental proofs were given that the ternary system water/EtOH/n-octanol forms a microemulsion area. A direct and detailed characterisation of the microemulsions formed in the ternary mixture are presented. At first, DLS measurements were performed along two paths with a fixed n-octanol of 10 and 20 wt%. Significant correlation functions were obtained near the phase boundary. Points far away from this boundary gave correlation functions typical of real soltutions. The apprearance of swollen micelles in the system was confirmed by SAXS and SANS experiments. The spectra were recorded by Dr. Isabelle Grillo and interpreted by Prof. Thomas Zemb and Dr. Olivier Diat. Further, small angle X-Ray scattering experiments were made in the Institut de Chimie Séparative de Marcoule by Dr. Olivier Diat.

III.2.2.2. Introduction

Surfactants in aqueous solutions can form micelles and liquid crystals above a certain temperature and concentration. Micelles can be distinguished from progressive aggregation via well-defined average aggregation number of molecules per micellar aggregate [40]. All known micelle-forming surfactants are in fast (ns to ms) exchange related to a minimum hydrophobic chain length and a sufficiently hydrophilic "headgroup". A simple OH-headgroup in fatty alcohols is not enough to form micelles, it must be either a charged headgroup or a non-ionic headgroup with sufficient length, for example four ethylene glycol groups plus OH- to ensure a sufficiently high amount of hydration. Molecules like short alcohols that do not fulfil these criteria can still be surface active, work as a cosurfactant or destroy defined surfactant aggregates and in that case are known as hydrotropes. In binary solutions with water, all alcohols form loose networks that can be seen as living polymers and form

a three-dimensional mesh that has specific signature in scattering [292, 293]. But these structures are neither micelles nor microemulsions. However, since over thirty years papers are published from time to time, in which so-called "surfactant-free" microemulsions are postulated. Their existence is claimed as a working hypothesis to explain some curious observations, such as the fact that enzymes requiring interfaces work well in such "surfactant-free microemulsions" [73, 84, 281]. The oldest papers go back to the 1970s [61, 64, 65]. The key observation at that time was the apparition of three optically clear domains in analytical ultracentrifuge, as well as a non-monotonic behaviour of conductivity along water dilution lines. Moreover, close to the phase separation boundary but "far" from critical point, these ternary systems exhibit DLS [294] that are experimentally identical to the one charactecteristic of micelles close to a critical point [283]. However, no real unambiguous structural investigations obtained by neutron or x-ray scattering have been performed to our knowledge with plausible explanations of the underlying mechanisms.

Sometimes, ternary surfactant-free model systems such as decane-water-isobutoxyethanol as studied by Shinoada and Kunieda show the so-called "Ouzo effect" [295]. Ouzo as other similar liquors contains water, methanol and anethole, an essential oil that is poorly soluble in water, but highly soluble in EtOH. Above a critical water concentration, such ternary mixtures are unstable; they spontaneously form very fine emulsions that are remarkably stable in time. This is the so-called Ouzo effect. The precondition for such "surfactant-free emulsions" is the mixture of two miscible solvents 1 and 2 with a solute that can be also a solvent, e.g. anethole (component 3). This component 3 must be highly soluble in one solvent (e.g. EtOH), but only poorly soluble or insoluble in the other one (e.g. water). In addition the two solvents 1 and 2 (here water and EtOH) must be miscible, either completely or at least to a large extent [89]. Whereas this Ouzo effect is more and more studied and rather

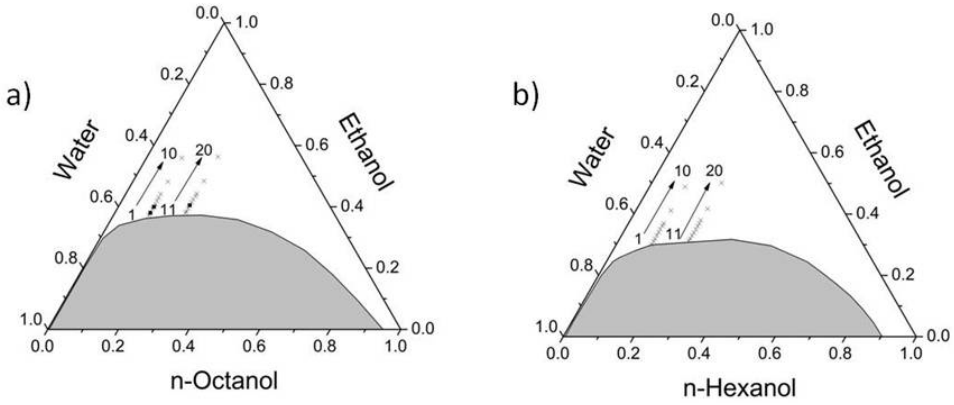

Figure III.27.: a) n-octanol and b) n-hexanol/water/EtOH ternary phase diagrams. The black squares give the location of samples investigated by contrast variation in SANS and SAXS. Compositions indicated by X on the dilution lines were investigated by light scattering.

understood, on the part in the phase diagram, where the water content is still low enough to get a homogeneous, stable, transparent one-phase system. The surprising structuring in these systems before phase separation upon the addition of higher amounts of water is called pre-Ouzo effect.

III.2.2.3. Results and discussion

III.2.2.3.1. Phase diagrams and partial pressure

Figure III.27 shows the resulting ternary phase diagrams for the systems water/ EtOH/n-octanol or n-hexanol. The change of the phase boundary at different temperature was investtgated as well. At higher temperature, the two phase region is decrease. The evolution is shown in Figure A.8 in the appendix.

To get further information about the partition of EtOH between the pseudo-phases (one is water-rich, the other one rich in octanol or hexanol) it is worth considering the partial pressure of EtOH above the liquid medium. Although they are difficult to measure, they can be estimated with sufficient precision from the NRTL gE-model.

	Vapour Pressure	**Neutron Scattering**
X_{EtOH}^{Water}	0.1365	0.2463
$X_{EtOH}^{Octanol}$	0.7780	0.5333
ω_{EtOH}^{Water}	0.2641	0.4261
$\omega_{EtOH}^{Octanol}$	0.5535	0.2879
Φ_{EtOH}^{Water}	0.3347	0.5099
$\Phi_{EtOH}^{Octanol}$	0.5656	0.2981
$\Phi_{WaterPhase}$	0.5160	0.7005
$\Phi_{OilPhase}$	0.4840	0.2995

Table III.1.: Overall composition of the sample shown by Vapour Pressure and SANS. The mole, mass and volume fractions of EtOH in the water and octanol phase are calculated. From neutron scattering experiments a EtOH distribuition of 4:1 between the aqueous and octanol phase was obtained from Prof. Thomas Zemb and Dr. Olivier Diat. Further, the volume fractions of the aqueous and oil phase are given.

At first, the binary NRTL-interactions were fitted to the different experimental data of the binary systems. On the base of these parameters the vapour-liquid equilibria for the given concentrations of the liquid phases of the ternary systems at 25 °C and 1 atm was calculated. The partial pressure of EtOH is a measure of its chemical activity and can be also used to infer the partition of EtOH between the two pseudo-phases. In Figure III.28 the resulting partial pressure of EtOH is plotted as a function of the mole fraction of EtOH in the ternary system for samples 1-10 (■) and 11-20 (▲) as denoted in Figure III.27 a). Further, the partial pressure of EtOH on the water-EtOH binary (●) is shown. This binary is taken from literature [296]. Assuming that EtOH "trapped" in the micelle has no contribution and the overall partial pressure of EtOH is only defined by the EtOH in the water-phase the distribution of EtOH in both pseudo-phases can be estimated. For a specific composition of the ternary system the partial pressure of EtOH can be deduced. Fitting a function to the binary, the mole fraction of EtOH can be calculated which resides in the water phase. In combination with the knowledge of the exact composition of the sample, values from can be obtained.

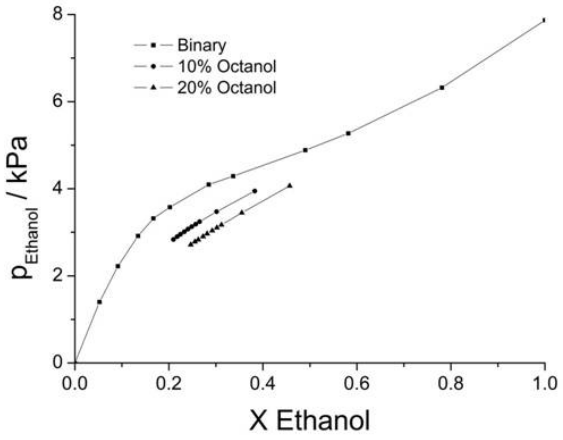

Figure III.28.: Partial pressure of EtOH as a function of the mole fraction in solution for the water/EtOH binary (●), and the two ternary systems for samples 1-10 (■) and 11-20 (▲) as denoted in Figure III.27. Values for the binary system were taken from literature [296]. The partial pressure in the ternary systems were calculated as described above.

III.2.2.3.2. Scattering experiments

In order to get a first insight into a molecular structuring, SLS and DLS have been performed along a composition line indicated in Figures III.27 a) and b). Time correlations in scattering intensity are observed with large characteristic periods, results that can be interpreted with the existence of spherical aggregates. The corresponding characteristic size can be attributed to the structures between few tenths of nanometers far away from the phase separation boundaries (binodal line) to more than 10 nm close to it. This can be interpreted as an increasing clustering from a true molecular ternary solution up to a well-defined microemulsion close to the phase separation composition. It should be noted, however, that this is not the signature of a classical long-range fluctuation close to a critical point. The observed correlations appear indeed even far from the binodal line. Of course, none of the three involved binary systems (composition along the sides of the triangles) shows

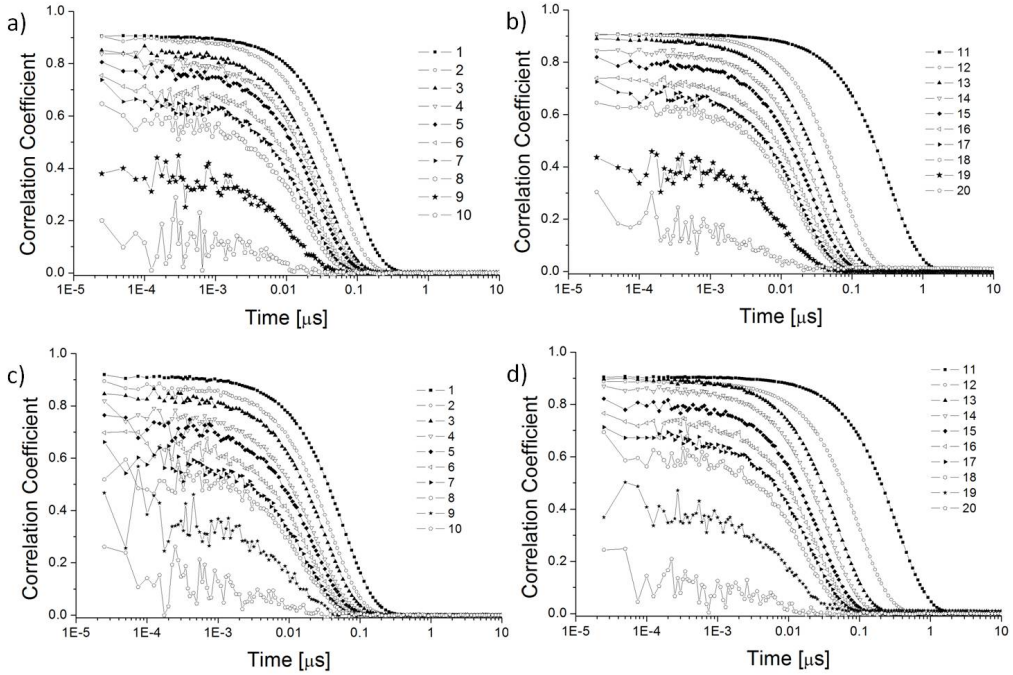

Figure III.29.: Time-dependent self-correlation functions as obtained by DLS following the paths as denoted in Figure III.27 with a) 10 wt% and b) 20 wt% of octanol or c) 10 wt% and d) 20 wt% of hexanol.

any microemulsion structure [292]. The explained results are presented in Figure III.29. Figure III.30 shows the evolution of the droplet sizes as function of the water content.

III.2.2.4. Conclusion

In this section, the concept of surfactant-less microemulsions was studied more in details. In total, there is a striking analogy with swollen micellar systems. However, in the case of the pre-Ouzo effect, the third hydrophobic molecule does not have to contain a linear hydrocarbon chain or a highly hydrated head group. It can be small or big, it should only consist of a hydrophobic (or more generally more solvophobic) part relative to one of the solvents and nevertheless at least a very small hydrophilic (solvophilic) part. All the rest is brought in by the second solvent. In this sense,

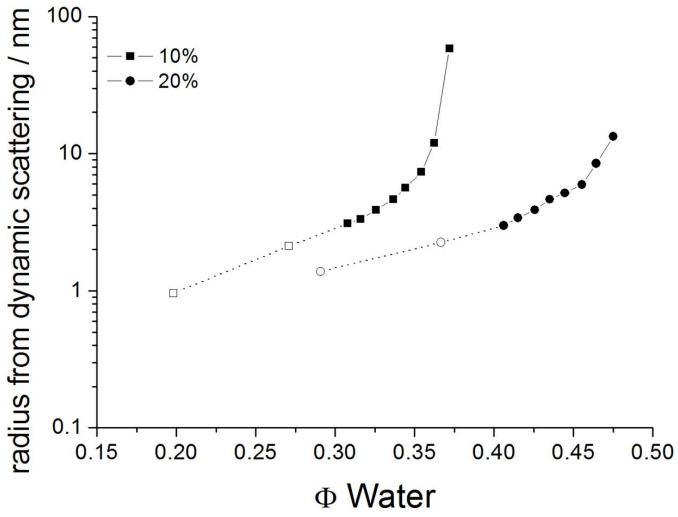

Figure III.30.: Apparent hydrodynamic radii observed when moving on a line with constant octanol percentage (10%, ■; 20%, ●) from the two-phase domain towards the water corner, along the dilution path shown in the phase diagram. The white symbols give the "calculated" radii of particles with correlation functions comparable to molecular solutions.

this type of micellar formation is much more general than surfactant micellisation, proposed many decades ago by McBain as the beginning of the science of association colloids. Consequently, it should occur in lots of well-known systems consisting of two miscible solvents with an additional component that is only miscible with one of them. It would be worth having a closer look to many of such mixtures. Surfactant-free enzymatic media are only one example. From the present study it should also be possible to design new structured liquid systems containing interfaces without using surfactants. This is of particular importance because surfactants have several drawbacks, such as environmental concerns.

III.2.3. Eco-solvents - cluster-formation, surfactant-less microemulsions and facilitated hydrotropy

III.2.3.1. Abstract

In this paragraph clusters in the ternary systems water/BA and EtOH, ethyl lactate or γ-valerolactone as found with the help of SLS and DLS scattering experiments are considered. These ternary mixtures are powerful solvent media and consist only of low-toxic solvents of natural origin. In the previous section (III.2.1), it has been shown that surfactant-less microemulsions are formed in the system water/EtOH/n-octanol. By contrast, in the systems studied here the sizes of the aggregates are too small to be considered as micelles. It can be postulated that the presence of clusters or larger structures as in surfactantless microemulsions is strongly influenced by the most hydrophobic compound. The phenomenon of facilitated hydrotropy is also investigated in the above mentioned systems. In this context, EtOH is considered as the primary hydrotrope and the more hydrophobic BA as the facilitating second hydrotrope. The hydrophobic dye Disperse Red 13 is used as a marker of facilitated hydrotropy. The results suggest that the degree of self-association of eco-solvent has a significant influence on the hydrotropic efficiency of BA.

III.2.3.2. Introduction

Principle 2 of the six principles of green extractions, as defined by Chemat [297], refers to the use of principally water or agro-solvents stemming from agricultural resources. Bio- or agro-based solvents (eco-solvents) are important classes of solvents that may replace solvents obtained from petrochemistry at least for some applications. Eco-solvents can be gained from biomass, such as wood, starch, vegetable oils and fruits. Nature produces 170 billion tons of biomass per year by photosynthesis. 75% belongs to the class of carbohydrates, and just 3-4% of these compounds are used by humans for food and nonfood purposes [298]. EtOH, ethyl lactate and γ-

valerolactone are three examples of eco-solvents derived from carbohydrates (sugars).

EtOH is the most common eco-solvent. The world production of bioethanol is estimated to be 22,000 millions of U.S. liquid gallons per year [225]. It can be produced by fermentation of sugar-rich materials such as sugar crops (sugar cane and sugar beet), starch crops (corn), or cellulosic feedstock (wood, grasses and agricultural residues) [299, 300]. Although EtOH is flammable and produces explosive emissions, it is used on a large scale because of its availability in high purity, its low price and low viscosity. Of course, it is completely biodegradable. Its boiling point is 78 °C.

Ethyl lactate (EL) is an environmentally acceptable solvent. Moreover, it is biodegradable and has a low viscosity. It is not a volatile organic compound (VOC). A way of producing EL is the esterification of lactic acid with EtOH [301]. The advantage of this process is that both reactants are obtained from renewable resources. The selling price for commonly used solvents in the USA is around \$0.90 to \$1.70 per pound. Processing advances have lowered the price of EL from \$1.50 to \$2.00 per pound to \$0.85 to \$1.00 per pound what makes it more competitive to petro-solvents [300, 302]. Its low melting (−26 °C) and high boiling points (151 − 155 °C) are also advantageous.

γ-valerolactone (GVL) is another sugar-based eco-solvent that attracted attention recently [303–307]. It can be produced at yields higher than 95 % by the hydrogenation of levulinic acid [308, 309] which can be derived from biomass [310, 311]. Horváth *et al.* showed recently that GVL is a promising green and sustainable solvent with interesting properties such as low melting (−31 °C) and high boiling (207 °C) points, a very low vapour pressure (0.65 kPa at 25 °C), no formation of

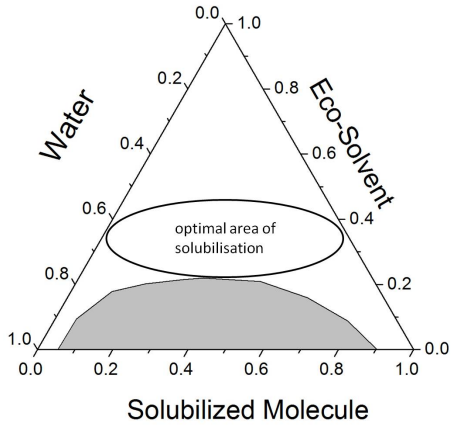

Figure III.31.: Illustration of the optimal region in the ternary phase diagram to solubilize a hydrophobic molecule with the minimum of cosolvent. This region is also characterised by optimum structuring. The white zone represents monophasic systems, the grey zone biphasic ones. The compositions are given in mass ratios.

measurable amount of peroxides, etc. [304].

It has already been shown that environmentally friendly microemulsions can be made without surfactants (Section III.2.1. The condition for this phenomenon, the so called "pre-ouzo" effect, is that at least three compounds are mixed where solvent A is miscible with solvent B, solvent B is miscible with compound C, and A and C are immiscible. Surfactantless microemulsions have already been known since the late 1970s but to date, only few articles deal with this topic and none of them deliver a satisfactory explanation [61, 64, 65, 79]. In Section III.2.2, it is shown that most pronounced structuring in terms of microemulsions is found close to the demixing (binodal) line. This is also the region where industrial extraction processes are made, and it is supposed that structuring is most important for efficient extraction [85].

Durand *et al.* [312] investigated the system water/BA/dimethyl isosorbide (DMI), the latter being also an eco-solvent derived from sugar, using DLS. Their results concerning the occurrence of significant correlation functions are comparable to the

results mentioned before. Concerning their model system they were not able to find a reasonable explanation for the formation of aggregates. Instead they focused on the concept of facilitated hydrotropy, which may have its origin in aggregate formation. The concept of facilitated hydrotropy consists of solubilising an insoluble amphiphilic compound in water in the presence of a co-solvent and a further more hydrophobic hydrotrope [313, 314]. In the present study the systems water/BA/ eco-solvent (EtOH, EL, GVL) were investigated with SLS and DLS to determine the structure. Further, the possibility of facilitated hydrotropy was checked. BA was chosen as a model of a hydrophobic hydrotrope molecule to be solubilised in the binary water/eco-solvent mixture. In order to study facilitated hydrotropy Disperse Red 13 (DR-13) was used as a hydrophobic molecule (octanol-water distribution log p = 5.2 [287]). According to the concept of facilitated hydrotropy [315], BA is the facilitating hydrotrope and the eco-solvents are hydrotropes to solubilise BA in the aqueous system. The work is part of a research program, initiated in our institute, aiming at a better understanding of solubilisation media and their mesoscopic structuring to optimise solvents and extraction media.

III.2.3.3. Results and discussion

III.2.3.3.1. Ternary phase diagrams

For a better understanding of facilitated hydrotropy the phase behaviour of the ternary systems water/BA/eco-solvent was studied first. In Figure III.32 the three ternary phase diagrams are shown. Two distinct areas can be found, a clear translucid single phase and a turbid two-phase zone. All three cosolvents are completely soluble in water and BA. Moreover, the three eco-solvents increase the cosolubility of water and BA significantly. Above a certain mass fraction of cosolvent (0.25 for EtOH, 0.35 for EL, and 0.55 for GVL), only a monophasic system is obtained for

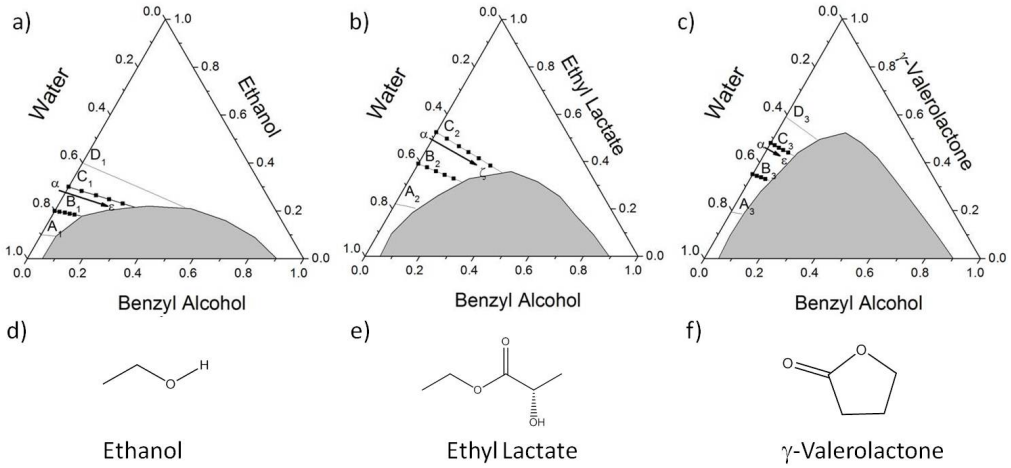

Figure III.32.: Phase diagrams of the systems water/BA/a) EtOH, b) EL, and c) GVL. All diagrams were recorded at 25 °C and the compositions are in mass fractions. The grey area represents the two phase, the white one the monophasic region. Lines A_i to D_i, with $i = 1 - 3$, represent the experimental paths for the solubility experiments. ■ on lines B and C correspond to the compositions investigated by DLS and SLS. From d) to f) the molecular structures of the eco-solvents are shown.

every water/BA ratio.

III.2.3.3.2. Light scattering experiments

Figure III.33 presents selected self-correlation functions from DLS along lines with increasing BA content for the systems water/BA/EtOH, EL, and GVL. Two phe-

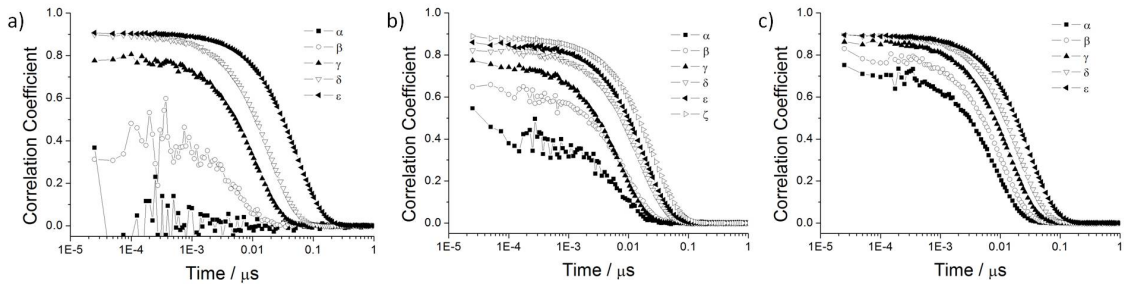

Figure III.33.: Time-dependent self-correlation functions as obtained by DLS for the ternary systems water/BA/a) EtOH, b) EL, and c) GVL at 25 °C. The results for the different compositions (α-ϵ,ζ) on the experimental paths C_i of Figure III.32 are presented.

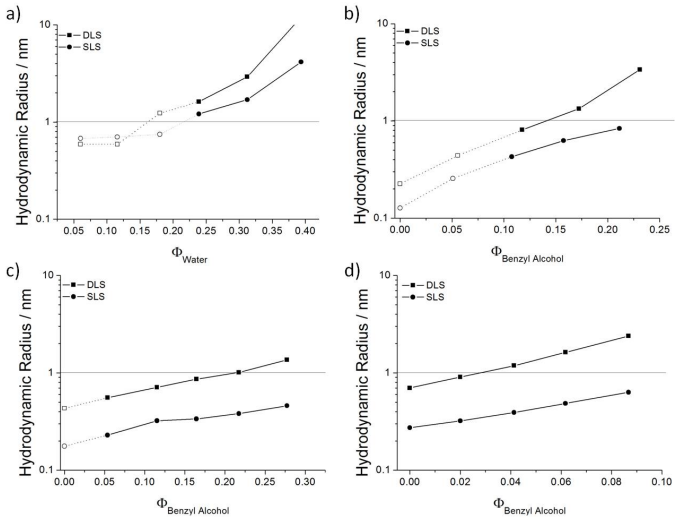

Figure III.34.: Estimated radii of scattering objects inferred from DLS (■) and SLS (●) assuming spherical geometry for the systems a) water/EtOH/n-octanol and water/BA/) b) EtOH, c) EL, and d) GVL. □ correspond to the correlation functions where it was not possible to fit properly and ○ to samples with a very low intensity of scattered light. The dotted lines should just indicate the evolution of the curves.

nomena can be distinguished. For EtOH and EL, the correlation becomes more and more pronounced, the closer the composition is to the phase separation composition. On the other hand, the correlation function of the binary system water/GVL is already significant. With the assumption of a spherical symmetry, the deduced radii of the particles get larger the closer the composition is to the phase boundary. Even relatively far away structures clearly occur, a fact that can be used to assume that these correlations are not a critical phenomenon with large fluctuations close to a critical point. Comparing the three curves α from Figure III.33 a)-c) which correspond to the binary system water/eco-solvent it can be seen that EtOH in water does not produce a significant correlation function. In the case of EL the formation of aggregates can be assumed, but only the correlation functions of the binary water/GVL can be properly fitted.

But DLS results alone are not a definitive argument for spherical structures in solution. Therefore, SLS measurements were performed at three angles (45 °, 90 ° and 135 °) to rule out the possibility of critical fluctuations (Ornstein-Zernicke scattering) which would give a strong angle dependence. The radii as derived from Rayleigh scattering at the three angles mentioned before did not differ by more than 1 %. In Figure III.34 b) to d) the radii derived from DLS and SLS with the assumption of spherical particles are shown as function of the BA mass fraction. In addition, Figure III.34 a) shows the graph obtained from the system water/EtOH/n-octanol shown in Section III.2.1. In contrast to the three curves mentioned before this figure is an example of a system with well-defined micelles. The difference to this system is the overall hydrodynamic radii measured. For the eco-solvents the objects are very small (almost always below 1 nm). In this case it cannot be spoken of well-defined micelles in the systems, but of cluster formation of the solvent molecules or of a pre-micellar area in the phase diagram. Though the particle sizes are very low, all three curves show a satisfactory agreement between the radii obtained from both techniques. This is a strong hint at the presence of more or less spherical clusters. This procedure of comparing DLS and SLS results has already identified micelles of defined sizes [283] and pre-micelles with strongly concentration dependent aggregation numbers for short chain surfactants [284].

III.2.3.3.3. Solubilisation experiments

To study the concept of facilitated hydrotropy, the solubilisation of a hydrophobic dye, DR-13, as function of the BA concentration was investigated. For this purpose, the water-to-eco-solvent mass ratio was kept constant and the amount of BA was successively increased. The compositions used for these experiments are shown in Figure III.32. In every system two experimental lines were chosen (B_i and C_i). For a better comparison of the three solvents, the molar ratio of water-to-eco-solvent was

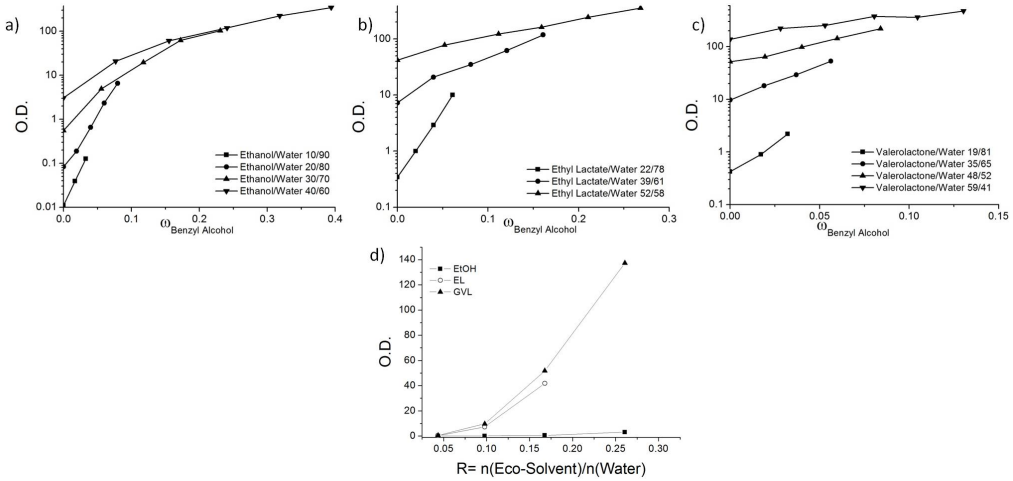

Figure III.35.: DR-13 solubilisation as a function of the BA mass fraction for the systems water/a) EtOH, b) EL, and c) GVL. In the legend of every figure, the mass ratio of the eco-solvent-to-water is given corresponding to the dilution lines in Figure III.32. d) Evolution of O.D. of the binary water/eco-solvent mixture. O.D. is plotted as a function of the molar ratio of eco-solvent-to-water.

kept constant. The solubilisation of DR-13 is expressed in units of optical density (O.D.). In Figure III.35 the O.D.s of the three solvents are plotted as a function of mass fraction. The addition of BA leads to an increase of solubility of DR-13 in the three systems. In Figure III.35 d) the dye solubility for the binary systems water/eco-solvent is plotted. The increase of O.D. is significant for EL and GVL with increasing eco-solvent concentration. A possible explanation for the different solubility properties could be the appearance or absence of clusters in the binary systems. EtOH forms no aggregates with water, so the solubility is very low. EL and GVL already form some cluster in water (see Figure III.33). This could be an argument for the higher solubility of DR-13.

But the eco-solvent concentration affects the DR-13 solubilisation as well. For samples with high amount of eco-solvent the increase of O.D. is not as remarkable as for lower concentrations. Bauduin *et al.* showed a way to characterise the hydrophobic efficiency α [288]. It is linked to the evaluation of the slopes of the linear part in

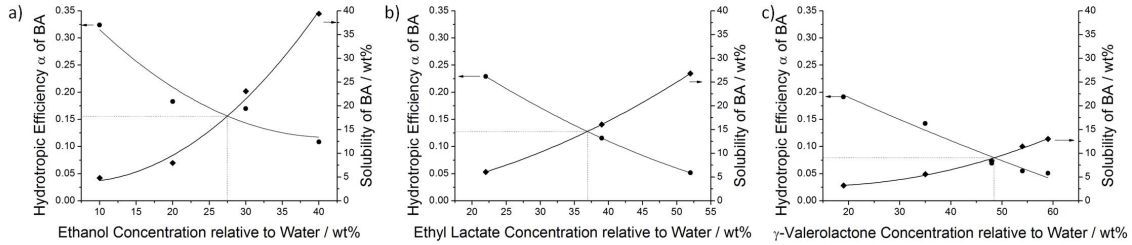

Figure III.36.: Hydrotropic efficiency of BA in the systems water/ a) EtOH , b) EL and c) GVL (circles) and BA solubility in the corresponding systems (diamonds) as a function of the eco-solvent-to-water ratio. The dotted lines show the crossing points of the two curves.

the log-linear plots of the solubility of the hydrophobic dye, which is defined with the following equation:

$$\alpha_{BA}^{DR13} = \frac{\delta log_{10} O.D.}{\delta [BA]} \tag{III.2}$$

In Figure III.36 a plot of the evolution of α for different water/eco-solvent ratios is shown together with the solubility of BA in these systems. With increasing water/eco-solvent ratio the BA solubility increases as well but the hydrophobic efficiency decreases. Since this occurs for every eco-solvent this seems to be a general phenomenon which has already been described by Durand *et al.* [312]. Another important aspect of the obtained curves is the crossing point of the efficiency and solubility curve. It is shifted in the same manner. For a high hydrotropic efficiency low hydrotrope concentrations are necessary. In a recent study on the mechanism of hydrophobic drug solubilisation Booth *et al.* [316] showed that self-association of hydrotopes decreases the solubilisation property. In other words, the self-association at high hydrotrope concentrations, which leads to a pronounced structure in the systems, as shown with DLS and SLS measurements, leads to a decrease of hydrotropic efficiency. The results in Figure III.36 are experimental proofs of this theory. Moreover, the absolute value of α in the water/eco-solvent binaries is highest for EtOH and decreases with EL and GVL. This is another hint that the self-aggregation of hydrotropes affects the facilitated hydrotropic efficiency.

III.2.3.4. Conclusions

In this section, the structuring and solubilisation properties of the ternary mixtures water/BA/eco-solvent were investigated. In these mixtures the solubility of the most hydrophobic molecule, in this case BA, was increased by the presence of the eco-solvent. In the single phase area, a region of optimal solubility located near the two-phase boundary was found. In this zone nano-structures occur. The size of these structures are too small to be considered as micelles. The appearance of micelles depends on the hydrophobicity of the solubilised molecule, and in the case of BA, this hydrophobicity is too small. Nevertheless, clusters of BA and eco-solvent are formed. This was proofed by the combination of DLS and SLS. In presence of the eco-solvent the hydrotropic efficiency decreased with the increase of the degree of self-association of the eco-solvent in water. Compared to the work of Booth, they only considered the simple direct hydrotropy, whereas in this work the joint effect of two hydrotropes were used in order to investigate the concept of facilitated hydrotropy. This fact makes the two studies different. The present work can thus be considered as a generalisation and extension of Booth's work.

Chapter IV.

IV Conclusion and Outlook

At the beginning of this work, pseudo-ternary phase diagrams with water, sodium dodedcyl sulfate as surfactant, 1-pentanol as cosurfactant and classic n-alkanes as oil phase were provided by Dr. Didier Touraud. In this former work, the evolution of the microemulsion area was investigated as function of the carbon atom number of the alkanes. The first aim of my studies was to formulate green, or let's say "greener", microemulsions, starting from compositions mentioned before.

In the first step, n-alkanes were replaced by sustainable alternatives. For this reason, limonene and FAME rapeseed biodiesel were used. Hereby, it was possible to generate large microemulsion areas. Moreover, on a macroscopic level, the PTPD produced with limonene was comparable to the ones obtained with short chain n-alkanes (heptane or octane) and the same counted for biodiesel and long chain alkanes (hexadecane). The results show that it was possible to replace certain n-alkanes by limonene and biodiesel in these formulations. Further, by mixing both oils, it was more or less possible to screen the whole spectrum of phase diagrams for the mid-chain alkanes.

Other sustainable possibilities as oil-phases are dibasic esters. With these oils it was possible to formulate fully and highly water dilutable microemulsions. But when

sodium oleate was used as surfactant, problems with the chemical stability of the esters occured. Due to the resulting high pH values with oleate, hydrolysis took place. This hydrolysis was slow at low water content and was accelerated with the addition of water. It was only possible to formulate highly water dilutable microemulsions with sodium oleate because at infinite dilution vesicles were formed.

As a last step, the influence of the addition of a short chain alcohol as cosolvent was examined. The "greenest" formulated microemulsion was found in the system water/sodium oleate/citronellol/ethanol/limonene. Ethanol was used to extend the microemulsion area, which was very limited in the system with only citronellol as cosurfactant. Moreover, at a specific concentration of ethanol, even the formulation of a highly water dilutable system was possible.

In a complementary work, this concept of extending the microemulsion area with the addition of ethanol was investigated more intensively. The experiments with with citronellol and limonene, showed that with the addition of ethanol the system was transformed from an anti-percolative to a percolative one (confirmed with conductivity measurements). So ethanol has a significant influence on the film rigidity of the system. A more flexible film is obtained with the addition of ethanol. To investigate this concept, the system water/sodium oleate/FAME rapeseed biodiesel was used with different mid and long chain alcohols as cosurfactants (1-heptanol, 1-dodecanol) and their branched analoga (Guerbet alcohols). The result of these experiments was that the hydrophobicity of the involved components plays an important role. Everything depends on the partition of ethanol in the different phases. With more hydrophobic oils and cosurfactants, ethanol stays in the aqueous phase and does not partition in the interfacial film.

Besides the formulation of green microemulsions, the investigation of surfactant-less microemulsions was of great importance in this work. The motivation of this effect was different at the beginning. The starting point was the so called Ouzo Effect. During the study of the phase diagrams of such systems it was discovered that nanostructures occur already in the one phase area at certain compositions. This area was investigated with the combination of several techniques. At first, the ternary phase diagrams of the system water/ethanol/octanol were recorded. With DLS and SLS, the particles size was determined to be approximately 1 nm, far away from the two phase region. The droplet size increased up to 10 nm close to the border. These results were confirmed with SAXS and SANS measurements, conducted by Prof. Thomas Zemb and Dr. Olivier Diat.

In both cases (green and surfactant-less microemulsions) plenty of investigations can still be envisaged. Another task in the work of green microemulsion is the formulation of water-free systems. An alternative would be for example glycerol. Glycerol was used already in replacement of water in ternary systems with decanol and ethanol. In this system, significant correlation functions were found. Ionic liquids could be used as polar phase as well. But in this case, it is questionable to speak about green microemulsions any more. Concerning the addition of short chain alcohols as cosolvents to extend the microemulsion area, the use of other alcohols as propanol or butanol could help to improve the understanding of this concept. The understanding of surfactant-less microemulsions is still a challange. This concept seems to be responsible for many phenomena. In a recent work for example, it was tried to link the formation of these structures in perfume tinctures to the application as eau de toilette etc. So, many other systems are conceivable.

Appendix A.

A Supplementary

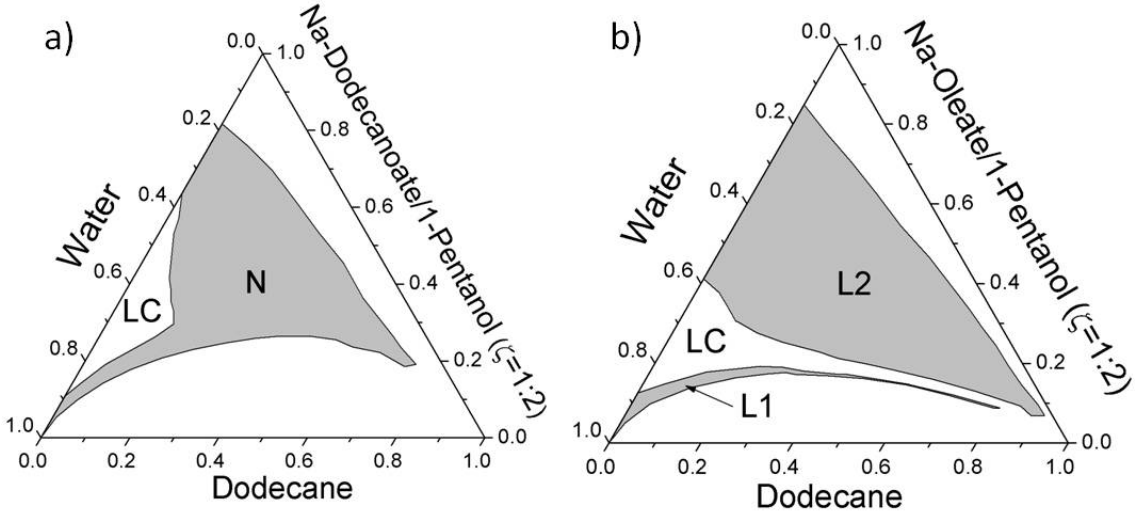

Figure A.1.: PTPDs of the systems water/1-pentanol/dodecane and a) sodium dodecanoate or b) sodium oleate. All compositions are in mass fraction.

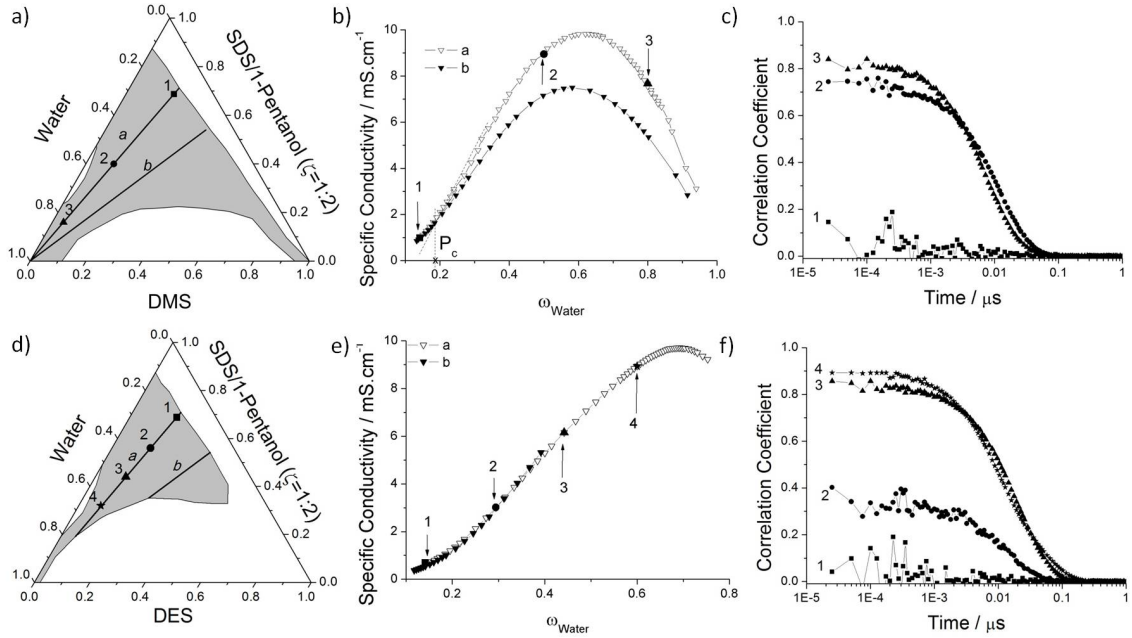

Figure A.2.: In this figure the PTPDs obtained using a) DMS and d) DES respectively as oils are shown again in order to associate the topology of the realms of existence of the single phase to conductivity and DLS measurements. Paths a and b are the two lines were the conductivity experiments were performed. The different points located on path a are the corresponding compositions investigated with DLS. Curves b) and e) show the results of conductivity measurements following path a (▼) and b ($\bigtriangledown$). The arrows give the compositions investigated by DLS. Curves c) and f) show the correlation functions obtained by DLS measurements for these points. The symbols of the DLS curves correspond to the same symbols as shown in a) and d).

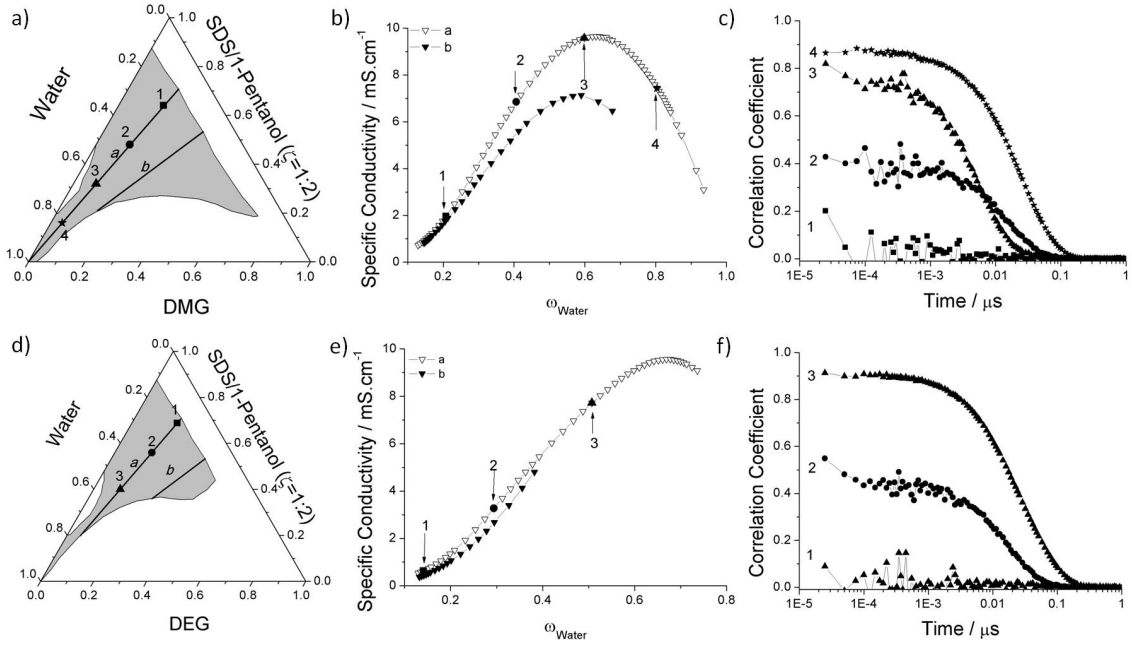

Figure A.3.: In this figure the PTPDs obtained using a) DMG and d) DEG respectively as oils are shown again in order to associate the topology of the realms of existence of the single phase to conductivity and DLS measurements. Paths *a* and *b* are the two lines were the conductivity experiments were performed. The different points located on path *a* are the corresponding compositions investigated with DLS. Curves b) and e) show the results of conductivity measurements following path *a* (▼) and b (▽). The arrows give the compositions investigated by DLS. Curves c) and f) show the correlation functions obtained by DLS measurements for these points. The symbols of the DLS curves correspond to the same symbols as shown in a) and d).

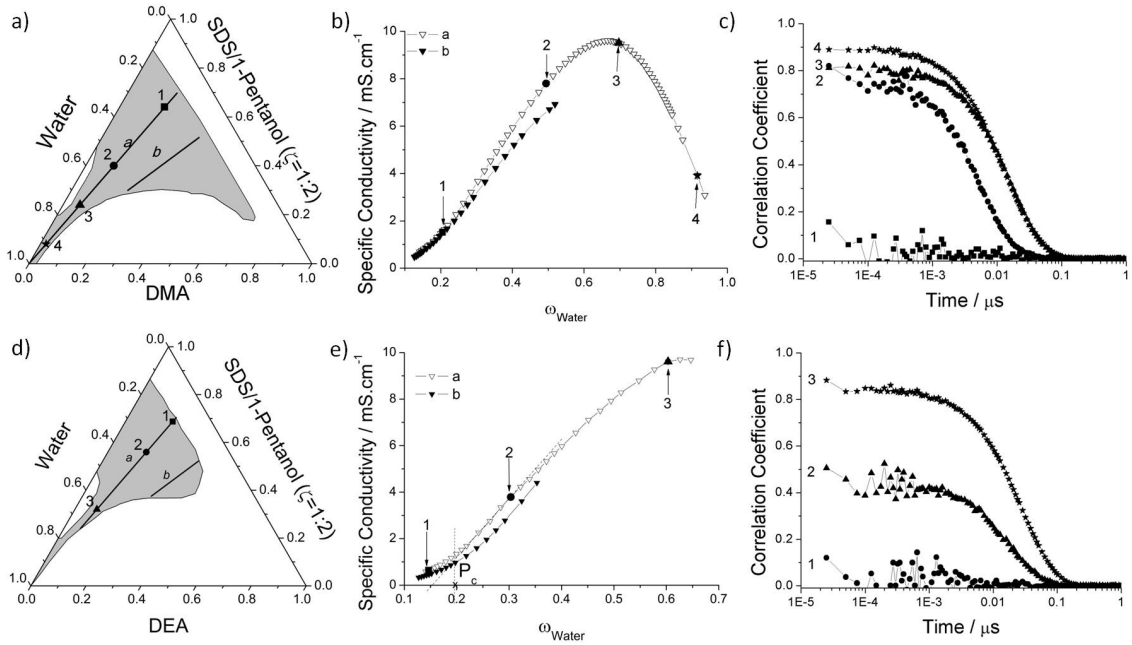

Figure A.4.: In this figure the PTPDs obtained using a) DMA and d) DEA respectively as oils are shown again in order to associate the topology of the realms of existence of the single phase to conductivity and DLS measurements. Paths *a* and *b* are the two lines were the conductivity experiments were performed. The different points located on path *a* are the corresponding compositions investigated with DLS. Curves b) and e) show the results of conductivity measurements following path *a* (▼) and b (▽). The arrows give the compositions investigated by DLS. Curves c) and f) show the correlation functions obtained by DLS measurements for these points. The symbols of the DLS curves correspond to the same symbols as shown in a) and d).

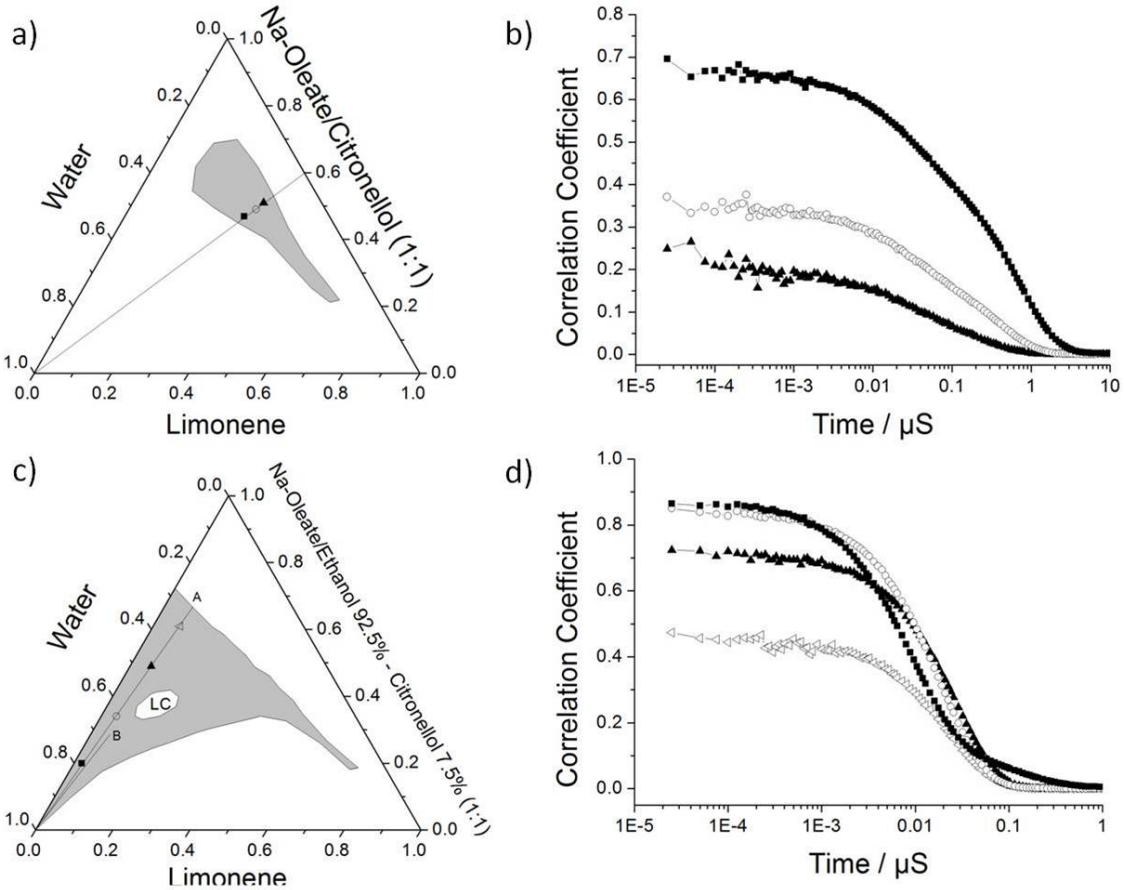

Figure A.5.: a) and c) show the experimental paths along which DLS measurements were performed. The symbols on the paths give the compositions of the samples and the same symbols are used for the respective curves in b) and d). b) and d) show the self-correlation functions. With the addition of water, the correlation functions become more significant.

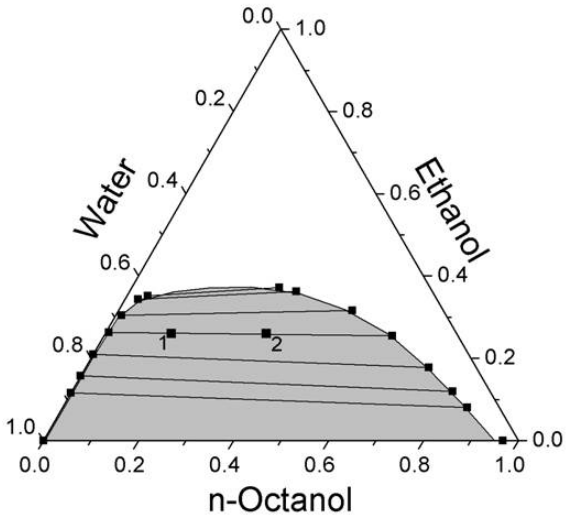

Figure A.6.: Ternary phase diagram of the system water/ethanol/n-octanol recorded at 25 °C. The lines in the two phase region correspond to the tie lines and were taken from literature [317]. The black squares represent experimental compositions to prove the accuracy of the tie lines. All compositions are in mass fraction.

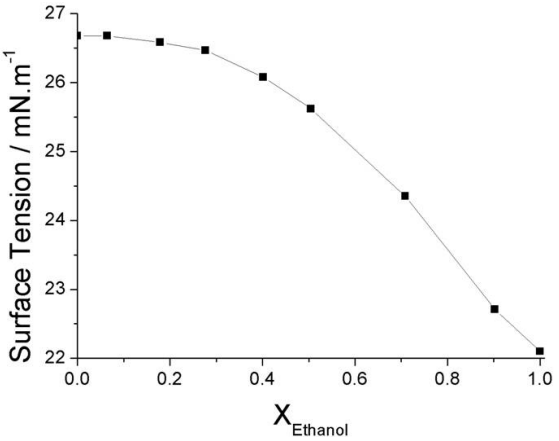

Figure A.7.: Evolution of the surface tension of octanol with the addition of ethanol expressed in mole fraction.

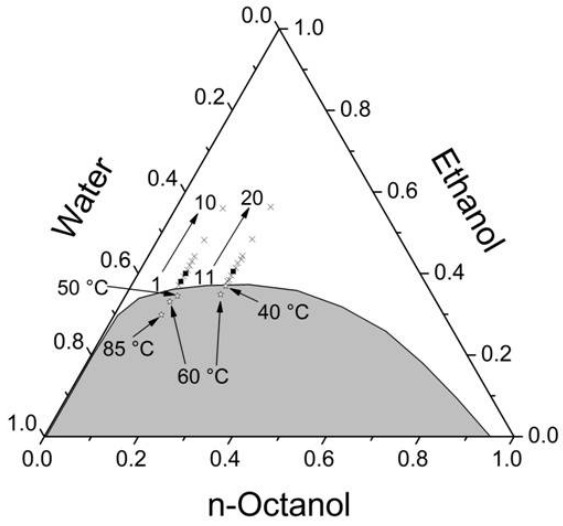

Figure A.8.: Evolution of the phase boundary with temperature. All compositions are in mass fraction.

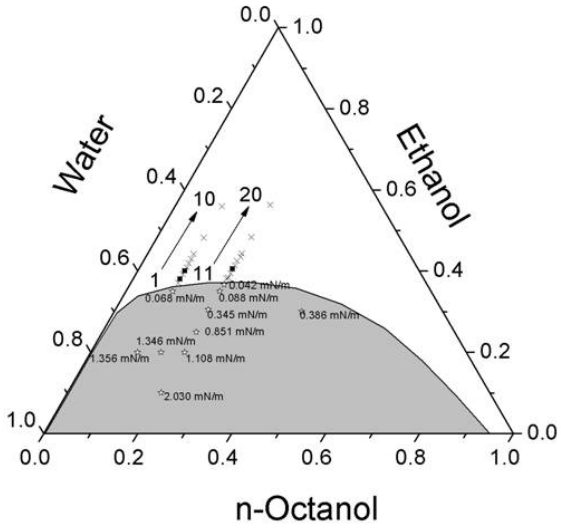

Figure A.9.: Interfacial tension within the two phase region. All compositions are in mass fraction.

List of Figures

Bibliography

[1] Marcus, Y. *The Properties of Solvents*; John Wiley & Sons Ltd, WEst SUssex, England, 1998.

[2] Nelson, W. M. *Green Solvents for Chemistry*; Oxford University Press, USA, 2003.

[3] Reichardt, C. *Solvents and Solvent Effects in Organic Chemistry*; VCH Publishing, Weinheim, Germanry, 1988.

[4] Walsh, K. A. *Chem. Week* **1996**, *158*, 38.

[5] Constable, D. J. C.; Curzons, A. D.; Cunningham, V. L. *Green Chem.* **2002**, *4*, 521–527.

[6] Sullivan, D. A.; Thiebaud-Roux, T. *Kirk-Othmer Encyclopedia of Chemical Technology*; John Wiley & Sons Inc., New York, USA, 2000.

[7] Leitner, W. *Green Chem.* **2009**, *11*, 603.

[8] Lancaster, M. *Green Chemistry: An Introductory Text*; Royal Society of Chemistry, Cambridge, England, 2002.

[9] Best Management Practices for Pollution Prevention in the Textile Industry. U. S. Environmental Protection Agency, Washington D.C., 1996.

[10] DeSimone, J. M. *Science* **2002**, *297*, 799–803.

[11] http://www.soyfoods.org/wp-content/uploads/Regulatory%20Expert%20Document Barry%20Swanson%20revised.pdf,.

[12] Anastas, P. T.; Warner, J. C. *Green Chemistry: Theory and Practice*; Oxford University Press, New York, USA, 2000.

[13] Tanaka, K. *Solvent-free Organic Synthesis*; Wiley-VCH, Weinheim, Germany, 2003.

[14] Leitner, W.; Poliakoff, M. *Green Chem.* **2008**, *10*, 730.

[15] Jacobs, L. J. M.; Kemmere, M. F.; Keurentjes, J. T. F. *Green Chem.* **2008**, *10*, 731–738.

[16] Earle, M. J.; Seddon, K. R. *Pure Appl. Chem.* **2000**, *72 (7)*, 1391–1398.

[17] Zhao, H.; Xia, S.; Ma, P. *J. Chem. Technol. Biotechnol.* **2005**, *80*, 1089–1096.

[18] Kerton, F. M.; Marriott, R. In *Alternative Solvents for Green Chemistry, Chapter 6: Room Temperature Ionic Liquids and Eutectic Mixtures*; Clark, J. H., Kraus, G. A., Eds.; RSC, Thomas Graham House, Science Park, Milton Road, Cambridge, CB4 0WF, UK, 2009; pp 23–43.

[19] Ryu, I.; Matsubara, H.; Emnet, C.; Gladysz, J. A.; Takeuchi, S.; Nakamura, Y.; Curran, D. P. In *en Reaction Media in Organic Synthesis Chapter 3: Fluorous Solvents*; Koichi, M., Ed.; Wiley-Blackwell; 1 edition, 2005.

[20] Kerton, F. M.; Marriott, R. In *Alternative Solvents for Green Chemistry, Chapter 7: Fluorous Solvents and Related Systems*; Clark, J. H., Kraus, G. A., Eds.; RSC, Thomas Graham House, Science Park, Milton Road, Cambridge, CB4 0WF, UK, 2009; pp 143–169.

[21] Kerton, F. M.; Marriott, R. In *Alternative Solvents for Green Chemistry, Chapter 2: 'Solvent free' Chemistry*; Clark, J. H., Kraus, G. A., Eds.; RSC, Thomas Graham House, Science Park, Milton Road, Cambridge, CB4 0WF, UK, 2009; pp 23–43.

[22] Jessop, P. G. *Green Chem.* **2011**, *13*, 1391–1398.

[23] Capello, C.; Fischer, U.; Hungerbühler, K. *Green Chem.* **2007**, *9*, 927–934.

[24] Curran, P.; Mail, J.; Ostrowski, P.; Ublacker, G.; Linclau, B. *Top. Curr. Chem.* **19999**, *206*, 79–106.

[25] Gani, R.; Jiménez-Gonzalez, C.; Kate, A.; Crafts, P. A.; Jones, M.; Powell, L.; Atherton, J. H.; Cordiner, J. L. *Chem. Eng.* **2006**, *1*, 30–41.

[26] Sacaiko, B. *World Ethanol and Biofuels Report* **2004**, *2 (17)*, 20–22.

[27] Noyori, R. *Chem. Rev.* **1999**, *99*, 353–354.

[28] Koller, G.; Fischer, U.; Hungerbühler, K. *Ind. Eng. Chem.* **2000**, *39*, 960–972.

[29] *Environmental management - Life Cycle Assessment - Principles and framework*; 1997.

[30] Alfonsi, K.; Colberg, J.; Dunn, P. J.; Fevig, T.; Jennings, S.; Johnson, T. A.; Kleine, H. P.; Knight, C.; Nagy, M. A.; Perry, D. A.; Stefaniak, M. *Green Chem.* **2008**, *10*, 31–36.

[31] Hansen, C. H. *Hansen Solubility Parameters: a User's Handbook*; CRC Press, Boca Raton, FL, USA, 2nd edition, 2007.

[32] Kamlet, M. J.; Taft, R. W. *J. Am. Chem. Soc.* **1976**, *98*, 377–383.

[33] Taft, R. W.; Kamlet, M. J. *J. Am. Chem. Soc.* **1976**, *98*, 2886–2894.

[34] Kamlet, M. J.; Abboud, J. L.; Taft, R. W. *J. Am. Chem. Soc.* **1977**, *99*, 6027–6038.

[35] Moity, L.; Durand, M.; Benazzouz, A.; Pierlot, C.; Molinier, V.; Aubry, J.-M. *Green Chem.* **2012**, *14 (4)*, 1132–1145.

[36] Durand, M.; Molinier, V.; Kunz, W.; Aubry, J.-M. *Chem. Eur. J.* **2011**, *17*, 5155–5164.

[37] Rico-Lattes, I.; Perez, E.; Franceschi-Messant, S.; Lattes, A. *CR Chim* **2011**, *14 (7-8)*, 700–715.

[38] Schwuger, M.-J.; Stickdorn, K. *Chem. Rev.* **1995**, *95*, 849–864.

[39] Eicke, H. F. *Top. Curr. Chem.* **1980**, *87*, 85–145.

[40] Lindman, B.; Wennerstroem, H. *Top. Curr. Chem.* **1980**, *87*, 1–83.

[41] Hoar, T. P.; Schulman, J. H. *Nature* **1943**, *152*, 102–103.

[42] Winsor, P. A. *Trans. Faraday. Soc.* **1948**, *44*, 376–382.

[43] Schulman, J. H.; Stoeckenius, W.; Prince, L. M. *J. Phys. Chem.* **1959**, *63*, 1677–1680.

[44] Adamson, A. W. *J. Colloid Interface Sci.* **1969**, *29 (2)*, 261–267.

[45] Friberg, S. E.; Mandell, L.; Larsson, M. *J. Colloid Interface Sci.* **1969**, *29 (1)*, 155–156.

[46] Danielsson, I.; Lindman, B. *Colloid Surface* **1981**, *3(4)*, 391–392.

[47] Bodet, J. F.; Bellare, J. R.; Davis, H. T.; Scriven, L. E.; Miller, W. G. *J. Phys. Chem.* **1959**, *63 (10)*, 1898–1902.

[48] Jahn, W.; Strey, R. *J. Phys. Chem.* **1988**, *92*, 2294–2301.

[49] Lichterfeld, F.; Schmeling, T.; Strey, R. *J. Phys. Chem.* **1986**, *90*, 5762–5766.

[50] Chen, S. H. *Ann. Rev. Phys. Chem.* **1986**, *37*, 351–399.

[51] Kahlweit, M. et al. *J. Colloid Interface Sci.* **1987**, *118(2)*, 436–453.

[52] Chevalier, Y.; Zemb, T. *Rep. Prog. Phys.* **1990**, *53 (3)*, 279–371.

[53] Stilbs, P.; Lindman, B.; Rapacki, K. *J. Colloid Interf. Sci.* **1983**, *95*, 583–585.

[54] Bowcott, I. E.; Schulman, I. H. *Z. Elektrochem.* **1955**, *59*, 283–288.

[55] Anderson, J. L.; Ding, J.; Welton, T.; Armstrong, D. W. *J. Am. Chem. Soc.* **2002**, *124*, 14247–14254.

[56] Scriven, L. E. *Nature* **1976**, *263*, 123–125.

[57] Langevin, D. *Annu. Rev. Phys. Chem.* **1992**, *43*, 341–369.

[58] Sassen, C. L.; Casielles, A. G.; Loos, T. W. D.; J. De Swaan Arons From Fluid Phase Equilibria (1992), .-., 72 *Fluid Phase Equilibr.* **1992**, *72*, 173–187.

[59] Pizzino, A.; Molinier, V.; Catte, M.; Salager, J.-L.; Aubry, J.-M. *J. Phys. Chem. B* **2009**, *113*, 16142–16150.

[60] Smith, G. D.; Garrett, B. B.; Holt, S. L.; Barden, R. E. *J. Phys. Chem.* **1976**, *80 (15)*, 1708–1713.

[61] Smith, G. D.; Donelan, C. E.; Barden, R. E. *J. Colloid Interface Sci.* **1977**, *60 (3)*, 488–496.

[62] Aveyard, R.; Mitchell, R. W. *Trans. Faraday. Soc.* **1969**, *65 (10)*, 2645–2653.

[63] Knickerbocker, B. M.; Pesheck, C. V.; Scriven, L. E.; Davis, H. T. *J. Phys. Chem.* **1979**, *83 (15)*, 1984–1990.

[64] Keiser, B. A.; Varie, D.; Barden, R. E.; Holt, S. L. *J. Phys. Chem.* **1979**, *83 (10)*, 1276–1280.

[65] Borys, N. F.; Holt, S. L.; Barden, R. E. *J. Colloid Interface Sci.* **1979**, *71 (3)*, 526–532.

[66] Prince, L. M. *J. Colloid Interf. Sci.* **1967**, *23 (2)*, 165–173.

[67] Prince, L. M. *J. Colloid Interf. Sci.* **1975**, *52 (1)*, 182–188.

[68] Shooley, J. N.; Alder, B. J. *J. Chem. Phys.* **1955**, *23*, 805–811.

[69] Knickerbocker, B. M.; Pesheck, C. V.; Davis, H. T.; Scriven, L. E. *J. Phys. Chem.* **1982**, *86*, 393–400.

[70] Puig, J. E.; Hemker, D. L.; Gupta, A.; Davis, H. T.; Scriven, L. E. *J. Phys. Chem.* **1987**, *91*, 1137–1143.

[71] Lara, J.; Perron, G.; Desnoyers, J. E. *J. Phys. Chem.* **1981**, *85 (11)*, 1600–1605.

[72] Lund, G.; Holt, S. L. *J. Am. Oil Chem. Soc.* **1980**, *57 (8)*, 264–267.

[73] Zoumpanioti, M.; Stamatis, H.; Papadimitriou, V.; Xenakis, A. *Colloid Surf B* **2006**, *47 (1)*, 1–9.

[74] Khmelnitsky, Y. L.; van Hock, A.; Veeger, C.; Visser, A. J. W. G. *J. Phys. Chem.* **1989**, *93*, 872–878.

[75] Drapeau, J.; Verdier, M.; Touraud, D.; Kroeckel, U.; Geier, M.; Rose, A.; Kunz, W. *Chem. Biodivers.* **2009**, *6 (6)*, 934–947.

[76] Luisi, P. L.; Giomini, M.; Pileni, M. P.; Robinson, B. H. *Biochim. Biophys. Acta* **1988**, *947 (1)*, 209–246.

[77] Xu, J.; Yin, A.; Zhao, J.; Li, D.; Hou, W. *J. Phys. Chem. B* **2013**, *117*, 450–456.

[78] Clausse, M.; Nicolas-Morgantini, L.; Zradba, A.; Touraud, D. In *Surfactant Science Series, Microemulsion Systems*; Rosano, H. L., Clausse, M., Eds.; Dekker: New York, 1987.

[79] Keiser, B. A.; Holt, S. L. *Inorg. Chem.* **1982**, *21*, 2323–2327.

[80] Khmelnitsky, Y. L.; Zharinova, I. N.; Berezin, I. V.; Levashov, A. V.; Martinek, K. *Annals New York Acad. Sci.* **1987**, *501*, 161–164.

[81] Khmelnitsky, Y. L.; Levashov, A. V.; Klyachko, N. L.; Martinek, K. *Enzyme Microb. Technol* **1988**, *10*, 710–724.

[82] O'Connor, C. J.; Cleverly, D. R. *Biocatal. Biotransf.* **1995**, *12 (3)*, 193–204.

[83] Vulfson, E. N.; Ahmed, G.; Gill, I.; Kozlov, I. A.; Law, P. W. G. B. A. *Biotechnol. Lett.* **1991**, *13 (2)*, 91–96.

[84] Zoumpanioti, M.; Karali, M.; Xenakis, A.; Stamatis, H. *Enzyme Microb. Tech.* **2006**, *39 (4)*, 531–539.

[85] Schott, R.; Pfennig, A. *Mol. Phys.* **2004**, *102 (4)*, 331–339.

[86] Li, Z.; Cheng, H.; Li, J.; Hao, J.; Zhang, L.; Hammouda, B.; Han, C. C. *J. Phys. Chem. B* **2011**, *115*, 7887–7895.

[87] Al-Bawab, A.; Bozeya, A.; Friberg, S. E.; Ge, L.; Guo, R. *Colloid Surf. A* **213**, *418*, 1–6.

[88] Klossek, M. L.; Touraud, D.; Zemb, T.; Kunz, W. *Chem. Phys. Chem.* **2012**, *13 (18)*, 4116–4119.

[89] Vitale, S. A.; Katz, J. L. *Langmuir* **2003**, *19*, 4105–4110.

[90] Grillo, I. *Colloid Surf. A* **2003**, *225*, 153–160.

[91] Sitnikova, N. L.; Sprik, R.; Wegdam, G.; Eiser, E. *Langmuir* **2005**, *21 (16)*, 7083–7089.

[92] Carteau, D.; Pianet, I.; Brunerie, P.; Guillemat, B.; Bassani, D. M. *Langmuir* **2007**, *23 (7)*, 3561–3565.

[93] Botet, R. *J. Phys. Conf. Ser.* **2012**, *352*, 1–10.

[94] Stainmesse, S.; Orecchioni, A. M.; Nakache, E.; Puisieux, F.; Fessi, H. *Colloid Polym. Sci.* **1995**, *273 (5)*, 505–511.

[95] Kim, J. Y.; Lee, H. K.; Baik, K. J.; Kim, S. C. *J. Appl. Polym. Sci.* **1997**, *65 (13)*, 2643–2653.

[96] Aubry, J.; Ganachaud, F.; Addad, J.-P. C.; Cabane, B. *Langmuir* **2009**, *25 (4)*, 1970–1979.

[97] Lagues, M.; Ober, R.; Taupin, C. *J. Physique Lett.* **1978**, *39 (24)*, L487–L491.

[98] Lagues, M. *J. Physique Lett.* **1979**, *40 (14)*, 331–333.

[99] Kirkpatrick, S. *Phys. Rev. Lett.* **1971**, *27 (25)*, 1722–1725.

[100] Sahimi, M., Ed. *Applications of Percolation Theory*; Taylor & Francis, London 1994.

[101] Ede, D.; Elias, J. *Measurement of Suspended Particles by Quasi-Elastic Light Scattering*; Wiley Interscience, New York, 1983.

[102] Pecora, R. *Dynamic Light Scattering: Applications of Photon Correlation Spectroscopy*; Plenum Press, New York, 1985.

[103] Berne, B. J.; Pecora, R. *Dynamic Light Scattering: With Applications to Chemistry, Biology, adn Physics*; Dover Pubn Inc., New York, 2000.

[104] Brown, W. *Dynamic Light Scattering*; Clarendon Press, Oxford, 1993.

[105] Hassan, P.; Kulshreshtha, S. *J. Colloid Interf. Sci.* **2006**, *300*, 744–748.

[106] Morrison, I. D.; Grabowski, E. F.; Herb, C. A. *Langmuir* **1985**, *1*, 496–501.

[107] Provencher, S. W. *Comput. Phys. Commun* **1982**, *27*, 229–242.

[108] Koppel, D. E. *J. Chem. Phys.* **1972**, *57*, 4814.

[109] Moreels, E.; Ceuninck, W. D.; Finsy, R. *J. Chem. Phys.* **1987**, *86 (2)*, 618–623.

[110] Wahid, H. *J. Mol. Liqu.* **1993**, *55*, 1–18.

[111] Chu, B. *Laser Light Scattering*; Academic Press, London, 2nd edition, 1991.

[112] Papadimitriou, V.; Pispas, S.; Syriou, S.; Pournara, A.; Zoumpanioti, M.; Sotiroudis, T.; Xenakis, A. *Langmuir* **2008**, *24*, 3380–3386.

[113] Do, L.; Withayyapayanon, A.; Harwell, J.; Sabatini, D. *J. Surfact. Deterg.* **2009**, *12*, 91–99.

[114] Gao, Y.; Wang, S.; Zheng, L.; Han, S.; Zhang, X.; Lu, D.; Yu, L.; Ji, Y.; Zhang, G. *J. Colloid Interface Sci.* **2006**, *301*, 612–616.

[115] Liu, C.-H.; Chang, F.-Y.; Hung, D.-K. *Colloid Surface B* **2011**, *82*, 63–70.

[116] Kogan, A.; Garti, N. *Adv. Colloid Interface Sci.* **2006**, *123*, 369–385.

[117] Wellert, S.; Karg, M.; Imhof, H.; Steppin, A.; Altmann, H.-J.; Dolle, M.; Richardt, A.; Tiersch, B.; Koetz, J.; Lapp, A.; T. Hellweg, T. *J. Colloid Interface Sci.* **2008**, *325*, 250–258.

[118] Gao, H.; Li, J.; Han, B.; Chen, W.; Zhang, J.; Zhang, R.; Yan, D. *Phys. Chem. Chem. Phys.* **2004**, *6*, 2914–2916.

[119] Saito, H.; Shinoda, K. *J. Colloid Interface Sci.* **1970**, *32*, 647.

[120] Shinoda, K.; Friberg, S. *Adv. Colloid Interface Sci.* **1975**, *4*, 281–300.

[121] Shinoda, K. *Prog. Colloid Polym. Sci.* **1983**, *68*, 1.

[122] Talmon, Y.; Prager, S. *J. Chem. Phys* **1978**, *69*, 2984.

[123] Jouffray, J.; Levinson, P.; DeGennes, P. *J. Phys* **1982**, *43*, 1241.

[124] Endo, H.; Mihailescu, M.; Monkenbusch, M.; Allgaier, J.; Gompper, G.; Richter, D.; Jakobs, B.; Sottmann, T.; Strey, R.; Grillo, I. *J. Chem. Phys* **2001**, *115*, 580–600.

[125] Mihailescu, M.; Monkenbusch, M.; Endo, H.; Allgaier, J.; Gompper, G.; Stellbrink, J.; Richter, D.; Jakobs, B.; Sottmann, T.; Farago, B. *J. Chem. Phys* **2001**, *115*, 9563–9577.

[126] Lindman, B.; Kamenka, N.; Kathopoulis, T. M.; Brun, B.; Nilsson, P. G. *J. Phys. Chem.* **1980**, *84*, 2485–2490.

[127] Bodet, J. F.; Bellare, J. R.; Davis, H. T.; Scriven, L. E.; Miller, W. G. *J. Phys. Chem.* **1988**, *92*, 1898–1902.

[128] Burauer, S.; Belkoura, L.; Stubenrauch, C.; Strey, R. *Colloids Surf., A* **2003**, *228*, 159–170.

[129] Note, C.; Ruffin, J.; Tiersch, B.; Koetz, J. *J. Disp. Sci. Technol.* **2007**, *28*, 155–164.

[130] Dvolaitzky, M.; Lagues, M.; Pesant, J. P. L.; Ober, R.; C.Sauterey,; Taupin, C. *J. Phys. Chem.* **1980**, *84*, 1532–1535.

[131] Lagourette, B.; Peyrelasse, J.; Boned, C.; Clausse, M. *Nature* **1979**, *281*, 60–63.

[132] Lagues, M. *J. Phys. Lett.* **1979**, *40(14)*, 331–333.

[133] Alexandridis, P.; Holzwarth, J. F.; Hatton, T. A. *J. Phys. Chem.* **1995**, *99*, 8222–8232.

[134] Zemb, T. *Colloid Surface A* **1997**, *1291, 130*, 435–454.

[135] Solans, C., (Eds.), H. K., Eds. *Microemulsions in cosmetic, Industrial Applications of Microemulsions*; Marcel Dekker, New York, 1997.

[136] von Rybinski, W.; Hloucha, M.; Johansson, I. In *Microemulsions in cosmetics and detergents, Microemulsions: Background, New Concepts, Application, Perspectives*; Stubenrauch, C., Ed.; John Wiley & Sons, Ltd, Chichester, 2009.

[137] Hloucha, M.; Haake, H.-M.; Pellon, G. *Cosmetics & Toiletries* **2009**, *124*, 58.

[138] http://www.cognis.com/company/Businesses/Care+chemicals/Products+and+concept+innovations/personal+care/Plantasil.htm,.

[139] Lawrence, M. J.; Rees, G. D. *Adv. Drug Deliv. Rev.* **2000**, *45*, 89–121.

[140] Paul, B.; Moulik, S. P. *Curr. Sci.* **2001**, *80*, 990–1001.

[141] Garti, N. *Curr. Opin. Colloid Interface Sci.* **2003**, *8*, 197–211.

[142] Flanagan, J.; Singh, H. *Crit. Rev. Food Sci. Nutr.* **2006**, *46*, 221–237.

[143] Sottmann, T.; Stubenrauch, C. In *Microemulsions: Background, New Concepts, Application, Perspectives*; Stubenrauch, C., Ed.; Blackwell Publishing Ltd, 2009.

[144] Harwell, J. H.; Sabatini, D. A.; Knox, R. *Colloids Surf., A* **1999**, *151*, 255–268.

[145] Jayanti, S.; Britton, L. N.; Dwarakanath, V.; Pope, G. A. *Environ. Sci. Technol.* **2002**, *36*, 5491–5497.

[146] Wellert, S.; Imhof, H.; Dolle, M.; Altmann, H.-J.; Richardt, A.; Hellweg, T. *Colloid Polym. Sci.* **2008**, *286*, 417–426.

[147] http://www.cognis.com/company/Businesses/agroSolutions/microemulsions,.

[148] http://www.cognis.com/NR/rdonlyres2101DE9F8DE0-4A0E-95BA-D3D1E3735080/0/Cognis_APG_Broschure_USA.pdf,.

[149] Sabatini, D. A.; Knox, R. C.; Harwell, J. H.; Wu, B. *J. Contam. Hydrol.* **2000**, *45*, 99–121.

[150] Childs, J. D.; Acosta, E.; Knox, R. C.; Harwell, J. H.; Sabatini, D. A. *J. Contam. Hydrol.* **2004**, *71*, 27–45.

[151] Chin, C.-P.; Lan, C.-W.; Wu, H.-S. *Ind. Eng. Chem. Res.* **2012**, *51*, 4710–4718.

[152] Hill, K. *Pure Appl. Chem.* **2000**, *72*, 1255–1264.

[153] de Castro Dantas, T. N.; da Silva, A.; Neto, A. *Fuel* **2001**, *80*, 75–81.

[154] Silva, E. J.; Zaniquelli, M. E. D.; Loh, W. *Energy Fuels* **2007**, *21*, 222–226.

[155] Ma, F.; Hanna, M. A. *Bioresour. Technol.* **1999**, *70*, 1–15.

[156] Knothe, G.; Steidley, K. R. *Ind. Eng. Chem. Res.* **2011**, *50*, 4177–4182.

[157] Knothe, G., Gerpen, J. V., Krahl, J., Eds. *The Biodiesel Handbook*; AOCS Publishing, 2005.

[158] Mittelbach, M., Remschmidt, C., Eds. *Biodiesel: The Comprehensive Handbook*; Martin Mittelbach, 2006.

[159] Foidl, N.; Foidl, G.; Sanchez, M.; Mittelbach, M.; Hackel, S. *Bioresour. Technol.* **1996**, *58*, 77–82.

[160] Chisti, Y. *Biotechnol. Adv.* **2007**, *25*, 294–306.

[161] Wolf, R.; Graham, S.; Kleiman, R. *J. Am. Oil Chem. Soc.* **1983**, *60*, 103–104.

[162] Knothe, G.; Cermak, S. C.; Evangelista, R. L. *Energy Fuels* **2009**, *23*, 1743–1747.

[163] Wilson, T.; Miwa, T.; Smith, C. *J. Am. Oil Chem. Soc.* **1960**, *37*, 675–676.

[164] Hu, J.; Du, Z.; Tang, Z.; Min, E. *Ind. Eng. Chem. Res.* **2004**, *43*, 7928–7931.

[165] Clark, J. H.; Tavener, S. J. *Org. Process Res. Dev.* **2007**, *11*, 149.

[166] Kerton, F. M. In *Alternative Solvents for Green Chemistry, Chapter 5*; Clark, J. H., Kraus, G. A., Eds.; RSC, Thomas Graham House, Science Park, Milton Road, Cambridge, CB4 0WF, UK, 2009.

[167] Wildes, S. *Chem. Health Saf.* **2002**, *5/6*, 24.

[168] Miller, N.; Mudge, S. M. *Spill Sci. Tech. Bull.* **1997**, *4*, 17–33.

[169] Salehpour, S.; Dubé, M. A. *Green Chem.* **2008**, *10*, 321–326.

[170] Salehpour, S.; Dubé, M. A.; Murphy, M. *Can. J. Chem. Eng.* **2009**, *87*, 129–135.

[171] Spear, S. K.; Griffin, S. T.; Granger, K. S.; Huddleston, J. G.; Rogers, R. D. *Green Chem.* **2007**, *9*, 1008–1015.

[172] Strey, R.; Nawrath, A.; Sottmann, T. US 2007/0028507 A1. 2007.

[173] Bemert, L.; Engelskirchen, S.; Simon, C.; Strey, R. *Prepr. Pap.-Am. Chem. Soc., Div. Fuel Chem.* **2009**, *54*, 290–291.

[174] Strey, R.; Sottmann, T.; Nawrath, A.; Rottländer, K.; Bemert, L.; Engelskirchen, S. WO 2010/133627 A2. 2010.

[175] Geller, D. P.; Goodrum, J. W.; Knapp, S. J. *Ind. Crop. Prod.* **1999**, *9*, 85.

[176] Khan, N.; Warith, M.; Luk, G. *J. Air and Waste Manage Assoc* **2007**, *57*, 286–296.

[177] DeMello, J. A.; Carmichael, C.; Peacock, E. E.; Nelson, R.; Arey, J. S.; Reddy, C. M. *Mar. Pollut. Bull.* **2007**, *54*, 894–904.

[178] Dinjus, E.; Arnold, U.; Dahmen, N.; Höfer, R.; Wach, W. In *Sustainable Solutions for Modern Economies, Chapter 8 Green Fuels – Sustainable Solutions for Transportation*; Höfer, R., Ed.; RSC, Thomas Graham House, Science Park, Milton Road, Cambridge, CB4 0WF, UK, 2009.

[179] Vrana, B.; Mills, G. A.; Dominiak, E.; Greenwood, R. *Environ. Pollut.* **2006**, *142*, 333–343.

[180] Gonzalez, Y. M.; de Caro, P.; Thiebaud-Roux, S.; Lacaze-Dufaure, C. *J. Solution Chem.* **2007**, *36*, 437–446.

[181] Thész, J.; Boros, B.; Király, Z. WO 2008/096187 A1. 2008.

[182] Sun, J. *Altern. Med. Rev.* **2007**, *12*, 259–264.

[183] Matura, M.; Goossens, A.; Bordalo, O.; Garcia-Bravo, B.; Magnusson, K.; Wrangsjö, K.; Karlberg, A. T. *J. Am. Acad. Dermatol* **2002**, *47*, 709–714.

[184] http://www.ppiatlanta.com/pdfs/DataSheets/D-Limonene-%20uses.pdf, 2012.

[185] Willkins, J. S. US5575822. 1996.

[186] Li, T. CN 101319146 (A). 2008.

[187] Fanun, M. *Household and Personal Care* **2011**, *2*, 10–12.

[188] Drapier, J.; Galvez, M.; Kerzmann, N.; Jakubicki, G. US 6048834. 2000.

[189] http://www.airproducts.com/∼/media/Downloads/Other/i-and-i-formulary%20brochure.ashx.

[190] Jameson, C. *Toxicology and Carcinogenesis Studiesof d-Limonene*; 1990.

[191] Crowell, P. L.; Gould, M. N. *Crit. Rev. Oncog.* **1994**, *5*, 1–22.

[192] Okabe, H.; Obata, Y.; Takayama, K.; Nagai, T. *Drug Des. Delivery* **1990**, *6*, 229–238.

[193] Karlberg, A.-T.; Boman, A.; Melin, B. *Ann. Occup. Hyg.* **1991**, *35(4)*, 419–426.

[194] Touraud, D. Ph.D. thesis, Compiégne, 1991.

[195] Clausse, M.; Peyrelasse, J.; Heil, J.; Boned, C.; Lagourette, B. *Nature* **1981**, *293*, 636–638.

[196] http://www.rhodia.com/en/markets_and_products/brands, 2012.

[197] Gross, S. F.; Doerr, M.; Morris, T. C. US 20070093404 A1. US 20070093404 A1, 2007.

[198] Pabalan, R. T.; Aymes, C.; Graham, S.; Sehgal, A.; Trivedi, S.; Fluck, D.; Langlois, B. WO 2011US01000. WO 2011US01000 20110602, 2011.

[199] Fluck, D.; Sehgal, A.; Trivedi, S.; Pabalan, R. T.; Aymes, C. WO 2011US01967. WO 2011US01967, 2012.

[200] Kordosh, J. WO 2011US45684. WO 2011US45684, 2012.

[201] Evans, J. *J. Chem. Austr.* **2005**, *72(2)*, 8–11.

[202] Frees, R. M.; Bortz, P. C. S. H. US 20070101902 A1. US 20070101902 A1, 2007.

[203] Machac, J. R.; Marquis, E. T.; Woodrum, S. A.; Darragas, K. WO 2003062325 A2. WO 2003062325 A2 20030731, 2003.

[204] S.Trivedi,; Fluck, D.; Sehgal, A. WO 2011028274 A2. WO 2011028274 A2, 2011.

[205] Wei, Y.; Cheng, F.; Li, H.; Yu, J. *J. Appl. Polym. Sci.* **2004**, *92*, 351–356.

[206] Katz, H.; Iovino, C. A. WO 2006108082 A2. WO 2006108082 A2, 2006.

[207] Kaplan, W. A. WO 2007092005 A1. WO 2007092005 A1 20070816, 2007.

[208] Katrib, Y.; Calvé, S. L.; Mirabel, P. *J. Phys. Chem. A* **2003**, *107*, 11433–11439.

[209] Cukalovic, A.; Stevens, C. V. *Biofuel Bioprod. Bior.* **2008**, *2*, 505–529.

[210] Zeikus, J. G.; Jain, M. K.; Elankovan, P. *Appl. Microbiol. Biotechnol.* **1999**, *51*, 545–552.

[211] Bechthold, I.; Bretz, K.; Kabasci, S.; Kopitzky, R.; Springer, A. *Chem. Eng. Technol.* **2008**, *31 (5)*, 647–654.

[212] Willke, T.; Vorlop, K. D. *Appl. Microbiol. Biotechnol.* **2004**, *66*, 131–142.

[213] Song, H.; Lee, S. Y. *Enyzme Microb. Tech.* **2006**, *39*, 352–361.

[214] Rossi, C.; Hauber, J.; Singer, T. P. *Nature* **1964**, *204*, 167.

[215] Ling, E. T.; Dibble, J. T.; Houston, M. R.; Lockwood, L. B.; Elliott, L. P. *Appl. Environ. Microbiol.* **1978**, *35*, 1213–1215.

[216] Guettler, M. V.; Rumler, D.; Jaint, M. K. *Int. J. Syst. Bacteriol.* **1999**, *49*, 207.

[217] Lee, P.; Lee, S.; Hong, S.; Chang, H. *Bioprocess. Biosyst. Eng.* **2003**, *26*, 63–67.

[218] http://www.chemicals-technology.com/projects/agro-industrie plant/, 2012.

[219] Moss, C. W.; Kaltenbach, C. M. *Appl. Microbiol.* **1974**, *27 (2)*, 437–439.

[220] Draths, K. M.; Frost, J. W. *J. Am. Chem. Soc.* **1994**, *116*, 399–400.

[221] http://www.chemsystems.com/reports/search/docs/abstracts/0809_2_abs.pdf, 2012.

[222] http://www.rennovia.com/LinkClick.aspx?fileticket=_G2xXL0Yes%3D&tabid=62, 2012.

[223] http://verdezyne.com/verdezyne/News/documents/Verdezyne PilotPlantReleaseBusinessFINAL.pdf, 2012.

[224] Ewbank, E.; Tummers, D. US 6620437B2. US 6.620.437B2, 2001.

[225] http://ethanolrfa.3cdn.net/d4ad995ffb7ae8fbfe_1vm62ypzd.pdf, 2012.

[226] Werle, P.; Morawietz, M. In *Ullmann's Encyclopedia of Industrial Chemistry - Alcohols, Polyhydric*; Elvers, B., Ed.; Wiley-VCH: Weinheim, 2002.

[227] Kaufman, D.; Reeve, W. *Org. Synth.* **1946**, *26*, 83–85.

[228] Xu, W.; Wang, H.; Liu, X.; Ren, J.; Wang, Y.; Lu, G. *Chem. Commun.* **2011**, *47*, 3924–3926.

[229] Cistola, D. P.; Hamilton, J. A.; Jackson, D.; Small, D. M. *Biochemistry* **1988**, *27*, 1881–1888.

[230] Kinecky, J. R.; Shah, D. O. *J. Colloid Interface Sci.* **2002**, *256*, 201–207.

[231] http://www.ddbst.com/en/EED/PCP/VAP_C11.php, 2012.

[232] http://www.chemspider.com/Chemical Structure.13839441.html, 2012.

[233] Garti, N.; Yaghmur, A.; Leser, M. E.; Clement, V.; Watzke, H. J. *J. Agric. Food Chem.* **2001**, *49*, 2552–2562.

[234] Spernath, A.; Yaghmur, A.; Aserin, A.; Hoffman, R.; Garti, N. *J. Agric. Food Chem.* **2002**, *50*, 6917–6922.

[235] Rao, J.; McClements, D. J. *J. Agric. Food Chem.* **2011**, *59*, 5026–5035.

[236] Suratkar, V.; Mahapatra, S. *J. Colloid Interface Sci.* **2000**, *225*, 32–38.

[237] Fischer, E.; Fieberand, W.; Navarro, C.; Sommer, H.; di, D. B.; Velazco, M.; Schönhoff, M. *J. Surfact. Deterg.* **2009**, *12*, 73–84.

[238] Tchakalova, V.; Fieber, W. *J. Surfact. Deterg.* **2012**, *15*, 167–177.

[239] Kahlweit, M.; Busse, G.; Faulhaber, B.; Eibl, H. *Langmuir* **1995**, *11 (11)*, 4185–4187.

[240] Kahlweit, M.; Busse, G.; Faulhaber, B. *Langmuir* **1997**, *13 (20*, 5249–5251.

[241] Stubenrauch, C.; Paeplow, B.; Findenegg, G. H. *Langmuir* **1997**, *13 (14)*, 3652–3658.

[242] Kanei, N.; Tamura, Y.; Kunieda, H. *J. Colloid Interface Sci.* **1999**, *218 (1)*, 13–22.

[243] Amar, I.; Aserin, A.; Garti, N. *J. Agric. Food Chem.* **2003**, *51*, 4775–4781.

[244] Ratjika, C. US2007087104 (A1). 2007.

[245] Nishimi, T. *Macromol. Symp.* **2008**, *270*, 48–57.

[246] Fanun, M. In *Biocompatible microemulsions in Colloids in Biotechnology, Surfactant Series*; Fanun, M., Ed.; Taylor and Francis/CRC press, Boca Raton, 2010.

[247] Fanun, M. *Colloids Surf A* **2010**, *369*, 246–252.

[248] Xing, Y.; Xiaonian, X.; Li, L.; Ye, G.; Haibin, Y.; Chunyan, B. CN101982109 (A). 2011.

[249] Fanun, M. *J. Mol. Liq.* **2008**, *142*, 103–110.

[250] Nguyen, T. T.; Sabatini, D. A. *J. Surfact. Deterg.* **2009**, *12*, 109–115.

[251] http://accessdata.fda.gov/scripts/cdrh/cfdocs/cfcfr/CFRSearch.cfm?FR=172.863, 2012.

[252] Choia, S. Y.; Oh, S. G.; Bae, S. Y.; Moon, S. K. *Korean J. Chem. Eng.* **1999**, *16(3)*, 377–381.

[253] Yaghmur, A.; Campo, L. D.; Aserin, A.; Garti, N.; Glatter, O. *Phys. Chem. Chem. Phys.* **2004**, *6*, 1524–1533.

[254] Walderhaug, H.; Knudsen, K. D. *Langmuir* **2008**, *24*, 10637–10645.

[255] Zhang, H.; Feng, F.; Li, J.; Zhan, X.; Wei, H.; Li, H.; Wang, H.; Zheng, X. *Eur. Food Res. Technol.* **2008**, *226*, 613 – 619.

[256] Santos, P.; Watkinson, A. C.; Hadgraft, J.; Lane, M. E. *Skin Pharmacol. Phys.* **2008**, *21*, 246–259.

[257] Yu, B.; Mattox, J. R. EP 648414 A2. 1995.

[258] Spernath, A.; Aserin, A.; Garti, N. *J. Colloid Interface Sci.* **2006**, *299*, 900–909.

[259] Kogan, A.; Kesselman, E.; Danino, D.; Aserin, A.; Garti, N. *Colloids Surf B* **2008**, *66*, 1–12.

[260] Mehta, S. K.; Kaur, G.; Mutneja, R.; Bhasin, K. K. *J. Colloid Interf. Sci.* **2009**, *338*, 542–549.

[261] Uddin, H.; Kanei, N.; Kunieda, H. *Langmuir* **2000**, *16*, 6891–6897.

[262] Vlad, F. J.; Mounier, R.; Wong, K.; Daugeron, A.; Herd, T. WO 2006043177 A1. 2006.

[263] Tchakalova, V.; Testard, F.; Wong, K.; Parker, A.; Benczédi, D.; Zemb, T. *Colloids Surf. A* **2008**, *331*, 40–47.

[264] Solè, I.; Solans, C.; Maestro, A.; González, C.; Gutiérrez, J. M. *J. Colloid Interface Sci.* **2012**, *376*, 133 – 139.

[265] Gebicki, J. M.; Hicks, M. *Nature* **1973**, *243*, 232–234.

[266] Morigaki, K.; Walde, P. *Curr. Opin. Colloid Interface Sci.* **2007**, *12*, 75–80.

[267] Chen, S. I.; Evans, D. F.; Ninham, B. W. *J. Phys. Chem.* **1984**, *88*, 1631–1634.

[268] Maghraby, G. M. E. *Int. J. Pharm.* **2008**, *355*, 285–292.

[269] Aboofazeli, R.; Lawrence, M. J. *Int. J. Pharm* **1994**, *106*, 51–61.

[270] Zana, R. *Adv. Colloid. Interfac.* **1995**, *57*, 1–64.

[271] Healy, R. N.; Reed, R. L. *Soc. Pet. Eng. J.* **1974**, *14 (5)*, 491–501.

[272] Lindman, B.; Stilbs, P.; M. E. Moseley J. Colloid Interface Sci. 83, . . *J. Colloid Interface Sci.* **1981**, *83*, 569–582.

[273] Bourrel, M.; Chambu, C. *Soc. Pet. Eng. J.* **1983**, *23 (2)*, 327–338.

[274] Overbeek, J. T. G.; Verhoeckx, G. J.; Bruyn, P. L. D.; Lekkerkerker, H. N. W. *J. Colloid Interf. Sci.* **1987**, *119 (2)*, 422–441.

[275] http://www.zenitech.com/documents/guerbet_chemistry.pdf, 2013.

[276] http://www.sasoltechdata.com/tds/ISOFOL.pdf, 2012.

[277] Murphy, J. B.; Jr., S. L. H.; Holt, E. M. *Inorg. Chim. Act.* **1981**, *48 (1)*, 29–32.

[278] Lavallee, D. K.; Huggins, E.; Lee, S. *Inorg. Chem.* **1982**, *21 (4)*, 1552–1553.

[279] Khmelnitsky, Y. L.; Gladilin, A. K.; Neverova, I. N.; Levashov, A. V.; Martinek, K. *Collect. Czech. Chem. C.* **1990**, *55 (2)*, 555–563.

[280] O'Connor, C. J.; Aggett, A.; Williams, D. R.; Stanley, R. A. *Aust. J. Chem.* **1991**, *44 (1)*, 53–60.

[281] Zoumpanioti, M.; Merianou, E.; Karandreas, T.; Stamatis, H.; Xenakis, A. *Biotechnol. Lett.* **2010**, *32 (10)*, 1457–1462.

[282] Asare, K. O. *Adv. Colloid. Interfac.* **1991**, *37 (1-2)*, 123–173.

[283] Corti, M.; Degiorgio, V. *J. Phys. Chem.* **1981**, *85*, 711–717.

[284] Zemb, T.; Drifford, M.; Hayoun, M.; Jehanno, A. *J. Phys. Chem.* **1983**, *87 (22)*, 4524–4528.

[285] Tanford, C. *The hydrophobic effect: Formation of micelles and biological membranes*; John Wiley & Sons Inc., 1973.

[286] http://www.chemspider.com/Chemical Structure.4511298.html,.

[287] Bhat, K. L.; Garg, A.; Bock, C. W. *Dyes Pigments* **2002**, *52*, 145–159.

[288] Bauduin, P.; Renoncourt, A.; Kopf, A.; Touraud, D.; Kunz, W. *Langmuir* **2005**, *21 (15)*, 6769–6775.

[289] Bauduin, P.; Testard, F.; Zemb, T. *J. Phys. Chem. B* **2008**, *112 (39)*, 12354–12360.

[290] Osakai, T.; Ebina, K. *J. Phys. Chem. B* **1998**, *102 (29)*, 5691–5698.

[291] Bouanz, M.; Beysens, D. *Chem. Phys. Lett.* **1994**, *231 (1)*, 105–110.

[292] Dixit, S.; Crain, J.; Poon, W. C. K.; Finney, J. L.; Soper, A. K. *Nature* **2002**, *416*, 829–832.

[293] Tomsic, M.; Jamnik, A.; Fritz-Popovski, G.; Glatter, O.; Vlcek, L. *J. Phys. Chem. B* **2007**, *111 (7)*, 1738–1751.

[294] Ivanov, D. A.; Winkelmann, J. *J. Chem. Phys* **2006**, *125*, 104507.

[295] Ganachaud, F.; Katz, J. L. *ChemPhysChem* **2005**, *6*, 209–216.

[296] Othmer, D. F.; Moeller, W. P.; Englund, S. W.; Christopher, R. G. *Ind. Eng. Chem.* **1951**, *43*, 707.

[297] Chemat, F.; Vian, M. A.; Cravotto, G. *Int. J. Mol. Sci.* **2012**, *13*, 8615–8627.

[298] Röper, H. *Starch-Starke* **2002**, *54*, 89–99.

[299] Runge, C. F.; Senauer, B. Council on Foreign Affairs,. May/June 2007.

[300] Pereira, C. S. M.; Silva, V. M. T. M.; Rodrigues, A. E. *Green Chem.* **2011**, *13*, 2658–2671.

[301] Delgado, P.; Sanz, M. T.; Beltrán, S.; nez, L. A. N. *Chem. Eng. J.* **2010**, *165 (2)*, 693–700.

[302] http://web.anl.gov/techtransfer/pdf/fact_sheets/ethyl_lactate.pdf, 2006.

[303] Horváth, I. T. *Green Chem.* **2008**, *10*, 1024–1028.

[304] Horváth, I. T.; Mehdi, H.; Fabos, V.; Boda, L.; Mika, L. T. *Green Chem.* **2008**, *10*, 238–242.

[305] Deng, L.; Li, J.; Lai, D. M.; Fu, Y.; Guo, Q. X. *Angew. Chem., Int. Ed* **2009**, *48*, 6529–6532.

[306] Deng, L.; Zhao, Y.; Li, J. A.; Fu, Y.; Liao, B.; Guo, Q. X. *ChemSusChem* **2010**, *3*, 1172–1175.

[307] Wettstein, S. G.; Alonso, D. M.; Chonga, Y.; Dumesic, J. A. *Energy Environ. Sci.* **2012**, *5*, 8199–8203.

[308] Yan, Z. P.; Lin, L.; Liu, S. J. *Energy Fuels* **2009**, *23*, 3853–3858.

[309] Du, X. L.; He, L.; Zhao, S.; Liu, Y. M.; Cao, Y.; He, H. Y.; Fan, K. N. *Angew. Chem., Int. Ed.* **2011**, *50*, 7815–7819.

[310] Werpy, T.; Petersen, G. 2004.

[311] Bozell, J. J.; Petersen, G. R. *Green Chem.* **2010**, *12*, 539–554.

[312] Durand, M.; Stoppa, A.; Molininer, V.; Touraud, D.; Aubry, J.-M. *J. Solution Chem.* **2012**, *41*, 555–565.

[313] Gupta, B.; Mishra, D. S.; Cheng, C. H.; Yalkowsky, S. H. *Toxicol. Environ. Chem.* **1991**, *33*, 7–21.

[314] Yalkowsky, S. H., Ed. *Solubility and Solubilization in Aqueous Media, 1 edition*; American Chemical Society Publication, 1999.

[315] Simamora, P.; Alvarez, J. M.; Yalkowsky, S. H. *Int. J. Pharm.* **2001**, *213*, 25–29.

[316] Booth, J. J.; Abbott, S.; Shimizu, S. *J. Phys. Chem. B* **2012**, *116 (51)*, 14915–14921.

[317] Moriyoshi, T.; Sakamoto, T.; Uosaki, Y. *J. Chem. Thermodynamics* **1989**, *21*, 947–954.

Publications

Parts of this work have already been published:

- Michael L. Klossek, Didier Touraud, and Werner Kunz, *Green Chem.*, 2012, **14**, 2017-2023
- Michael L. Klossek, Didier Touraud, Thomas Zemb, and Werner Kunz, *Chem. Phys. Chem.*, 2012, **13 (18)**, 4116–4119
- Michael L. Klossek, Julien Marcus, Didier Touraud, and Werner Kunz, *Colloid Surf. A*, 2013, doi.org/10.1016/j.colsurfa.2012.12.061
- Michael L. Klossek, Didier Touraud, and Werner Kunz, *PCCP*, 2013, submitted
- Michael L. Klossek, Julien Marcus, Didier Touraud, and Werner Kunz, *Colloid Surf. A*, 2013, submitted
- Michael L. Klossek, Didier Touraud, and Werner Kunz, *SCAE*, 2013, submitted

Declaration

Herewith I declare that I have made this existing work single-handed. I have only used the stated utilities.

Michael L. Klossek
March 13, 2013